# 國 立 交 通 大 學

## 應用化學研究所

## 博士論文

# 矽化鈦奈米結構之成長及其鑑定

# Growth and Characterization of Titanium Silicide Nanostructures

研 究 生：林煌凱

指導教授：裘性天 博士

李紫原 博士

# Contents

Contents ........................................................................................ I
Abstract ........................................................................................ IV
Acknowledgments ........................................................................ VIII
List of Tables ................................................................................ X
List of Figures ............................................................................. XI

Chapter 1 Introduction ...................................................................... 1
1.1 Introduction ................................................................................. 1
1.2 Metal Silcide ............................................................................... 2
1.3 Titanium Silcide .......................................................................... 4
1.3.1 Structure and Properties of Titanium Silicide ............................ 4
1.3.2 Synthesis of Titanium Silicide ................................................... 6
1.4 Metal Silicide Nanowires .............................................................. 7
1.4.1 Synthetic Methods of Metal Silicide NWs ................................. 9
1.4.1.1 Silicidation of Si or Metal NWs ............................................. 9
1.4.1.2 Deposition of Si Sources on Metal Films ............................... 10
1.4.1.3 Reaction between Metal Vapor Sources and Si Substrates ....... 10
1.4.1.4 Deposition of Metal and Si on the Substrates Simultaneously ... 11
1.4.2 Applications of Metal Silicide NWs ........................................... 13
1.5 Introduction of Electron Field Emission ......................................... 15
1.6 Aim of This Thesis ....................................................................... 18
1.7 References ................................................................................... 19

Chapter 2 $Ti_5Si_3$ Nanowire and Its Field Emission Property....................27

2.1 Introduction....................................................................27

2.2 Experimental Section..........................................................28

2.2.1 Materials..................................................................28

2.2.2 Synthesis Procedure.....................................................28

2.2.3 Characterization Instruments.........................................29

2.3 Results and Discussion........................................................30

2.3.1 SEM and EDX Characterizations....................................31

2.3.2 XRD Characterizations.................................................33

2.3.3 TEM Studies..............................................................33

2.3.4 Influence of the Growth Conditions for the Synthesis of NWs..........................................................................36

2.3.5 Proposed Reaction Pathway..........................................37

2.4 Electron Field Emission Property Studies..............................38

2.5 Conclusions.......................................................................40

2.6 References........................................................................41

Chapter 3 Chemical Vapor Deposition of TiSi Nanowires on C54 $TiSi_2$ Thin Film – An Amorphous Titanium Silicide Interlayer Assisted Nanowire Growth..........................................................................44

3.1 Introduction....................................................................44

3.2 Experimental Section..........................................................48

3.2.1 Growth of Titanium Silicide Samples..............................48

3.2.2 Instruments for Characterizations..................................48

3.3 Results and Discussion........................................................49

3.3.1 SEM and EDX Characterizations....................................50

3.3.2 XRD Characterizations.................................................52

3.3.3 TEM Studies of TiSi NWs ....................................................55
3.3.4 Characterization of the Interface between TiSi NWs and C54 $TiSi_2$ Film....................................................57
3.3.5 Growth Pathway of TiSi NWs ....................................................62
3.3.6 Electron Field Emission Properties of Titanium Silicide Samples ....................................................67
3.4 Conclusions....................................................69
3.5 References....................................................70
Chapter 4 Chemical Vapor Deposition of $Ti_xSi_y$ Film and Single Crystalline C49 $TiSi_2$ Nanoplates ....................................................76
4.1 Introduction....................................................76
4.2 Experimental Section....................................................77
4.2.1 Synthesis Procedure....................................................77
4.2.2 Characterization Instrument....................................................77
4.3 Results and Discussion....................................................78
4.3.1 Titanium Silicide Films Grown at Different Temperatures ....................................................79
4.3.2 Titanium Silicide Film Grown at Different Time ..............82
4.3.3 Synthesis of C49 $TiSi_2$ Nanoplates....................................................86
4.3.3.1 Characterization of the C49 $TiSi_2$ Nanoplates .........86
4.3.3.2 Proposed Reaction Pathway of the C49 $TiSi_2$ Nanoplates....................................................88
4.4 Conclusions....................................................91
4.5 References....................................................92
Chapter 5 Conclusions....................................................94
List of Publications ....................................................96

Growth and Characterization of Titanium Silicide Nanostructures

Student: Huang-Kai Lin Advisor: Dr. Hsin-Tien Chiu
Dr. Chi-Young Lee

Institute of Applied Chemistry, National Chiao Tung University

## Abstract

Recently, synthesis of various metal silicide nanowires (NWs) has raised many attentions due to their excellent physical properties. In this work, we demonstrate the synthesis of titanium silicide nanowires, nanoplates, and thin films via a unique chemical vapor deposition process, using $TiCl_4$ and Ti powder as the precursors, without the usage of template and catalysts. Field emission properties, growth mechanism of these titanium silicide samples were also investigated.

Titanium silicide NWs, including single crystalline $Ti_5Si_3$ NWs and crystalline TiSi NWs, were prepared by reacting titanium subchlorides $TiCl_x$ (x = 1-3), generated by the reaction between $TiCl_{4(g)}$ and Ti metal in the high temperature zone at 1173 K initially, and the Si substrates in the lower temperature zone at 723 - 1073 K. The diameters of the nanowires are 20 - 80 nm, and the lengths are several micrometers. The growth directions of the $Ti_5Si_3$ and TiSi NWs are determined to be along the [001] and [010] axes, respectively. An amorphous titanium silicide interlayer was observed between the NWs and the C54-$TiSi_2$ film. This interlayer, probably existed as a quasi-liquid thin film during the growth, appears to be the key factor to assist the NW development.

The C49 $TiSi_2$ nanoplates on Si substrate were obtained at a low $TiCl_4$ vapor pressure condition. The preferred basal plane of the C49-$TiSi_2$ nanoplates was determined to be parallel to the (010) plane. This could be attributed to the anisotropic

crystal structure nature of the C49-$TiSi_2$. The characterization and the growth mechanism of the two-dimensional nanostructure will be discussed below. Comparing with preferred growth direction the titanium silicide NWs, [001] and [010] for $Ti_5Si_3$ NWs and TiSi NWs, respectively. The crystal structure nature takes an important role on the growth of anisotropic nanostructures.

The field emission properties of the titanium silicides samples have been studied. The results show that the field emission performances are highly dependent on the morphology and crystal structures of the NWs and thin films. The high aspect ratio nature of the NWs has improved the performance of field emission properties. The field emission property obtained from $Ti_5Si_3$ and TiSi NWs on C54 -$TiSi_2$ thin film demonstrates low turn-on fields Eo of 5.4 and 5.25 V/μm and high field enhancement factor β of 816 and 876, respectively. These remarkable results suggest that titanium silicide nanoemitters could serve as promising candidates for future field emission devices.

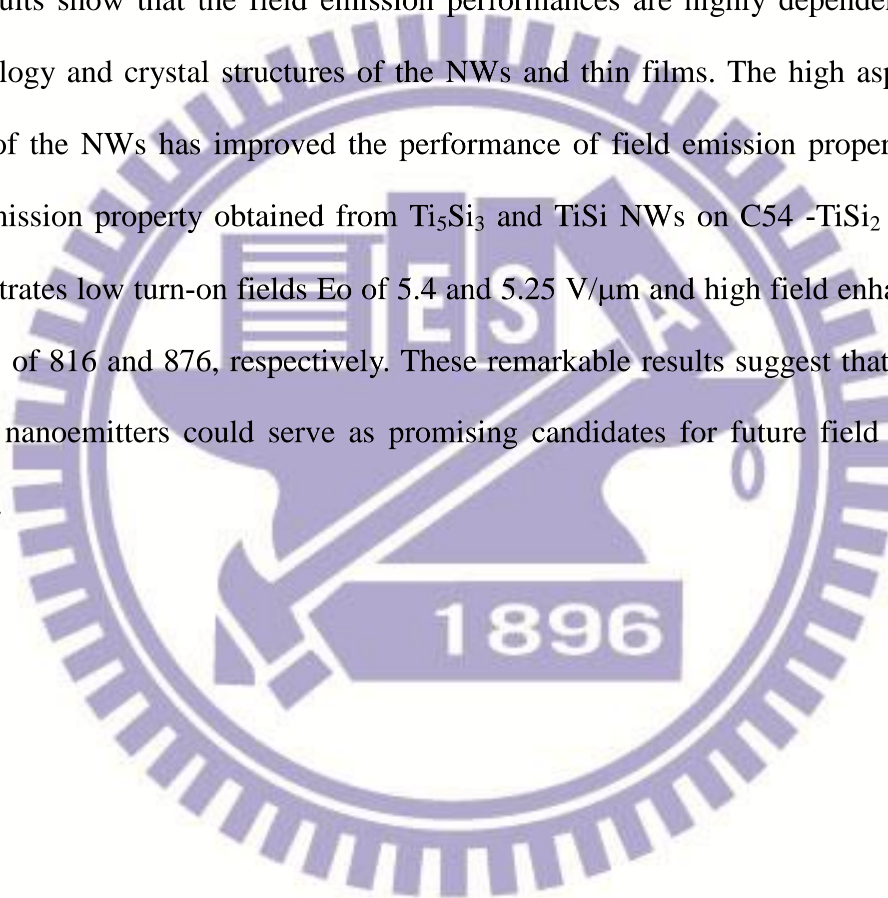

# 矽化鈦奈米結構之成長及其鑑定

研究生：林煌凱　　　　　　　　　　　　　指導教授：裘性天 博士

李紫原 博士

國立交通大學應用化學所

## 摘　要

金屬矽化物奈米線具有低電阻、良好的熱穩定度等優異的特性。近年來，製備各種金屬矽化物奈米線成為重要的研究議題。本研究中我們提出利用化學氣相沉積法以四氯化鈦與鈦金屬為反應前驅物，並且在不使用模版或金屬催化劑的條件下成長矽化鈦奈米線、二維奈米片狀產物及薄膜。此外本研究也對矽化鈦奈米材料的成長機制以及電子場發射性質作了詳細的探討。

首先，我們利用在 1173 K 由四氯化鈦與鈦金屬生成的 $TiCl_x$ (x=1-3)與在低溫區 (723 – 1073 K) 的矽基材反應後可以得到各種矽化鈦奈米線。本研究中所得矽化鈦奈米線具有兩種不同的結晶型態，分別為三矽化五鈦($Ti_5Si_3$)以及矽化鈦(TiSi)。矽化鈦奈米線的直徑分布大約為 20 – 80 奈米，線長可長達數個微米。$Ti_5Si_3$ 及 TiSi 奈米線的成長方向經過鑑定分別為[001]以及[010]方向。在奈米線以及其下方的矽化鈦薄膜之間可以觀察到一層非晶相矽化鈦薄膜，此半液相薄膜在奈米線的成長裡扮演了相當重要的角色。

利用相同的反應，在 $TiCl_4$ 前驅物的蒸氣壓於相對低的條件下，可以得到 C49 二矽化鈦二維奈米結構。經過分析，此二維結構傾向展露出(010)晶面，此一特性源自 C49 二矽化鈦本身的層狀晶體結構。由此二矽化鈦二維奈米結構及前述奈米線的結果可知本論文中提及奈米結構的非等向性成長與材料本身的晶體結構排列有相當大的關聯。

經由探討矽化鈦樣品的電子場發射性質，顯示出樣品的形貌及結晶性與其場

發射特性具相當的關聯性。可知矽化鈦奈米線具有很高長寬比使得其場發射特性具有很好的表現。結果顯示 $Ti_5Si_3$ 與 TiSi 奈米線具有很低的起始電場 Eo 分別為 5.4 與 5.25 V/㎛，以及優異的場增強因子β 可達到 816 與 876。從研究結果顯示矽化鈦奈米線在未來的場發射元件上具有相當大的潛力。

# Acknowledgments

終於，也到了這一天，我要離開待了九年半的交大。當初懵懂的大一新生已經要拿到博士學位。回想這些日子所遇到的人、發生的事，心中充滿了滿滿的溫暖與感動。感謝這一路上給我支持、陪伴、幫助與鼓勵的每一個人。陪我一起渡過這些辛苦忙碌卻又充實豐富的日子，並且順利地完成這本論文。

心中要感謝的人真的很多，首先感謝我的指導老師—裘性天老師以及李紫原老師。我很幸運能夠有兩位指導老師，不論是學術研究、待人處世我從兩位老師身上分別學到了很多。

從大一的普化課開始就感受到裘老師的風趣與幽默。大三的無機化學課更讓學生訂下了日後研究的方向。進入實驗室後，老師以淵博的學識與無限的創意，不斷的給予我深入的指導。裘老師給予我架設場發射機台以及出國參加研討會的機會，這些經驗大大地開拓了學生的視野。在生活上，老師自由、親民的作風讓我的研究生涯不那麼枯燥乏味，與老師的午餐約會總是羨煞其他的老師與學生們，也讓學生學到了許多待人處世的道理。

由於實驗有很多部分在清大完成，再加上論文的主軸—矽化鈦的合成是接續李老師之前的研究，與李老師的互動比其他交大的夥伴多了很多。很感謝老師一直以來在實驗上細心與耐心的指導。此外，老師的愛心也讓學生感到十分敬佩，老師兼具科技與人文氣質的風範更是學生學習的榜樣。真的非常感謝兩位老師一路來的指導、照顧以及包容，這份恩情，學生會永遠銘記在心。

在此，也感謝論文口試委員陳登銘教授、李積琛教授、周立人教授、黃暄益教授與吉凱明教授對此論文的批評與指導，使學生的論文更加完善。此外也特別感謝李積琛老師在晶體結構與成長上的建議以及周立人老師在電子顯微鏡上的支援。謝謝每一位老師的用心指導以及鼓勵。

感謝交大實驗室裡的每一位同伴，張裕煦學長對實驗認真嚴謹，對人風趣幽

默的態度一直是我的模範。此外簡俊雄學長、王隆昇學長、Baken、黃志豪、小黑與彭治偉學長在實驗上提供了很多的協助。亭凱、進興、高翔、宇婕、Sif、嘉芳、Goby、昕君、大支、季勳、馨緯、最美麗的媽咪佳兒學姐、不需多說老室友蕭蕭、搞笑又負責的昱良、可愛的亦諄、貼心又善良的Wei Wei、悶騷的大銘、帥氣的文志、有氣質的佑蕙、美食專家與籃球高手心安、手藝高超的 Kimi、康樂股長奕廷、善良的小栗、人很好的凱捷、認真又細心的小童與鄒宗育。很高興能夠與你們在同一個實驗室，讓我的研究生活多采多姿，也謝謝還在實驗室的大家陪我渡過最後這一段日子。

清大實驗室裡的老人們鈺芬、正得、旻橋、奕仁以及聰盈。還記得當初大家在材料中心一起奮鬥的光景，如今大家都已各奔前程。很感謝有你們的幫助與經驗的分享，讓我成長了許多。弘麒、名輝、彥百、鑑嘉、博欽、婷婷與久萱也謝謝你們陪我度過了很多充滿歡笑與汗水的時光。

此外，清大TEM的余宜真小姐，清大ESCA蔡靜雯小姐、交大SEM陳悅婷小姐、陳聯珠小姐以及吳艾軒小姐，謝謝你們的幫助讓我能得到高品質的實驗數據。

謝謝Sunny這九年半來一直陪在我的身邊，鼓勵我、支持我。很高興能夠與你分享生活中的所有喜怒哀樂，是你給我力量讓我能夠克服所有的艱難，此生有你是我最幸福的事。最後要感謝我的父母與姊姊這些年來默默的支持，你們的付出與栽培讓我能無後顧之憂地往目標邁進，順利完成學業。謝謝你們。

# List of Tables

Chapter 1

Table 1.1 Physical properties of some common used metal silicides.........3

Table 1.2 Crystal parameters and physical properties of the titanium silicides. ........................................................................................4

Chapter 2

Table 2.1 Summary of Samples ..............................................................31

Chapter 3

Table 3.1 Summary of Titanium Silicide Samples ...................................47

Table 3.2 Assignments of the XRD Peaks in Figure 3.4 ..........................54

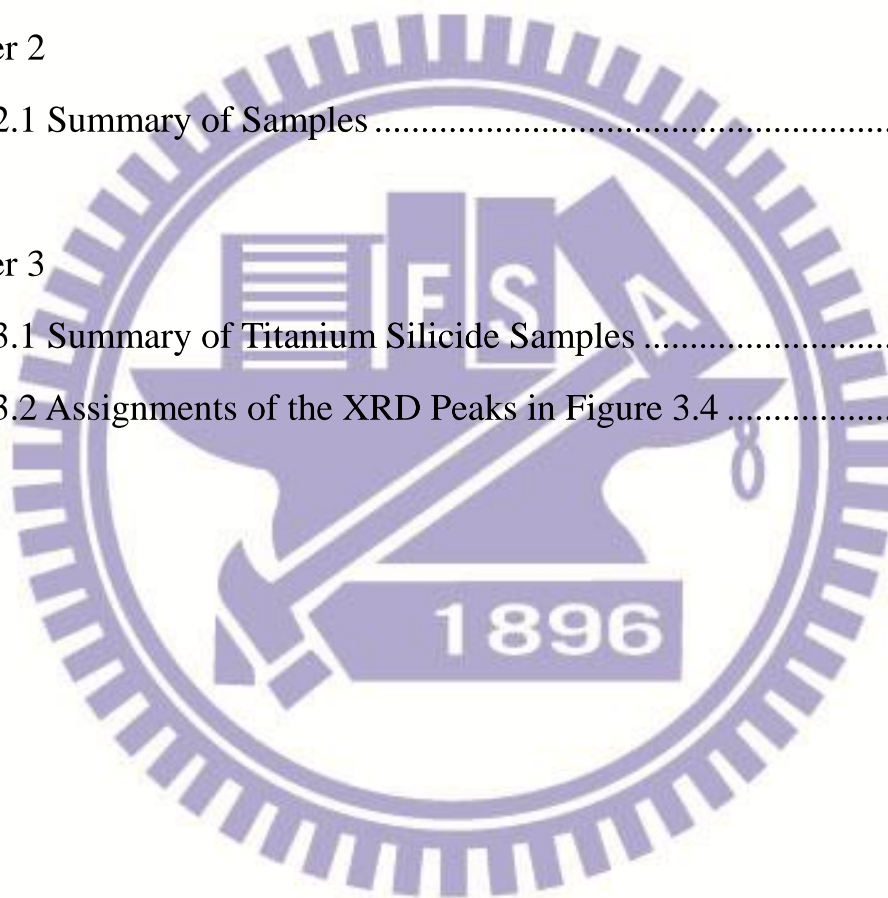

# List of Figures

**Chapter 1**

**Figure 1.1** Binary phase diagram for Ti-Si system. ..................................3

**Figure 1.2** Crystal structures of the titanium silicides. (a) ab projection and side view for $Ti_5Si_3$ crystal structure, (b) bc projection for TiSi crystal structure, (c) ab projection for C54 $TiSi_2$..................................................6

**Figure 1.3** (a) Schematic diagram for silicide NWs synthesized by Chemical vapor transport (CVT), (b) Synthesis of silicide NWs through single source precursor chemical vapor deposition (CVD)......................12

**Figure 1.4** Energy diagram of metal-vacuum level (a) without electric field, (b) under high electric field. ..........................................................15

**Chapter 2**

**Figure 2.1** Experimental setup of the CVD system. ................................29

**Figure 2.2** Setup of the home-built electron field emission (EFE) system. .............................................................................................................30

**Figure 2.3** SEM images of sample I grown on Si. (a) Top view, (b) high magnification image, (c) EDX, and (d) side view image. ........................32

**Figure 2.4** SEM images of II (a), (b) and III (c), (d) grown on Si. ..........32

**Figure 2.5** XRD patterns of samples I, II, and III. ..................................33

**Figure 2.6** TEM studies of a NW isolated from I. (a) Low magnification

image, (b) SAED pattern of the sample in (a) showing a [1-10] zone axis, (c) high-resolution image from the selected section in (a). ......................34

**Figure 2.7** Auger depth profile of I. ......................................................35

**Figure 2.8** (a) TEM image of NW isolate from sample II, (b) SAED pattern showing that the NW is amorphous, (c) EDX of the selected area in (a) indicates that the composition of the NW are Ti and Si. The NWs in II could be designated as *a*-$Ti_xSi_y$ NWs................................................35

**Figure 2.9** SEM images of samples grown at similar condition but different precursors with sample I. (a) without the Ti metal, (b) without the $TiCl_4$. ......................................................................................36

**Figure 2.10** Proposed Growth Steps of $Ti_5Si_3$ NWs. ..............................38

**Figure 2.11** Electron field emission current density as a function of applied electric field of samples I – III. Inset shows their corresponding Fowler-Nordheim plots.......................................................................39

**Chapter 3**

**Figure 3.1** SEM images of I grown on Si. (a) Top-view and EDX (inset), (b) high magnification image, (c) low magnification side-view, and (d) high magnification side-view image......................................................50

**Figure 3.2** SEM top-view and side-view (inset) of (a) II, (b) III, (c) IV, and (d) V.......................................................................................52

**Figure 3.3** XRD patterns of I - V. Assignment of peaks: spheres, C54-$TiSi_2$; square: TiSi (020); diamond: $Ti_5Si_3$ (002); triangle: Si (020), this forbidden signal only appears in several samples grown on a specific batch of Si substrates. For clarity, Si (400) at 69.2$^o$ is not shown. ...........53

**Figure 3.4** (a) Detailed XRD of I from 25$^o$ to 38$^o$, (b) XRD of I from 20$^o$ to 80$^o$ (spheres, C54-$TiSi_2$; square: TiSi; triangles: Si), and (c) XRD of the Si wafer used to grow silicides in samples I – III. 33.2$^o$: Si (200), 56.5$^o$: Si (311), 69.5$^o$: Si (400), 61.7$^o$ and 65.9$^o$: unable to assign. ....................54

**Figure 3.5** (a) TEM image of a NW isolated from I, (b) SAED pattern and (c) HRTEM image from the circled region in (a), and (d) TEM and EDX elemental line profiles of another NW from I. ...............................56

**Figure 3.6** (a) TEM image of a NW isolated from I, (b) high magnification image from (a), (c) SAED pattern from the circled region in (a), and (d) HRTEM image of the squared area in (b). ........................56

**Figure 3.7** (a) SEM side-view of I showing an interlayer between TiSi NWs and a $TiSi_2$ film, (b) enlarged view of (a), (c) SEM side-view of IV showing a $TiSi_2$ thin film, and (d) enlarged view of the rectangular region in (c). ........................................................................................57

**Figure 3.8** SEM EDX analyses of (a) I and (b) V. Chemical compositions of the circled areas are listed below. .......................................................58

**Figure 3.9** Cross-sectional SEM EDX line-scans of (a) I and (b) V. The

arrows mark the limits of the interlayers. ...............................................59

**Figure 3.10** (a) Low-magnification cross-sectional TEM image of I showing the presence of NWs on top of a thin film and (b) high-magnification image of the dashed rectangular area in (a). .............59

**Figure 3.11** (a) Low-magnification cross-sectional TEM image of I showing the presence of NWs on top of a thin film and (b) high-magnification image of the dashed rectangular area in (a). .............60

**Figure 3.12** (a) Cross-sectional TEM image of the interface in I, (b) HRTEM image and (c) SAED pattern from the solid square region in (a). EDX spectra from (d) the solid and (e) the dotted circled areas in (a). The Cu signal is from the Cu TEM grid. .......................................................61

**Figure 3.13** HRTEM images of the selected crystallites shown in Figure 3.11d. Possible crystal plane assignments are designated in the images. .62

**Figure 3.14** Proposed growth pathway of the TiSi NWs. (x denotes variables). ...........................................................................................63

**Figure 3.15** Crystal models of orthorhombic TiSi viewing along (a) *a*, (b) *b*, and (c) *c* axes. The short Si-Si bonds (0.2171 nm) are linked in yellow sticks. Orthorhombic TiSi (JCPDS 17-0424, ICSD 43494): space group P*nma* (no. 62), *a* = 0.6544 nm, *b* = 0.3638 nm, ***c*** = 0.4997 nm. ..............66

**Figure 3.16** Crystal models of hexagonal $Ti_5Si_3$ viewing along (a) *a* and (b) *c* axes. Viewing along *b* axis is equivalent to viewing along *a* axis. The short Ti-Ti bonds (0.25754 nm) are linked in yellow sticks. Hexagonal $Ti_5Si_3$ (JCPDS 78-1429, ICSD 62591): space group $P6_3$/mcm (no. 193), $a$ = 0.7610 nm, $c$ = 0.51508 nm. ............................................66

**Figure 3.17** EFE current density as a function of applied electric field of samples I, and III–V. Inset shows their corresponding Fowler-Nordheim plots. ........................................................................................68

**Chapter 4**

**Figure 4.1** Top-view and side-view SEM images of samples grown at different reaction temperatures for 60 min. (a)-(b) 723 K (I), (c)-(d) 773 K (II), (e)-(f) 873 K (III), (g)-(h) 973 K (IV), and (i)-(j) 1023 K (V). .....80

**Figure 4.2** High-resolution XPS spectra of the film grown at 973 K for 60 min. (a) Ti 2p1/2 and Ti 2p3/2 electrons and (b) Si 2P electron..........81

**Figure 4.3** XRD patterns of samples prepared at different temperatures for 60 min (I-V). ............................................................................82

**Figure 4.4** ........................................................................................84

**Figure 4.5** XRD patterns of samples synthesized at 973 K for different time. ........................................................................................85

**Figure 4.6** Characterization of sample **IX**, grown on Si wafer at 973 K for 30 min as the $TiCl_4$ was immersed in an ice bath. SEM studies: (a)

low magnification image, and EDX spectrum (inset), (b) high magnification image of the nanoplates, (c) enlarged-view of the nanoplats, and (d) XRD pattern. ........................................................................87

**Figure 4.7** TEM studies of sample **IX**. (a) Low-magnification TEM image, (b) EDX spectrum, (c) SAED, and (d) HRTEM image were obtained at the square area in (a). ............................................................88

**Figure 4.8** Crystal models of orthorhombic C49-$TiSi_2$ viewing along (a) *a*, (b) *a*, (c) *b*, and (d) *c* axes. The short Si-Si bonds (0.232 nm) are linked in yellow sticks in (a). The Si-Si and Ti-Si, with the shortest distance, are linked in yellow sticks for clarity in (b)-(d). Orthorhombic C49-$TiSi_2$ (JCPDS 10-0225): space group C*mcm* (no. 63), *a* = 0.362 nm, *b* = 1.376 nm, *c* = 0.3605 nm. ........................................................................90

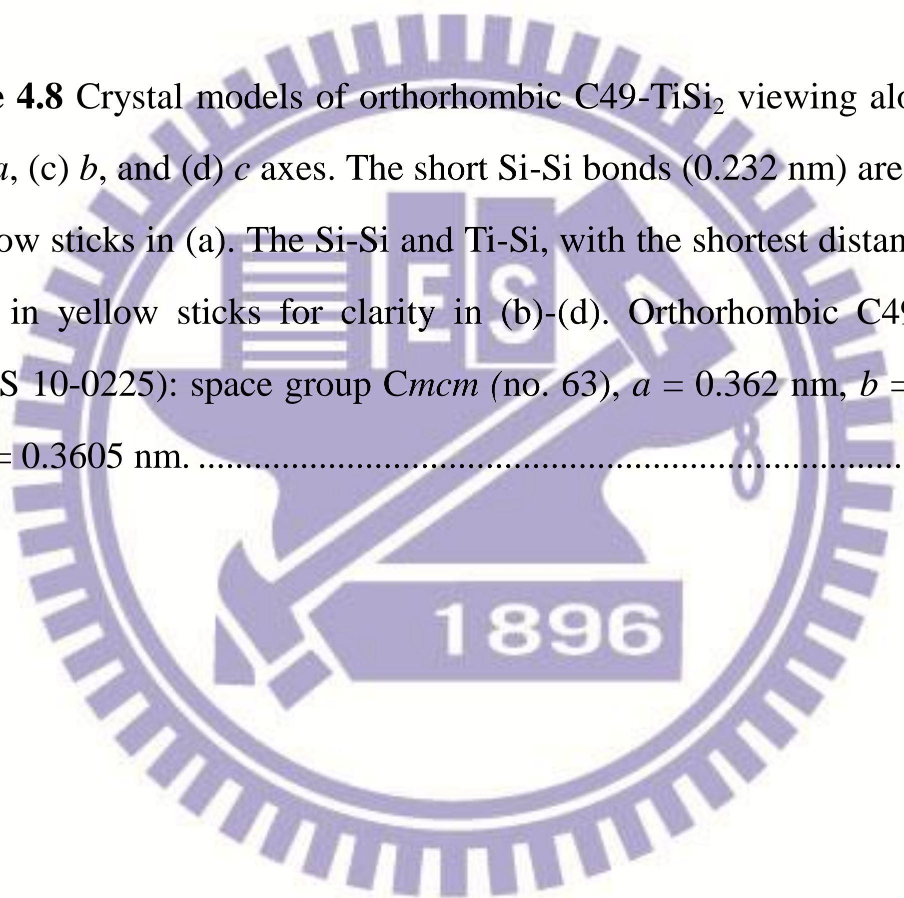

# Chapter 1

# Introduction

## 1.1 Introduction

Transition metal silicides, intermetallic compounds between metals and silicon, show unique and various physical and chemical properties that are important in both scientific and engineering aspect, especially for Si based integrated circuit devices.[1-4] Among the most studied silicides, such as silicides of Ti, Cr, Fe, Co, and Ni, titanium silicides show high thermal stability, low electrical resistivity, low work function, and low density.[3,5,6] Thus, many efforts have been devoted to the researches about the application of titanium silicides.

Novel physical and chemical properties are often obtained when dimensions of the materials are reduced to nanoscale. One-dimensional nanomaterials have attracted tremendous amounts of attention for technological applications, such as sensors,[7] laser devices,[8] and electrical systems.[9] An increasing effort has been devoted to fabricating nanomaterials for new field emitters, such as CNTs (carbon nanotubes),[10] nano-diamond coated Si nanowires (NWs),[11] SiC NWs and nanotubes,[12,13] metal oxides[14] and metal silicides. Recently, many studies about the fabrication of free standing silicide nanowires of Ti,[15-24] V,[25] Cr,[26-29] Mn,[30,31] Fe,[32-35] Co,[36-42] Ni,[43-58] Ta,[59-61] and Pt[62-65] have been reported because of their superior properties and compatibility with Si based integrated circuit devices. Among them, titanium silicides are potential candidates for building blocks for nanoelectronics and field emission devices due to their relative low resistivity (10 – 60 μΩ cm), high thermal stability, and low work function.[3,5,6] For titanium silicide NWs, the fabrication of $TiSi_2$

NWs,[15,20,24] TiSi nanopins,[16,17] and $Ti_5Si_4$ nanobats[21] through various processing techniques, including chemical vapor deposition (CVD) and physical vapor deposition (PVD), have been demonstrated recently.

In this dissertation, we will reveal the growth of different kind of titanium silicdes samples, including $Ti_5Si_3$ NWs, TiSi NWs, C49-$TiSi_2$ nanoplates and titanium silicides thin films (C49-$TiSi_2$ and C54-$TiSi_2$) via a unique CVD process.[66] Microstructures, growth mechanism and and field emission properties of the titanium silicdes NWs and thin films will be discussed in detail.

## 1.2 Metal Silcide

Metal silicides have attracted attention because their superior properties, such as low and metal-like resistivities (μΩcm – mΩcm) and high thermal stability, which could meet the requirements for modern Si-based electronic devices.[3] The most studied silicdes are $NiSi_2$, $CoSi_2$, $TiSi_2$, and $FeSi_2$. $NiSi_2$ has the best lattice mach to silicon, $CoSi_2$ and $TiSi_2$ possessed low resistivities and often used in the electronics devices. $FeSi_2$ is a direct energy gap semiconductor with a small gap of 0.87 eV. The physical properties of the most used metal silicides are listed in Table 1.1. The applications of metal silcides are summarized as below: (1) diffusion barrier,[67-69] (2) ohmic contact and interconnect,[70,71] (3) Schottky diode,[71] (4) polycide gate,[72,73] (5) multilevel metallization,[74,75] (6) shallow silicide contact,[69] (7) epitaxial silicides,[76-78] (8) thermoelectric material,[79,80] and (9) photovoltaic application.[81] Besides, for many metal silicides, varying the synthesis conditions could alter the metal to silicon composition ratio and the crystal phase. Consequently, properties of the silicides are changed as well. Thus, it is possible to prepare silicide samples with diverse properties within one reaction system.

**Table 1.1** Physical properties of some common used metal silicides.[3]

| Silicides | Space group | M.P. (K) | Resistivity (μΩcm) | Density (g/cm$^3$) | Microhard-ness (GPa) |
|---|---|---|---|---|---|
| $TiSi_2$ (C54) | Fddd Orthorhombic | 1773 | 10-20 | 4.07 | 7.7-8.9 |
| $FeSi_2$ | $P_4$/mmm Tetragonal | 1493 | Semicon-ductor | 4.99 | 10-13 |
| $CoSi_2$ | $P2_13$/mmm Cubic | 1599 | 15 | 4.9-6.65 | 0.77-9 |
| $NiSi_2$ | Fm3m Cubic | 1266 | 10-35 | 4.8 | 2-15 |
| $CrSi_2$ | $P6_222$ Hexagonal | 763 | Semicon-ductor | 4.98 | 11.3 |

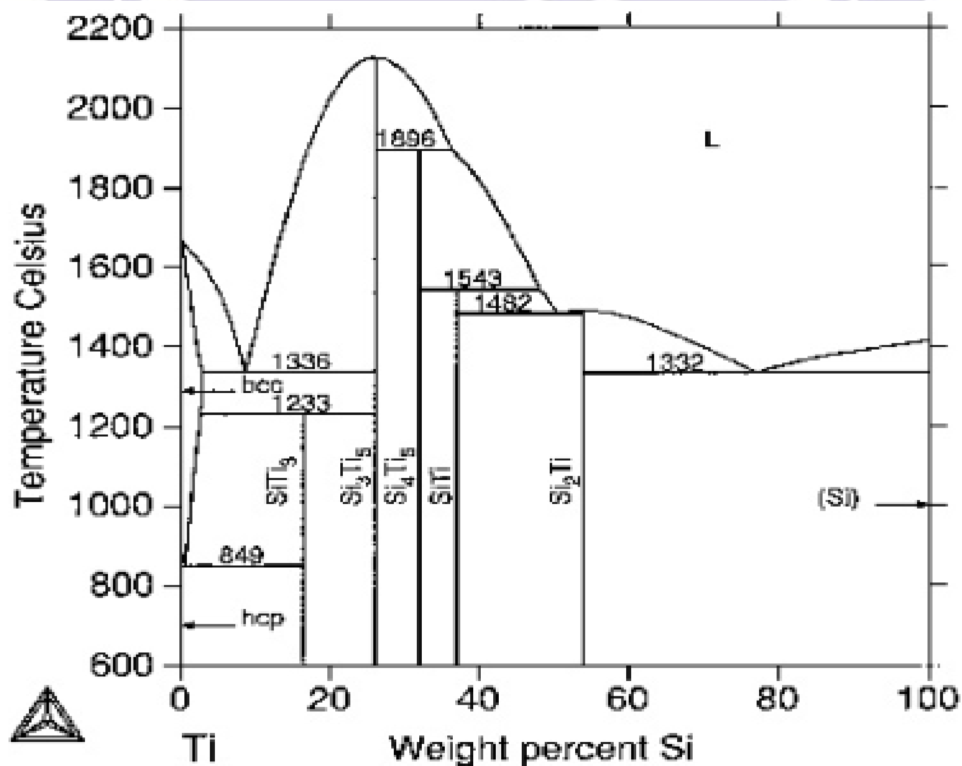


**Figure 1.1** Binary phase diagram for Ti-Si system.[82]

# 1.3 Titanium Silcide

Among the most studied silicdes, titanium silicides show higher melting points low electrical resistivities, and lower density, which made them good candidates for electronics technology. According to binary phase diagram of the Ti-Si system, shown in Figure 1.1, several titanium silicides with different compositions, such as $Ti_3Si$, $Ti_5Si_3$, $Ti_5Si_4$, TiSi and $TiSi_2$, could exist in the Ti-Si system.[82] Besides, there are two crystal polytypes of $TiSi_2$, one is the metastable C49 phase and the other is C54 phase. The crystal parameters and physical properties of those titanium silicides are summarized in Table 1.2.[3]

**Table 1.2** Crystal parameters and physical properties of the titanium silicides.[3]

| Silicides | Space group | Lattice constants (Å) | | | M.P. (K) | Microhardness (GPa) |
|---|---|---|---|---|---|---|
| | | a | b | c | | |
| **$Ti_3Si$** | $P4_2/n$ Tetragonal | **10.39** | | **5.17** | **1443** | |
| **$Ti_5Si_3$** | $P6_3/mcm$ Hexagonal | **7.46** | | **5.15** | **2403** | 9.8 |
| **$Ti_5Si_4$** | $P4_12_12$ Tetragonal | **6.71** | | **12.17** | **2193** | |
| **TiSi** | Pnma Orthorhombic | **6.54** | **3.63** | **4.99** | **1843** | 10 – 18 |
| **$TiSi_2$ (C49)** | Cmcm Orthorhombic | **3.62** | **13.76** | **3.60** | **1773** | - |
| **$TiSi_2$ (C54)** | Fddd Orthorhombic | **8.26** | **8.55** | **4.79** | **1773** | 7 – 8 |

## 1.3.1 Structure and Properties of Titanium Silicide

The structure parameters and some physical properties of titanium silicides are summarized in Table 1.2. The structures of $Ti_5Si_3$, TiSi and C54-$TiSi_2$, which were obtained in this work, are illustrated as below.[83] Figure 1.2 shows the projection of the

crystal structures for the titanium silicides. The bigger circles denote Ti atoms and the smaller ones are Si atoms. The shading of the circle indicates the height above the projection plane. From white to black represent 0, 1/4, 1/2, and 3/4 of the lattice vector normal to the plane. $Ti_5Si_3$ possesses a hexagonal structure ($Mn_5Si_3$ type) with space group of $P6_3/mcm$ and lattice constants of $a$ = 7.4610 Å and $c$ = 5.1508 Å. Figure 1.2a shows the *ab* projection and side view for $Ti_5Si_3$. There are two independent crystallographic sites of Ti atoms in the $Ti_5Si_3$. These correspond to the white and dark gray (1) and the black and light gray (2) circles. $Ti_1$ has two $Ti_1$ first neighbors, six Si second neighbors, and six $Ti_2$ third neighbors. $Ti_2$ has two Si first neighbors, three Si second neighbors, two $Ti_2$ third neighbors, four $Ti_2$ fourth neighbors, and four $Ti_1$ fifth neighbors. Si has two $Ti_2$ frist neighbors, four $Ti_1$ second neighbors, three $Ti_2$ third neighbors, and four Si fourth neighbors. Figure 1.2b displays the orthorhombic TiSi structure with space group of Pnma. The lattice constants are $a$ = 6.54 Å, $b$ = 3.63 Å, and $c$ = 4.99 Å. Each Ti atom has seven Si atoms in the range of 4.92 – 5.15 Å and six Ti atoms at 6.06 Å The Si atoms have two nearest Si atoms and eight neighboring Ti atoms. Figure 1.2c demonstrates the ab projection for C54 $TiSi_2$. The structure is face-centered orthorhombic with space group of Fddd. The lattice lattice constants are 8.26 Å, 8.55 Å, and 4.79 Å for *a*, *b*, and *c*, respectively. The layer structure is an ABCD stacking of equivalent planes. Ti has four Si first neighbors, four Si second neighbors, two Si third neighbors, and four Ti fourth neighbors. Si has two Si first neighbors and two Ti second neighbors. $Ti_5Si_3$ has the highest melting point of 2403 K in the titanium silicides. On the other hand, C54-$TiSi_2$ has the lowest electrical resistance and is most used in electric device. In the aspect of integrated circuit, $TiSi_2$ possessed some attractive properties: (1) low resistivity (10 – 20 μmcm), (2) resist of oxidization, (3) better depression of hot electron than poly-Si made gate devices.

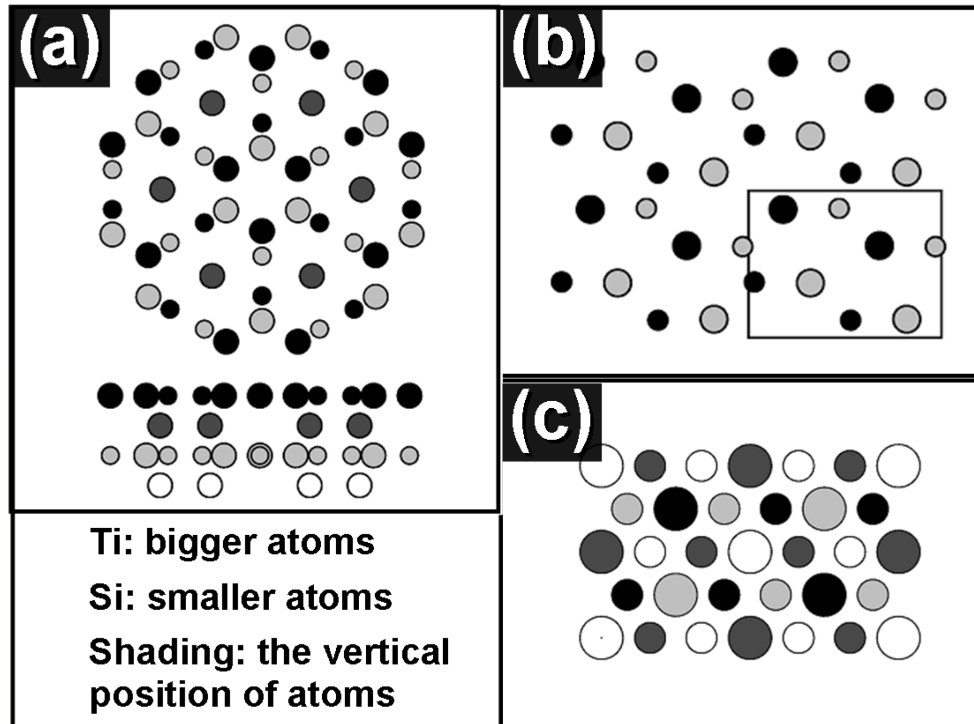


**Figure 1.2** Crystal structures of the titanium silicides.[83] (a) ab projection and side view for $Ti_5Si_3$ crystal structure, (b) bc projection for TiSi crystal structure, (c) ab projection for C54 $TiSi_2$.

## 1.3.2 Synthesis of Titanium Silicide

In order to apply titanium silicide to gate metallization, device interconnection, or Schottky diode, synthesis of thin film titanium silicides are required. There are three common used methods to fabricate titanium silicides thin films. First is the evaporation,[84] second is sputtering,[85] the last is chemical vapor deposition (CVD).[86] The Both evaporation and sputtering are physical methods. These two methods require two experimental steps, first is deposition of Ti or codeposition of Ti and Si on Si substrate. After that, the samples were annealed at high temperature to form silicides. In general Ti/Si thin film system, a thin layer of amorphous $Ti_xSi_y$ will be formed between Ti/Si interfaces after deposition at room temperature.[87] After annealing at around 673 K, the amorphous layer becomes thicker.[88] At higher temperatures, $Ti_5Si_3$, $Ti_5Si_4$, TiSi and C49-$TiSi_2$ along with amorphous $Ti_xSi_y$ layer are

formed. When the temperature was rised to 973-1073 K, C54-$TiSi_2$ will be the only existing phase.[87] Unfortunately, the annealing procedure usually damages the electronic devices. In the CVD method, by reaction between metal halides ($TiCl_4$, $WF_6$, etc) with silane or silicon chlorides, the reaction temperature could be lower and the annealing process is no longer necessary. Some examples of synthesis of titanium silicide thin film are shown below;[89-91]

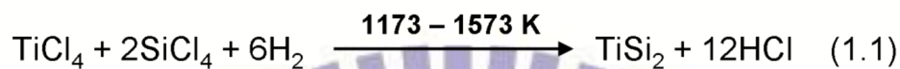

$$TiCl_4 + 2SiCl_4 + 6H_2 \xrightarrow{1173-1573\ K} TiSi_2 + 12HCl \quad (1.1)$$

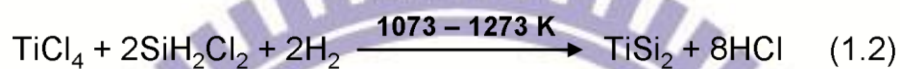

$$TiCl_4 + 2SiH_2Cl_2 + 2H_2 \xrightarrow{1073-1273\ K} TiSi_2 + 8HCl \quad (1.2)$$

$$TiCl_4 + 6SiH_4 \xrightarrow{873-1073\ K} TiSi_2 + 4SiH_3Cl + 6H_2 \quad (1.3)$$

As a consequence, CVD seems to be proper method to synthesis titanium silicides. However, the reactions required some explosive materials, such as $SiH_4$ and $H_2$. A unique CVD of titanium silicides was invented by Lee in 1999.[66] The reaction pathway is proposed to the reaction between the in situ generated $TiCl_x$(x=1-3), through reaction between $TiCl_4$ and Ti metal, and the Si substrate. This method provides a safe and easy way to synthesis titanium silicide.

## 1.4 Metal Silicide Nanowires

One-dimensional nanomaterials, such as wires, rods, belts, and tubes have demonstrated to possess distinct properties from their bulk materials. Furthermore, with the advancement in electronic technology, the dimensions of the electronics devices continue to scale down. Therefore, fabrications of metal silicide nanomaterials have turned into essential research topics. Most silicide compounds have multiple stoichiometries and complex phase behavior, rational and universal

chemical synthesis of silicide nanostructures can be quite difficult. Recently, growth of variety of silicide nanowires has been reported. These NWs could be grouped into two types: One is the epitaxial grown silicide NWs, which were lying on thy Si substrates. The other is the free standing silicide NWs, which is easier to be applied on electronic devices. The self-assembly epitaxial of rare-earth silicide NWs on Si was first shown by Preinesberger *et al*.[92,93] A sub-monolayer coverage of Dy on Si (001) results in the formation of nanowires under certain condition. Similar results were then discovered for Er,[94] Ho,[95] Sc, and Gd[96] silicides. The growth of the NWs is originated from the anisotropic lattice mismatch that is small in the long direction and large in the short direction. Epitaxial metal silicides NWs have also been observed in another system, such as Co/Si,[97] Fe/Si,[98] and Ti/Si,[99] which shown the "endotaxial' growth mechanism. The endotaxial mechanism does not require anisotropic lattice mismatch; it allows for a variety of metal and substrates and it allows tuning of the NW aspect ration via the growth temperature.

From the practical aspect, freestanding silicides NWs possess great potential than the epitaxial ones. More recently, several techniques have been used to synthesize free-standing silicide NWs, and could be classified into four groups: silicidation of Si NWs or Metal NWs, deposition of Si source on metal films, reaction between metal vapor sources and Si substrates, and deposition of metal and Si on the substrate simultaneously. In addition, the application of the free-standing silicide NWs will be reviewed below.

## 1.4.1 Synthetic Methods of Metal Silicide NWs

### 1.4.1.1 Silicidation of Si or Metal NWs

First technique involves taking Si NWs or metal NWs as templates and then reacting with their complementary elements, such as metal for Si NW and Si for metal NW. Through this concept, single crystalline $Pt_6Si_5$ NWs were fabricated through reaction between polycrystalline Pt NWs, synthesized using anodic aluminum oxide (AAO) templates by electrochemical deposition, and $SiCl_4/H_2$. And this is the first report of transition metal silicide NWs.[62] However, the reason for the transformation of polycrystalline Pt NWs into single crystalline $Pt_6Si_5$ NWs is under investigation. Other researches have shown fabrication of silicide NWs by evaporating metal, such onto the Si NWs template, synthesized through typical Au nanoparticle-assist VLS process. After annealing, metal silicide NWs were produced through solid state reaction. NiSi NWs was first prepared and reported by Lieber *et al*. In addition, epitaxial hetero junctions of NiSi/Si NWs were obtained and the NWs based field-effect transistors were also demonstrated.[44] Similar methods were applied to synthesize $FeSi_x$ NWs[34] and PtSi NWs.[34,63] Lately, in-situ high-resolution transmission electron microscopy (HRTEM) have exhibited powerful ability to study the kinetics of silicidation process. Si/silicide NW heterostructures were prepared by in situ annealing for point contact reaction between Si NWs and transition metal NWs, Ni[50] or Co,[38] in an in-situ TEM. Si NWs were fabricated through Au nanocatalyst VLS method, while metal NWs were prepared via electroplating deposition Ni or Co into AAO template. The results showed distinct diffusion behavior. Despite the low throughput as a synthetic technique, silicidation of single Si NW is a powerful method to study the silicidation process and may reveal the growth mechanism of other metal silicide NWs.

### 1.4.1.2 Deposition of Si Sources on Metal Films

Vapor-phase synthetic routes between metal vapor phase and Si thin film or Si vapor deposition on metal thin films and to spontaneously form various single crystalline metal silicides NWs. These synthetic methods are simple and become popular methods to fabricate silicide NWs. In addition, they are commonly obtained without the presence of the catalytic metal nanoparticles on the NWs. The first reported silicide NWs through vapor-phase reaction between Si vapor source and metal thin film was $NiSi_2$ NWs, which was demonstrated by Solanki *et al.* in 2004.[43] The $NiSi_2$ NWs was obtained by reaction between the $SiH_4$ and the Ni thin fiim. Several $NiSi_x$ NWs with different crystal phases ($NiSi_2$,[45] NiSi,[46,48,54] $Ni_2Si$,[45,54,57] $Ni_3Si_2$,[49] $Ni_{31}Si_{12}$,[56] and $Ni_3Si$[55]) were also reported recently. The growth mechanisms of most of the $NiSi_x$ NWs are seldom discussed. Taking $Ni_2Si$ NWs for example, $SiH_4$ decomposes and deposits on the Ni film to grow $Ni_2Si$ nanocrystals. As the reaction progress, elongation of the nanocrystals shrinks the sites on the surface for Ni diffusion. After the Ni incorporation rate matches the Si deposition, $Ni_2Si$ NWs are formed.[57] On the other hand, $NiO_x$ layer, serving as a diffusion barrier for Ni, was also regarded as an important key to the $NiSi_x$ NWs growth and was reported by Jo *et al*. Except $NiSi_x$ NWs, $Ti_5Si_4$ nanobats were fabricated on Ti foil via a vapor and condensation method with Si powder keeping at high temperature zone of 1373 K and Ti foil at low temperature zone of 1173 K.[21]

### 1.4.1.3 Reaction between Metal Vapor Sources and Si Substrates

Recently, some free-standing metal silicide NWs were fabricated by reacting pure metal vapors or anhydrous metal halides with Si substrates directly. $TaSi_2$ NWs were prepared through annealing samples composed with $FeSi_2$ thin film or $FeSi_2$ nanodots on the top of Si substrates in a Ta atmosphere.[59,60] Ta atom was deposited

and reacted with the Si atom, segregated from the $FeSi_x$ part, to form $TaSi_2$ nanocrystals. Under proper condition, certain facets shown preferred growth and one-dimensional nanostructure was observed. $TiSi_2$ NWs were first synthesized by a vapor deposition of Ti vapor onto the Si substrate in 2005.[15] Anhydrous metal halides were commonly used as the transition metal sources to react with Si substrate to grow silicide NWs. For example, $FeCl_3$ was vaporized at about 473 K and reacted with the Si substrate at 1373 K to form FeSi NWs.[32] Through this simple concept, NWs of $TiSi_2$,[20] TiSi,[22] $Ti_5Si_3$,[18] $CrSi_2$,[26,29] FeSi,[32] $Fe_5Si_3$,[35] CoSi,[37,42] $Co_2Si$,[37,42] and $Fe_{11-x}Co_xSi$[39] were fabricated. To date, no convincing mechanism has been porposed. Vopor-solid (VS) mechanism is usually employied to explain the NW growth, since the supersaturation condition of the metal halides shows great influence on the morphology and crystal phase of the NWs.

#### 1.4.1.4 Deposition of Metal and Si on the Substrates Simultaneously

Two techniques have been developed by transporting Si and metal sources to the substrate simultaneously to produce silicide NWs: one is chemical vapor transport (CVT), another is chemical vapor deposition (CVD) method. CVT method is a conventional solid-state crystal growth technique used to grow single crystals. The concept of CVT is exploiting the thermodynamically reversible reaction between source materials and transport agent (usually halogens) to produce gaseous precursor *in situ*. As shown in Figure 1.3a, silicide reacts with $I_2$ at $T_1$ to generated gaseous product. The gaseous precursor undergoes the reverse reaction to product silicide NWs at $T_2$. $CrSi_2$ NWs on $Si/SiO_2$ substrate, with dilute $Ni(NO_3)_2$ on the surface, were obtained using $CrSi_2$ powder as the source material and $I_2$ as the transport agent.[27] The Jin group has utilized the complementary chemical vapor transport (CVT) method to synthesis $CrSi_2$ NWs. The CVT process using $CrSi_2$ powder as the source

material and iodine as the transport reagent, which could transferred the solid $CrSi_2$ into gaseous $CrI_2$ and $SiI_4$. Through CVT the reaction temperature could be lower and the metal/silicide ration of the gaseous precousors will be similar with the desired $CrSi_2$ NWs, which could prevent the formation of multiple crystal phases. This CVT method has demonstrated to be general on other silicide NWs, such as δ-$Ni_2Si$[52] and β-$Ni_3Si$[51] NWs were obtained using $Ni_2Si$ and $TiSi_2$ as source materials respectively.

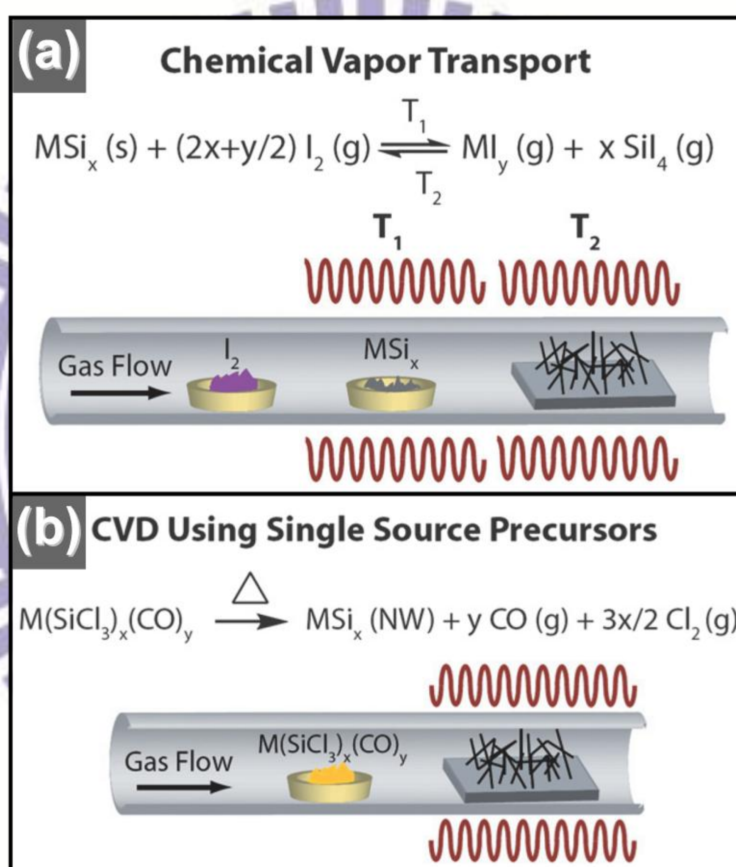


**Figure 1.3** (a) Schematic diagram for silicide NWs synthesized by Chemical vapor transport (CVT), (b) Synthesis of silicide NWs through single source precursor chemical vapor deposition (CVD).[100]

Chemical vapor deposition is commonly used to obtain transition metal silicide thin films. Using single source precursors (SSP), consisting metal and silicon atoms, in CVD is a simple method and allows controlling over the stoichiometry of the product precisely. CVD was used to obtain FeSi NWs on Si substrate, with a thin

oxide layer on the top, by using trans-$Fe(CO)_4(SiCl_3)_2$ as precursor, which undergoes a reductive elimination to $FeSiCl_2$ and further decomposes into FiSi in the gas phase.[33] This technique has been extended to CoSi[36] and $MnSi_{2-x}$ ($MnSi_{1.8}$) NWs[30] by using $Co(CO)_4SiCl_3$ and $Mn(CO)_5SiCl_3$, respectively. Moreover, Mixtures of $Co(CO)_4SiCl_3$ and trans-$Fe(CO)_4(SiCl_3)_2$ can be used as precursor to obtain $Fe_{1-x}Co_xSi$ alloy NWs.[38]

CVD with Si and metal sources has been used to prepare metal silicide thin film. Du *et al*. have shown the synthesis of TiSi naonpin with a particular shape on the deposited $Ti_5Si_3$ film by CVD with $TiCl_4$ and $SiH_4$ as precursors.[16,17] Moreover, C54 $TiSi_2$ NWs and two-dimensional C49 $TiSi_2$ nanonets have been obtained by using $TiCl_4$ and $SiH_4$ with $H_2$ and reported by Wang *et al*.[19,24] The C49 $TiSi_2$ nanonets shows preferred growth along [100] and [001] directions and could be attributed to the orthorhombic symmetry. Besides, single-crystalline $Mn_4Si_7$ NWs were prepared using SiO and $MnCl_2$ powder as the precursors.[31] The SiO and $MnCl_2$ were placed at different temperature zones to manipulate the evaporation rate of them respectively. The SiO and $MnCl_2$ could react directly to form $Mn_4Si_7$. Alternatively, $MnCl_2$ could react with the $SiCl_4$, gaseous byproduct of the reaction between $MnCl_2$ and SiO, to form $Mn_4Si_7$. Kim *et al* have demonstrated the synthesis of $V_5Si_3$ NWs on a V foil substrate on Si powder. The Si and metal sources are the Si powder and $VCl_3$, respectively. After reaction of $VCl_3$ and Si powder, $VSi_2$ and gas phase $SiCl_4$ are formed. In situ generated $SiCl_4$ could be served as another Si source for the growth of $V_5Si_3$ NWs.[25]

## 1.4.2 Applications of Metal Silicide NWs

Metal silicides possess superior properties and have been widely used in modern

electronic devices. As the dimension of silicide was limited to nanoscale, the scale of the devices decreases and other novel applications have been explored, such as nanoelectronics, cathode for electron field emitter, thermoelectrics, and solar energy conversion.

Low electrical resistivities and compatibility with silicon-base devices made silicide NWs a promising candidate for nanoelectronic devices. $Ni_2Si$ has demonstrated a low resistivity of 21 μΩcm and an extremely high failure current density of 108 A/cm$^2$.[52] Electron transportation properties of other silicide NWs were also reported.[36,44] Due to their low resistivity, high aspect ratio, and low work function, metal silicide NWs are promising candidates for electron field emitter. Field emission properties of various silicide NWs have been demonstrated including $TiSi_2$, TiSi, $Ti_5Si_4$, $Ti_5Si_3$, CoSi,[42] $NiSi_2$,[58] NiSi,[48,55] $Ni_{31}Si_{22}$,[56] $Ni_2Si$,[57] and $TaSi_2$.[60] The reported turn-on fields of the NWs are in the range of 3-4 V/μm. Recently, field emission properties of single NW have started to reveal the field emission mechanism in the nanoscale.[61] Metal silicides are candidates for thermoelectrics applications, which could generate electric potential through altering the temperature, and *vice versa*. $CrSi_2$ NWs has been prepared and its thermoelectric property has been studied through a unique technique. The result indicates that the phonon-surface scattering increased with the decreasing NW diameter at low temperature.[28] Titanium silicide have shown the ability to perform solar energy assisted catalytic water splitting.[101,102] $TiO_2$/$TiSi_2$ heterostructures, composed of C49 $TiSi_2$ nanonets coated with a $TiO_2$ layer, have show a high performance in photoelectrochemical water splitting. Burgeoning efforts have been devoted to expend the applications of silicide NWs. However, studies of metal silicide NWs have just begun about seven years; there are still a lot of territories needed to be explored.

# 1.5 Introduction of Electron Field Emission

Electron field emission (EFE) is a quantum tunneling phenomenon of electron from the surface of a material subjected to a strong electric field. When a sufficiently strong electric field was applied on a metal or semiconductor, electrons will tunnel through the surface potential barrier of the sample surface into vacuum level. As shown in Figure 1.4, under an applied strong electric field, the surface potential barrier reduced and the probability for electron extracted from the surface of solid into vacuum level increased. There is slightly difference between the field emission theories for metal and semiconductor; we only discuss the theory for metal below.[103]

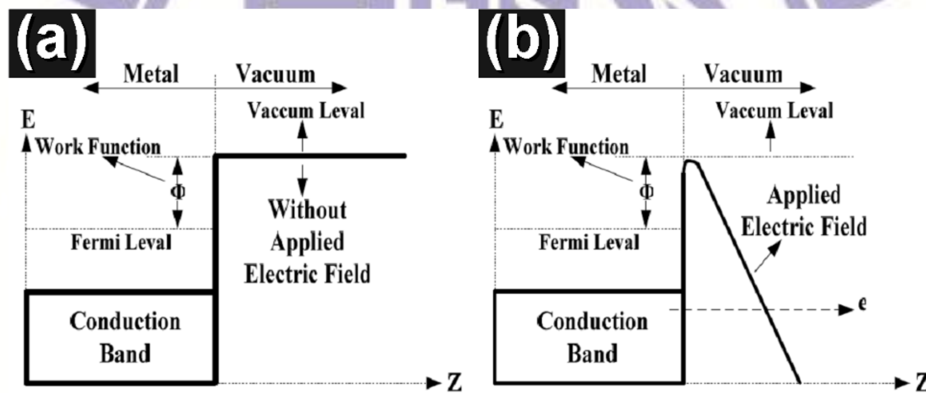


**Figure 1.4** Energy diagram of metal-vacuum level (a) without electric field, (b) under high electric field.

Fowler and Nordheim obtained the accurate description of field emission, based on tunneling of electrons through the surface potential barrier, in 1928.[104] Considering the emission of electrons from a object, the emission current could be defined by multiplying the number of electrons N(W,T) and the charge on the electron D(W). The number of emitted electrons is determined to multiply the flux of electron incident on the surface potential barrier and the tunneling probability of electrons to

overcome the potential barrier as shown below.

$$J(E,T) = e\int_0^{\infty} N(W,T)D(W)dW \tag{1.4}$$

Where E, T represent the applied electric field and the temperature, N(W,T) and D(W) are the function of E, and T. By integrating equation (1.4), it will change into

$$J(E,T) = \frac{e^3E^2}{16\pi^2 h\phi t^2(y_0)} \frac{\pi c_0 k_B T}{\sin(\pi c_0 k_B T)} \exp\left[-\frac{4}{3e}\left(\frac{2m}{h^2}\right)^{1/2} v(y_0)\frac{\phi^{3/2}}{E}\right] \tag{1.5}$$

While the time factor is

$$y_0 = 3.79\times10^{-4}\, E^{1/2}\big/\phi \tag{1.6}$$

The velocity is

$$V(y_0) \tag{1.7}$$

Set T approximate to zero to discuss the field emission, equation (1.5) could be shown as

$$J(F) = \mathrm{A}\, F^2 \exp\left[\frac{-\mathrm{B}\,\phi^{3/2}}{F}\right] \tag{1.8}$$

while $\mathrm{A} \equiv \frac{e^3}{16\pi^2\hbar\phi t^2(y_0)}$, and $\mathrm{B} \equiv \frac{4}{3e}\left(\frac{2m}{\hbar^2}\right)^{1/2} v(y_0)$

This is known as Fowler-Nordheim equation. Under the field emission condition, y is between 0-1, and the function of $v(y)$ and $t^2(y)$ could be approximated to:

$t^2(y) = 1.1$ , $v(y) = 0.95- y^2$

By substituting the approximation above, J = I/α, and F=βV into equation (1.8), the expression becomes

$$I = aV^2 \exp\left(\frac{-b}{V}\right) \tag{1.9}$$

where $a = \frac{\alpha \mathrm{A}\beta^2}{1.1\phi}\exp\left[\frac{\mathrm{B}(1.44\times10^{-7})}{\phi^{1/2}}\right]$ and $b = \frac{0.95\mathrm{B}\phi^{3/2}}{\beta}$

$\mathrm{A} = 1.54\times10^{-6}$，$\mathrm{B} = 6.87\times10^{7}$

A denotes the effective emission area and β is the field enhancement factor.

There are three factors, α, β, and ϕ, in equation (1.9) could influence the magnitude of

the field emission current density. Equation (1.9) can be further expressed as

$$\ln\left(\frac{I}{V^2}\right) = \ln a - b\left(\frac{1}{V}\right) \tag{1.10}$$

As a consequence, for a field emission data, by plotting of log($I/V^2$) versus 1/V, a straight line with negative slope could be obtained, and was designated as F-N plot. Through this plot, one can judge the field emission properties of a sample. When the work function of the sample is know, the field enhancement factor β could be calculated from the slope of F-N plot.

Shoulders had addressed that with a field amplification effect, which means the electric field lines are concentrated locally around a sharp object, the required electric field to election emission the could be lowered dramatically.[105] In 1968, Spindt had demonstrated a thin film field emission device with sharp Mo emission cathode.[106] As the advancement of nanotechnology, an increasing effort has been devoted to fabricating nanomaterials for new field emitters, such as CNTs (carbon nanotubes),[10] nano-diamond coated Si nanowires (NWs),[11] SiC NWs and nanotubes,[12,13] metal oxides[14] and metal silicides. Metal silicides NWs have excellent properties such as, high aspect ration, good conductivity, high thermal stability, and compatibility with Si based devices, makes them promising candidates for future field emission devices.

## 1.6 Aim of This Thesis

Titanium silicides possess outstanding physical properties and are widely used in electronic technology. The achievement in growth of metal silicide NWs represents a significant advance for application of silicide NWs in future nanodevices. However, free standing titanium silicides nanowires are rarely reported. This may resulted from the lack of easy and safe way to synthesis titanium silicdes without the usage of high-vacuum system (for PVD) or explosive materials, such as $SiH_4$ and $H_2$ (for CVD). In this thesis, we provide a unique CVD method by reaction between the $TiCl_x$(x=1-3), which is *in situ* generated through reaction between $TiCl_4$ and Ti metal, and the Si substrates to synthesis titanium silicde materials. By modifying the reaction conditions, such as time, temperature and partial pressure of the precursor, titanium silicide samples composed of different morphologies (nanowires, nanoplates, and thin films) and crystal structures could be obtained. The influence of growth conditions on the samples and the growth mechanism will be discussed in detail.

Titanium silicides have high thermal stability and low electrical resistivity. NWs have high aspect ratio and some distinct properties. As a consequence, the obtained titanium silicides NWs are believed to be good electric field emitters. Field emission properties of the titanium silicides samples are demonstrated and studied in this work.

## 1.7 References

(1) Chen, L.-J. *Silicide Technology for Integrated Circuits*; IEE: London, 2004.

(2) Kosolapova, T. Y. *Handbook of High Temperature Compounds: Properties, Production, Applications* Hemisphere Publishing Corporation: New York, 1990.

(3) Maex, K.; Rossum, M. V. *Properties of Metal Silicides*; IEE: London, 1995.

(4) Murarka, S. P. *Silicides for VLSI Applications*; Academic Press: Orlando, FL, 1983.

(5) Bucher, E.; Schultz, S.; Lux-Steiner, M. C.; Munz, P.; Gubler, U. G., F. *Appl. Phys. A* **1986**, *40*, 71.

(6) Murarka, S. P.; Fraser, D. B. *J. Appl. Phys.* **1980**, *51*, 350.

(7) Cui, Y.; Wei, Q.; Park, H.; Lieber, C. M. *Science* **2003**, *293*, 1289.

(8) Huang, M. H.; Mao, S.; Yan, H.; Wu, Y.-Y.; Kind, H.; Weber, E.; Russo, R.; Yang, P.-D. *Science* **2001**, *291*, 1897.

(9) Huang, Y.; Duan, X.; Wei, Q.; Lieber, C. M. *Science* **2001**, *291*, 630.

(10) Heer, W. A.; Chatelain, A.; Ugarte, D. *Science* **1995**, *270*, 1179.

(11) Tzeng, Y.-F.; Lee, Y.-C.; Lee, C.-Y.; Lin, I.-N.; H.-T., C. *Appl. Phys. Lett.* **2007**, *91*, 063117.

(12) Zhou, X.-T.; Lai, H.-L.; Peng, H.-Y.; Au, F. C.-K.; Liao, L.-S.; Wang, N.; Bello, I.; Lee, C.-S.; Lee, S.-T. *Chem. Phys. Lett.* **2000**, *318*, 58.

(13) Wang, C.-H.; Lin, H.-K.; Ke, T.-Y.; Palathinkal, T. J.; Tai, N.-H.; Lin, I.-N.; Lee, C.-Y.; H.-T., C. *Chem. Mater.* **2007**, *19*, 3956.

(14) Tseng, Y.-K.; Huang, C.-J.; Cheng, H.-M.; Lin, I.-N.; Liu, K.-S.; Chen, I.-C. *Adv.*

*Funct. Mater.* **2003**, *13*, 811.

(15) Xiang, B.; Wang, Q.-X.; Wang, Z.; Zhang, X.-Z.; Liu, L.-Q.; Xu, J.; Yu, D.-P. *Appl. Phys. Lett.* **2005**, *86*, 243103.

(16) Du, J.; Du, P.-Y.; Hao, P.; Huang, Y.-F.; Ren, Z.-D.; Han, G.-R.; Weng, W.-J.; Zhao, G.-L. *J. Phys. Chem. C* **2007**, *111*, 10814.

(17) Du, J.; Ren, Z.-D.; Tao, K.-Y.; Hu, A.-H.; Hao, P.; Huang, Y.-F.; Zhao, G.-L.; Weng, W.-J.; Han, G.-R.; Du, P.-Y. *Cryst. Growth Des.* **2008**, *8*, 3543.

(18) Lin, H.-K.; Tzeng, Y.-F.; Wang, C.-H.; Tai, N.-H.; Lin, I.-N.; Lee, C.-Y.; Chiu, H.-T. *Chem. Mater.* **2008**, *20*, 2429.

(19) Zhou, S.; Liu, X.-H.; Lin, Y.-J.; Wang, D.-W. *Angew. Chem. Int. Ed.* **2008**, *47*, 7681.

(20) Chang, C. M.; Chang, Y. C.; Chung, Y. A.; Lee, C. Y.; Chen, L. J. *J. Phys. Chem. C* **2009**, *113*, 17720.

(21) Chang, C.-M.; Chang, Y.-C.; Lee, C.-Y.; Yen, P.-H.; Lee, W.-F.; Chen, L.-J. *J. Phys. Chem. C* **2009**, *113*, 9153.

(22) Lin, H. K.; Cheng, H. A.; Lee, C. Y.; Chiu, H. T. *Chem. Mater.* **2009**, *21*, 5388.

(23) Ren, Z.; Hu, A.; Tao, K.; Du, J.; Weng, W.; Ma, N.; Du, P. *Thin Solid Films* **2009**, *517*, 5014.

(24) Zhou, S.; Liu, X.-H.; Lin, Y.-J.; Wang, D.-W. *Chem. Mater.* **2009**, *21*, 1023.

(25) In, J.; Seo, K.; Lee, S.; Yoon, H.; Park, J.; Lee, G.; Kim, B. *J. Phys. Chem. C* **2009**, *113*, 12996.

(26) Seo, K.; Varadwaj, K. S. K.; Cha, D.; In, J.; Kim, J.; Park, J.; Kim, B. *J. Phys. Chem. C* **2007**, *111*, 9072.

(27) Szczech, J. R.; Schmmitt, A. L.; Bierman, M. J.; Jin, S. *Chem. Mater.* **2007**, *19*, 3238.

(28) Zhou, F.; Szczech, J.; Pettes, M. T.; Moore, A. L.; Jin, S.; Shi, L. *Nano Lett.* **2007**, *7*, 1649.

(29) Yu, L.; Ma, Y.; Zhu, J.; Feng, H.; Wu, Q.; Lu, Y.; Lin, W.; Sang, H.; Hu, Z. *J. Phys. Chem. C* **2008**, *112*, 5865.

(30) Higgins, J. M.; Schmitt, A. L.; Guzei, L. A.; Jin, S. *J. Am. Chem. Soc.* **2008**, *130*, 16086.

(31) Ham, M.-H.; Lee, J.-W.; Moon, K.-J.; Choi, J.-H.; Myoung, J.-M. *J. Phys. Chem. C* **2009**, *113*, 8143.

(32) Quyang, L.; Thrall, E. S.; Deshmukh, M. M.; Park, H. *Adv. Mater.* **2006**, *18*, 1437.

(33) Schmitt, A. L.; Bierman, M. J.; Schmeisser, D.; Himpsel, F. J.; Jin, S. *Nano Lett.* **2006**, *6*, 1617.

(34) Yamamoto, K.; Kohno, H.; Takeda, S.; Ichikawa, S. *Appl. Phys. Lett.* **2006**, *89*, 083107.

(35) Varadwaj, K. S. K.; Seo, K. I., J.; Mohanty, P.; Park, J.; Kim, B. *J. Am. Chem. Soc.* **2007 .** *129*, 8594.

(36) Schmitt, A. L.; Zhu, L.; Schmeiber, D.; Himpsel, F. J.; Jin, S. *J. Phys. Chem. B* **2006**, *110*, 18142.

(37) Seo, K.; Varadwaj, K. S. K.; Mohanty, P.; Lee, S.; Jo, Y.; Jung, M.-H.; Kim, J.; Kim, B. *Nano Lett.* **2007**, *7*, 1240.

(38) Chou, Y. C.; Wu, W. W.; Cheng, S. L.; Yoo, B. Y.; Myung, N.; Chen, L. J.; Tu, K.

N. *Nano Lett.* **2008**, *8*, 2194.

(39) In, J.; Varadwaj, K. S. K.; Seo, K.; Lee, S.; Jo, Y.; Jung, M.-H.; Kim, J.; Kim, B. *J. Phys. Chem. C* **2008**, *112*, 4748.

(40) Schmitt, A. L.; Higgins, J. M.; Jin, S. *Nano Lett.* **2008**, *8*, 810.

(41) Seo, K.; Lee, S.; Yoon, H.; In, J.; Varadwaj, K. S. K.; Jo, Y.; Jung, M. H.; Kim, J.; Kim, B. *ACS Nano* **2009**, *3*, 1145.

(42) Tsai, C. I.; Yeh, P. H.; Wang, C. Y.; Wu, H. W.; Chen, U. S.; Lu, M. Y.; Wu, W. W.; Chen, L. J.; Wang, Z. L. *Cryst. Growth Des.* **2009**, *9*, 4514.

(43) Decker, C. A.; Solanki, R.; Freeouf, J. L.; Carruthers, J. R.; Evans, D. R. *Appl. Phys. Lett.* **2004**, *84*, 1389.

(44) Wu, Y.; Xiang, J.; Yang, C.; Lu, W.; Lieber, C. M. *Nature* **2004**, *430*, 61.

(45) Yan, X. Q.; Yuan, H. J.; Wang, J. X.; Liu, D. F.; Zhou, Z. P.; Gao, Y.; Song, L.; Liu, L. F.; Zhou, W. Y.; Wang, G.; Xie, S. S. *Appl. Phys. A* **2004**, *79*, 1853.

(46) Kim, J.; Anderson, W. A. *Thin Solid Films* **2005**, *483*, 60.

(47) Weber, W. M.; Geelhaar, L.; Graham, A. P.; Unger, E.; Duesberg, G. S.; Liebau, M.; Pamler, W.; Cheze, C.; Riechert, H.; Lugli, P.; Kreupl, F. *Nano Lett.* **2006**, *6*, 2660.

(48) Kim, C.-J.; Kang, K.; Woo, Y. S.; Ryu, K.-G.; Moon, H.; Kim, J.-M.; Zang, D.-S.; Jo, M.-H. *Adv. Mater.* **2007**, *19*, 3637.

(49) Kim, J.; Shin, D. H.; Lee, E.-S.; Han, C.-S.; Park, Y. C. *Appl. Phys. Lett.* **2007**, *90*, 253103.

(50) Lu, K.-C.; Wu, W.-W.; Wu, H.-W.; Tanner, C. M.; Chang, J. P.; Chen, L. J.; Tu, K. N. *Nano Lett.* **2007**, *7*, 2389.

(51) Song, Y.; Jin, S. *Appl. Phys. Lett.* **2007**, *90*, 173122.

(52) Song, Y.; Schmitt, A. L.; Jin, S. *Nano Lett.* **2007**, *7*, 965.

(53) Geng, Z. R.; Lu, Q. H.; Yan, P. X.; Yan, D.; Yue, G. H. *Phys. E* **2008**, *41*, 185.

(54) Kang, K.; Kim, S.-K.; Kim, C.-J.; Jo, M.-H. *Nano Lett.* **2008**, *8*, 431.

(55) Kim, J.; Lee, E.-S.; Han, C.-S.; Kang, Y.; Kim, D.; Anderson, W. A. *Microelectron. Eng.* **2008**, *85*, 1709.

(56) Lee, C.-Y.; Lu, M.-P.; Liao, K.-F.; Wu, W.-W.; Chen, L.-J. *Appl. Phys. Lett.* **2008**, *93*, 113109.

(57) Liu, Z. H.; Zhang, H.; Wang, L.; Yang, D. R. *Nanotechnology* **2008**, *19*, 375602.

(58) Lee, C. Y.; Lu, M. P.; Liao, K. F.; Lee, W. F.; Huang, C. T.; Chen, S. Y.; Chen, L. J. *J. Phys. Chem. C* **2009**, *113*, 2286.

(59) Chueh, Y. L.; Chou, L. J.; Cheng, S. L.; Chen, L. J.; Tsai, C. J.; Hsu, C. M.; Kung, S. C. *Appl. Phys. Lett.* **2005**, *87*, 223113.

(60) Chueh, Y.-L.; Ko, M.-T.; Chou, L.-J.; Chen, L.-J.; Wu, C.-S.; Chen, C.-D. *Nano Lett.* **2006**, *6*, 1637.

(61) Kim, J. J.; Shindo, D.; Murakami, Y.; Xia, W.; Chou, L.-J.; Chueh, Y.-L. *Nano Lett.* **2007**, *7*, 2243.

(62) Lu, J.-L.; Zhu, J. *Adv. Mater.* **2003**, *15*, 579.

(63) Liu, B.-Z.; Wang, Y.-F.; Dilts, S.; Mayer, T. S.; Mohney, S. E. *Nano Lett.* **2007**, *7*, 818.

(64) Lu, K.-C.; Tu, K.-N.; Wu, W.-W.; Chen, L.-J.; Yoo, B.-Y.; Myung, N. V. *Appl. Phys. Lett.* **2007**, *90*, 253111.

(65) Lin, Y.-C.; Lu, K.-C.; Wu, W.-W.; Bai, J.-W.; Chen, L.-J.; Tu, K.-N.; Huang, Y. *Nano Lett.* **2008**, *8*, 913.

(66) Lee, C.-Y. *Chem. Vap. Deposition* **1999**, *5*, 69.

(67) Nicolet, M. A. *Thin Solid Films* **1978**, *52*, 415.

(68) Ho, P. S. *Thin Solid Films* **1982**, *96*, 301.

(69) Tu, K. N. *J. Vac. Sci. Technol.* **1981**, *19*, 766.

(70) Yu, A. Y. C. *Solid State Electron* **1970**, *13*, 239.

(71) Murarka, S. P. *J. Vac. Sci. Technol.* **1980**, *17*, 775.

(72) Geipel, H. J.; Hsieh, J. N.; Ishaq, M. H.; Koburger, C. W.; White, F. R. *IEEE Trans. Electron Devices* **1980**, *ED-27*, 1417.

(73) Murarka, S. P.; Fraser, D. B. *J. Appl. Phys.* **1980**, *51*, 342.

(74) Saxena, A. N.; Pramanik, D. *Solid State Electron* **1984**, *27*, 1984.

(75) Sinha, A. K. *J. Vac. Sci. Technol.* **1981**, *19*, 778.

(76) Kawamura, T.; Shinoda, D.; Muta, H. *Appl. Phys. Lett.* **1967**, *11*, 1967.

(77) Buckley, W. D.; Moss, S. C. *Solid State Electron* **1972**, *15*, 1331.

(78) Gurp, G. J.; Langereis, C. *J. Appl. Phys.* **1975**, *46*, 431.

(79) Borisenko, V. E. *Semiconduction Silicides*; Springer: Berlin, 2000; Vol. 39.

(80) Rowe, D. M. *CRC Handbook of Thermoelectrics*; CRC Press: Boca Raton, 1994.

(81) Senthilarasu, S.; Sathyamoorthy, R.; Lalitha, S. *Sol. Energy Mater. Sol. Cells* **2004**, *82*, 299.

(82) Massalski, T. B.; Okamoto, H.; Subramanian, P. R.; Kacprzak, L. *Binary Alloy Phase Diagrams*; American Society for Metals: Metals Park, Ohio, 1990.

(83) Ekman, M.; Ozolins, V. *Physical Review B* **1998**, *57*, 4419.

(84) Chopra, K. L. *Thin Film Phenomena*; McGraw-Hill: New York, 1969.

(85) Hoffman, D. W.; Thronton, J. A. *Thin Solid Films* **1977**, *40*, 355.

(86) Ilderem, V.; Reif, R. *J. Electronchem. Soc.* **1988**, *135*, 2590.

(87) Wang, M. H.; Chen, L. J. *J. Appl. Phys.* **1992**, *71*, 5918.

(88) Lur, W.; Chen, L. J. *Appl. Phys. Lett.* **1989**, *54*, 1217.

(89) Yim, W. M.; Stotko, E. J. *J. Electrochem. Soc.* **1974**, *121*, 965.

(90) Lacombe, J.; Duchemin, J. P.; Bonnet, M.; Huyghe, D. *Eectron. Lett.* **1977**, *13*, 472.

(91) Hallais, J. P.; Boccon-Gibod, D.; Chane, J. P.; Durand. *J. Electrochem. Soc.* **1977**, *124*, 1290.

(92) Preinesberger, C.; Vandre, S.; Kalka, T.; Dahne, M. *J. Phys. D* **1998**, *31*, L43.

(93) Preinesberger, C.; Becker, S. K.; Vandre, S.; Kalka, T.; Dahne, M. *J. Appl. Phys.* **2002**, *91*, 1695.

(94) Chen, Y.; Ohlberg, D. A. A.; Medeiros, R. G.; Chang, Y.-A.; Williams, R. S. *Appl. Phys. Lett.* **2000**, *76*, 4004.

(95) Nogami, J.; Liu, B. Z.; Katkov, M. V.; Ohbuchi, C.; Birge, N. O. *Physical Review B* **2001**, *63*, 233305.

(96) Chen, Y.; Ohlberg, D. A. A.; Williams, R. S. *J. Appl. Phys.* **2002**, *91*, 3213.

(97) He, Z.; Smith, D. J.; Bennett, P. A. *Phys. Rev. Lett.* **2004**, *93*, 256102.

(98) Liang, S.; Islam, R.; Smith, D. J.; Bennett, P. A. *J. Cryst. Growth* **2006**, *295*, 166.

(99) Hsu, H.-C.; Wu, W.-W.; Hsu, H.-F.; Chen, L.-J. *Nano Lett.* **2007**, *7*, 885.

(100) Schmitt, A. L.; Higgins, J. M.; Szczech, J. R.; Jin, S. *J. Mater. Chem.* **2010**, *20*, 223.

(101) Li, Q.; Lu, G. *Catal. Lett.* **2008**, *125*, 376.

(102) Peter, R.; Andriy, K.; Marc, A. W. t.; Klaus, K.; Claudia, W.; Martin, D. *Angew. Chem., Int. Ed.* **2007**, *46*, 7770.

(103) Zhu, W. *Vacuum Microelectronics*; John Wiley, 2001.

(104) Fowler, R. H.; Nordheim, L. W. *Proc. R. Soc. London, Ser. A* **1928**, *119*, 173.

(105) Buck, D. A.; Shoulders, K. R. "An Approach to Microminiature Systems"; Procedure Eastern Joint Computer Conference, 1958.

(106) Spindt, C. A.; Brodie, I.; Humphrey, L.; Westerberg, E. R. *J. Appl. Phys.* **1976**, *47*, 5248.

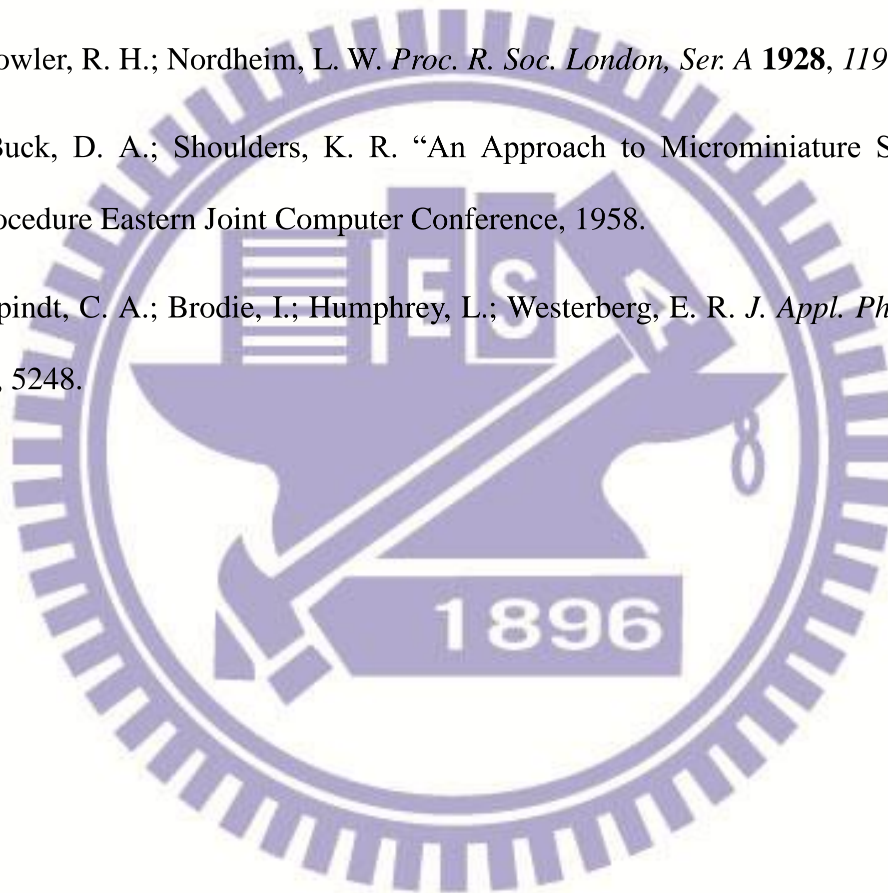

# Chapter 2

# $Ti_5Si_3$ Nanowire and Its Field Emission Property

## 2.1 Introduction

Because of their distinct properties, 1D nanostrutures have attracted tremendous amounts of attention for technological applications, such as sensors,[1] laser devices,[2] and electrical systems.[3] An increasing effort has been devoted to fabricating nanomaterials for new field emitters, such as CNTs (carbon nanotubes),[4] nano-diamond coated Si nanowires (NWs),[5] SiC NWs and nanotubes,[6] metal oxides[7] and metal silicides.[8] Many studies about the fabrication of free standing silicide nanowires of Ti, Cr, Fe, Co, Ni and Ta have been reported because of their superior properties and compatibility with Si based integrated circuit devices.[8-14] Among them, titanium silicides are potential candidates for field emission devices due to their relative low resistivity (10 – 28 μΩ cm), high thermal stability, and low work function.[15-17] Research on the fabrication of TiSi and $TiSi_2$ NWs and arrays through various processing techniques, including chemical vapor deposition (CVD) and physical vapor deposition (PVD), have been demonstrated recently.[9,18-20] On the other hand, fabrication of nanostructures of metal-rich titanium silicide $Ti_5Si_3$, which is a suitable refractory material with a melting point 2403 K, has not been reported. In this work, we report the first growth of $Ti_5Si_3$ NWs via a unique CVD process.[21] Microstructures and field emission properties of the NWs will be discussed in detail.

## 2.2 Experimental Section

### 2.2.1 Materials

| Reagent | Chemical Formula | Purity | Vendor |
|---|---|---|---|
| Titanium (IV) chloride | $TiCl_4$ | 99 % | Fluka |
| Titanium powder(~320 mesh) | Ti | 99.7 % | Aldrich |
| Si wafer (n-type) orientation (100) | Si | - | Semiconductor Wafer |
| Ammonium hydroxide | $NH_4OH$ | 25 % | Fluka |
| Hydrochloric acid | HCl | 37 % | Aldrich |
| Hydrofluoric acid | HF | 48 % | Aldrich |
| Hydrogen peroxide | $H_2O_2$ | 30 % | Aldrich |
| Nitric acid | $HNO_3$ | 70 % | Showa |
| Sulfuric acid | $H_2SO_4$ | 95 % | Fluka |
| Argon | Ar | 99 % | Chiah Lung |

### 2.2.2 Synthesis Procedure

All reactions were performed in a low-pressure horizontal hot-wall quartz tube reactor comprised of a pumping system, a reaction chamber heated by a three-zone tube furnace, and a precursor inlet control system. Ti powders (0.3 g) were placed at the highest temperature zone at 1173 K, which is the most upstream among the heating zones. Si (100) wafers, cleaned by RCA process and then immersed in a 48% HF/DI water (1/100 v/v) solution until the surface became hydrophobic right before the reaction were placed at a low temperature zone at 773 – 973 K downstream. After

the chamber was evacuated to 0.4 Pa, $TiCl_4$ was vaporized into the reaction chamber at a pressure of 2.67 Pa. After 1 - 6 h, the supply of $TiCl_4$ was stopped and the reaction system was cooled to room temperature. Samples of gray thin films deposited on Si substrates were collected for analysis. A summary of the representative samples prepared in this study is listed in Table 2.1.

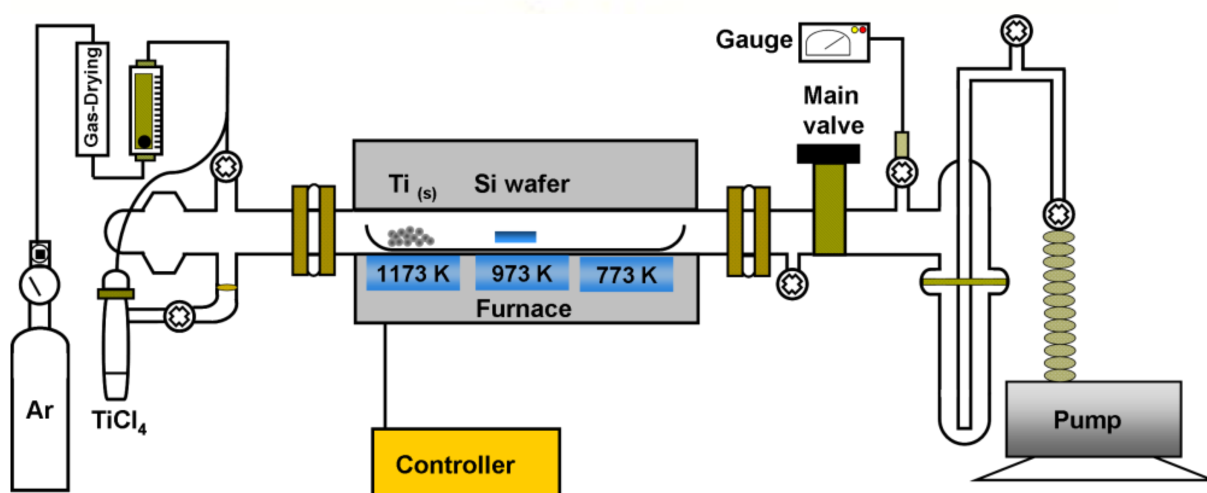


**Figure 2.1** Experimental setup of the CVD system.

### 2.2.3 Characterization Instruments

The SEM and EDX data were collected using JEOL JSM-6330F and Hitachi S-4700I at 15 kV. The TEM and SAED images were obtained on a JEOL JEM-2010 at 200 kV. The HRTEM images were acquired on a JEOL JEM-400EX at 400 kV. The Auger depth profile was obtained on a Physical Electronics Auger 670 PHI Xi. The XRD studies were carried out using a MAC MXP-18 and a BRUKER AXS D8 ADVANCE with Cu K$\alpha$1 radiation. The EFE properties of the samples were measured in a vacuum chamber at a pressure of $1.05 \times 10^{-3}$ Pa at room temperature with a spherical-shaped stainless-steel probe of 1 mm in diameter as the anode. The sample-to-anode distances, adjusted by the micrometer on the manipulator, were 150

μm, 135 μm, and 100 μm for samples **I**, **II**, and **III** respectively. The current-voltage (I-V) characteristics were measured using a Keithley 237. The maximum available voltage of the set-up is 1100 V, and the current was restricted to 10 mA.

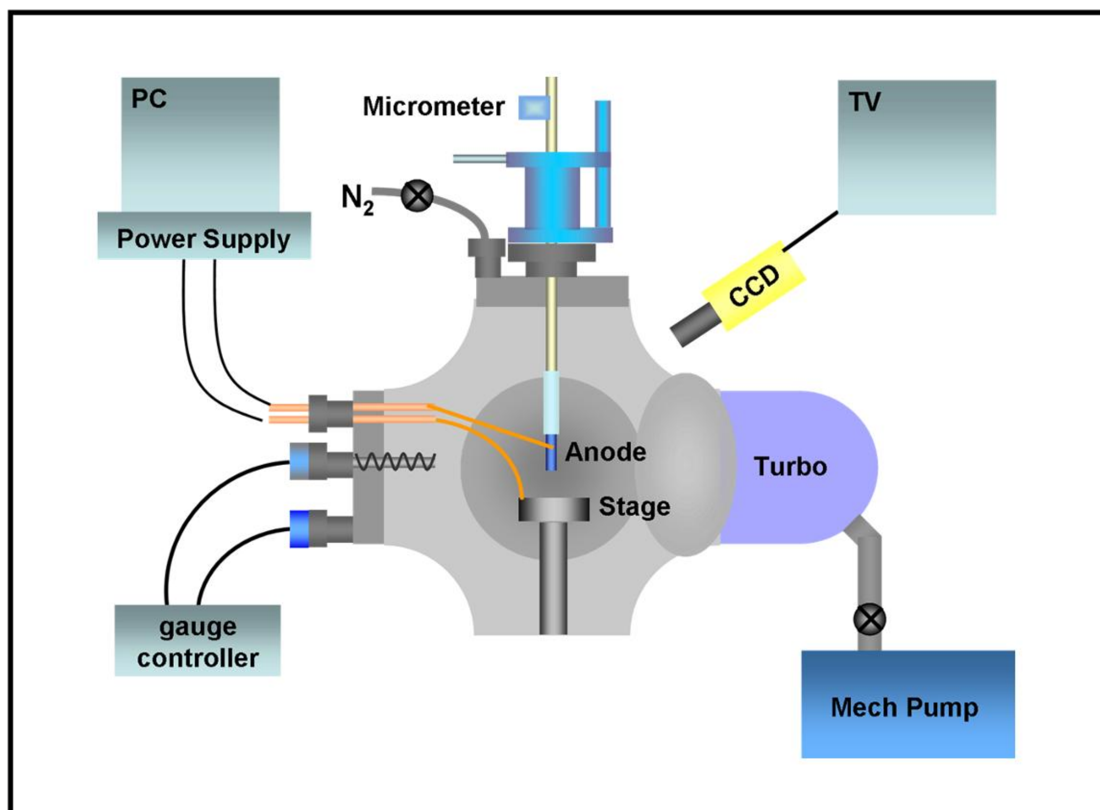


**Figure 2.2** Setup of the home-built electron field emission (EFE) system.

## 2.3 Results and Discussion

All reactions were performed in a low pressure horizontal hot-wall quartz tube reactor heated by a three-zone tube furnace. $TiCl_4$, the precursor, was vaporized into the reaction chamber at a controlled partial pressure. Close to the precursor inlet, Ti powders were placed at the heating zone at 1173 K. Si (100) wafers were placed at the center heating zone at 773 - 973 K. After 1 - 6 h, deposition of a gray layer on the substrates was observed. A summary of the representative samples prepared in this study is listed in Table 2.1.

**Table 2.1** Summary of Samples

| Sample | Growth Conditions | Morphologies and Phases | Eo [a] (V/μm) | [b] |
|---|---|---|---|---|
| I | 973K, 6h | $Ti_5Si_3$ NWs/ C54-$TiSi_2$ film | 5.4 | 816 |
| II | 773 K, 6h | *a*-$Ti_xSi_y$ NWs/ C54-$TiSi_2$ film | 7.6 | - [c] |
| III | 973 K, 1h | C54-$TiSi_2$ film | 10.4 | 343 |

[a] Turn-on field. [b] Field enhancement factor. [c] Cannot be obtained due to the lack of work function of amorphous $Ti_xSi_y$.

### 2.3.1 SEM and EDX Characterizations

Figure 2.3 shows the morphology and the chemical composition of sample **I** grown at 973 K on Si for 6 h. Figure 2.3a is a top-view scanning electron microscopic (SEM) image of **I**. It displays that on top of a deposited thin film, there are a considerable amount of thread-like NWs few micrometers long. A representative high-magnification SEM image in Figure 2.3b shows that the one-dimension (1D) nanostructures have diameters 20 - 50 nm. In addition, the image does not show evidence for the presence of metal particles, which may act as catalysts, on the tips of the wires. An energy-dispersive X-ray spectrum (EDX) of **I** in Figure 2.3c indicates that the sample contains Ti and Si only. A side view SEM image in Figure 2.3d reveals that numerous NWs with few micrometers in length extend randomly from the top of a deposited film with a thickness of ca. 6 μm on Si. Sample **II** grown at 773 K for 6 h, as displayed in Figure 2.4a, contains copious thread-like nanowires with length of few micrometers on the rough surface. Figure 2.4b, side view image of **II**, reveals numerous entangled NWs with few micrometers in length on the film with a thickness

of 3 μm. As shown in Figure 2.4c and d, **III** obtained at 973 K for 1 h also displays a 2.6 μm- thick film and scarce and short nanowires on it

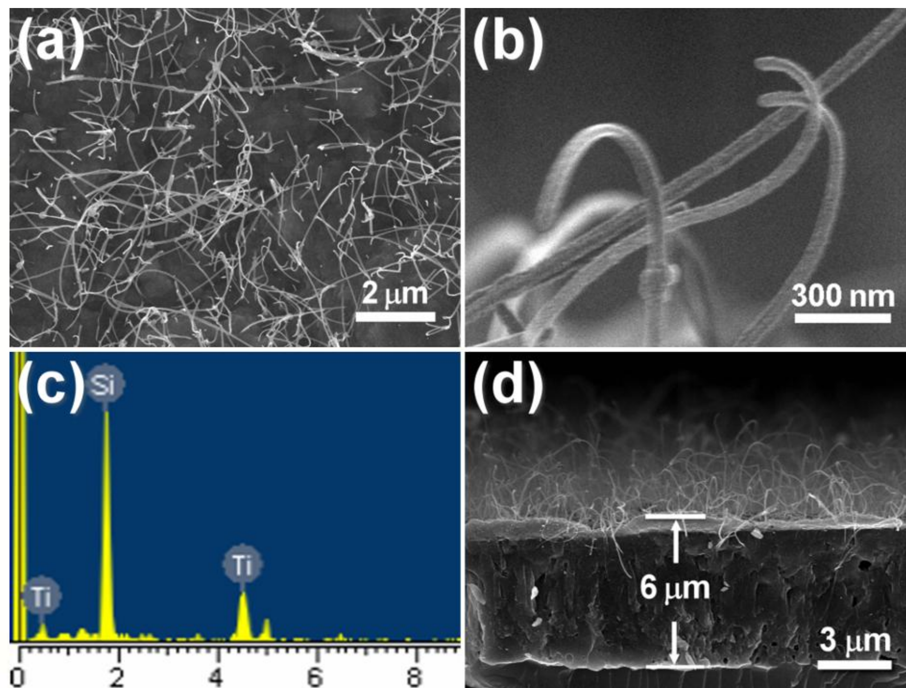


**Figure 2.3** SEM images of sample I grown on Si. (a) Top view, (b) high magnification image, (c) EDX, and (d) side view image.

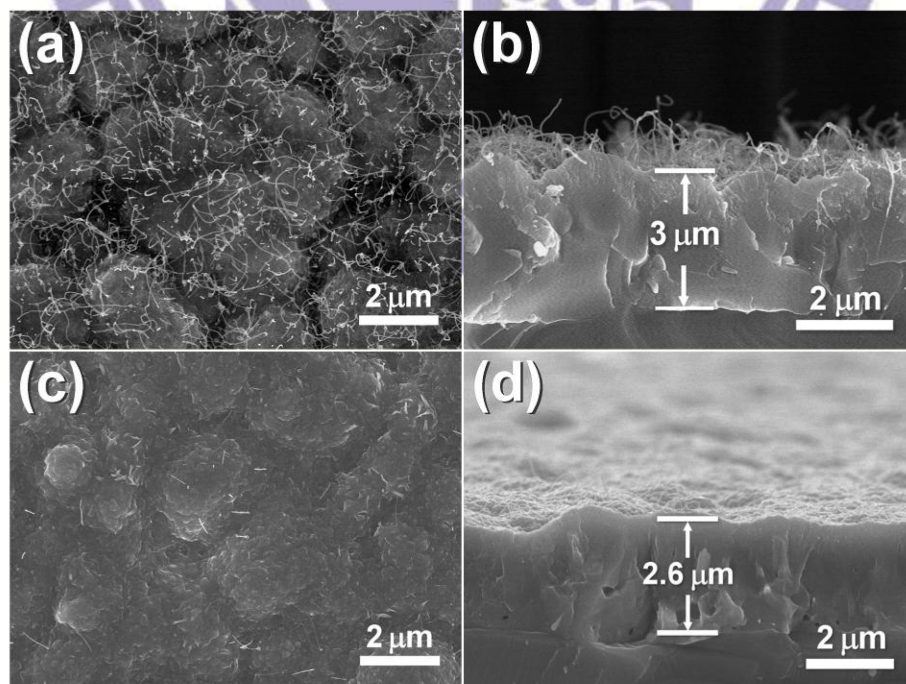


**Figure 2.4** SEM images of II (a), (b) and III (c), (d) grown on Si.

## 2.3.2 XRD Characterizations

X-ray diffraction (XRD), Figure 2.5, displays four peaks around 2θ = 39.1°, 42.3°, 43.5°, and 50° could be assigned to the (311), (040), (022), and (331) planes of C54-$TiSi_2$ (JCPDS 35-0785). This result suggests that all of the samples were composed mainly of orthorhombic C54-$TiSi_2$ phase (JCPDS 35-0785). However, transmission electron microscopic (TEM) studies of the NWs showed that the 1D material had a different titanium silicide phase.

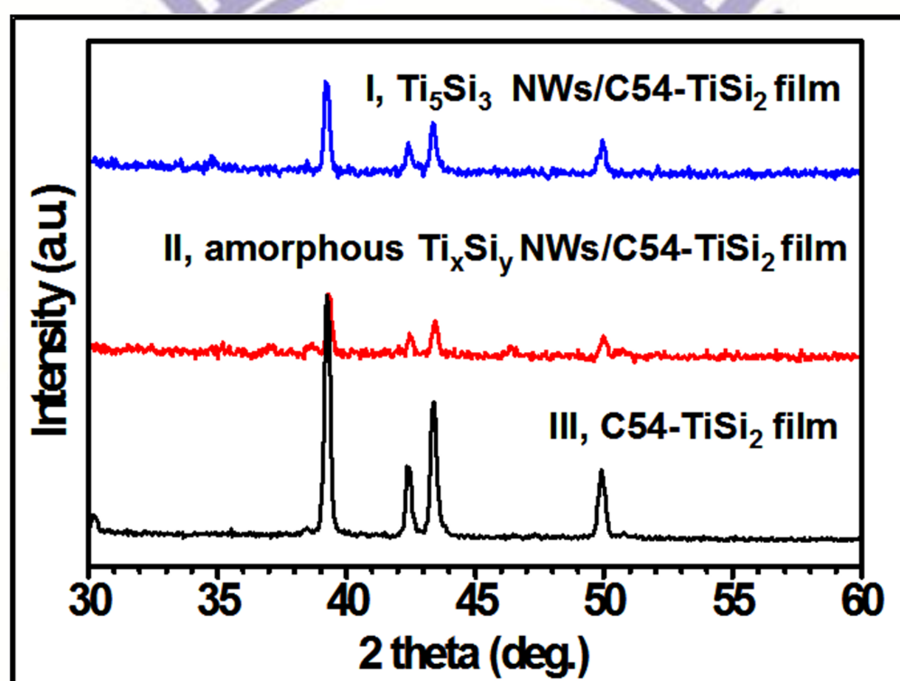


**Figure 2.5** XRD patterns of samples I, II, and III.

## 2.3.3 TEM Studies

A typical TEM image of NWs isolated from **I** is shown in Figure 2a. It reveals a long NW with a diameter ca. 30 nm. The image also confirms that on the tip of the wire, there is no evidence for the existence of any metal particles. A selected-area electron diffraction (SAED) image in Figure 2b, taken from the point indicated in

Figure 2a, displays a dot pattern. This could be assigned to (002) and (110) planes of single crystalline hexagonal $Ti_5Si_3$ with $[1\bar{1}0]$ zone axis. Figure 2c is the high-resolution TEM (HRTEM) image taken at the same place. From the image, two sets of fringes spaced at 0.25 nm and 0.37 nm apart could be assigned to the lattice spacing of (002) and (110) planes of $Ti_5Si_3$ phase, respectively. The wire growth direction is determined to be along the [002] axis of $Ti_5Si_3$. Thus, sample **I** is designated as $Ti_5Si_3$ NWs/$TiSi_2$. An Auger depth profile of **I**, Figure 2.7, also confirmed that the sample contained a high quantity of Ti on the surface while the Si content was rich inside the deposited layer.

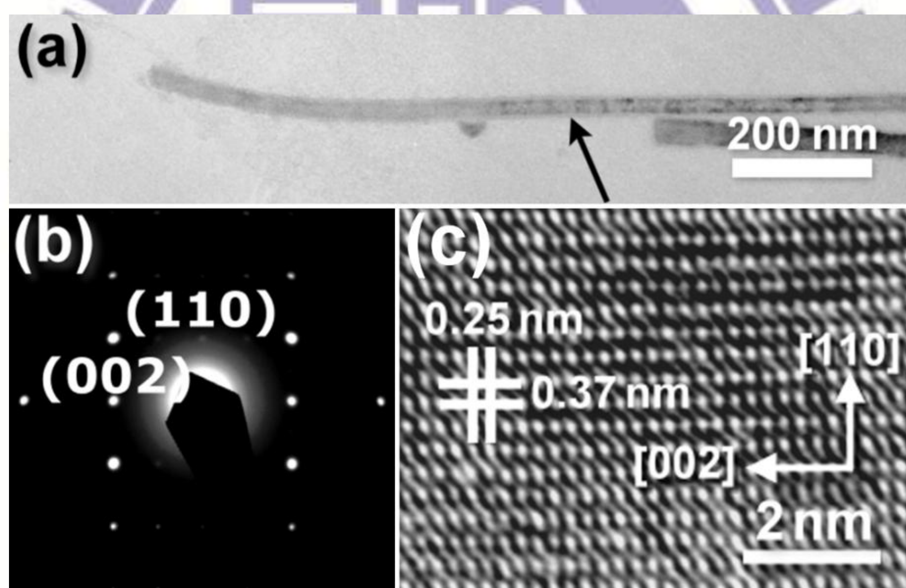


**Figure 2.6** TEM studies of a NW isolated from I. (a) Low magnification image, (b) SAED pattern of the sample in (a) showing a $[1\bar{1}0]$ zone axis, (c) high-resolution image from the selected section in (a).

As shown in Figure 2.8a, TEM image of NW isolate from **II** has diameter of 20 nm. Besides, there is no particle on the tip of the NW. Figure 2.8b is the corresponding selected-area electron diffraction (SAED) pattern, no significant diffraction spots or rings could be seen, suggested that the NW is amorphous. In

Figure 2.8c, EDX of the NWs in Figure 2.8a indicates that the compositions of the NW are Ti and Si. Combining the XRD studies mentioned in last section with the TEM results, sample **II** could be named as *a*-$Ti_xSi_y$ NWs/$TiSi_2$ film.

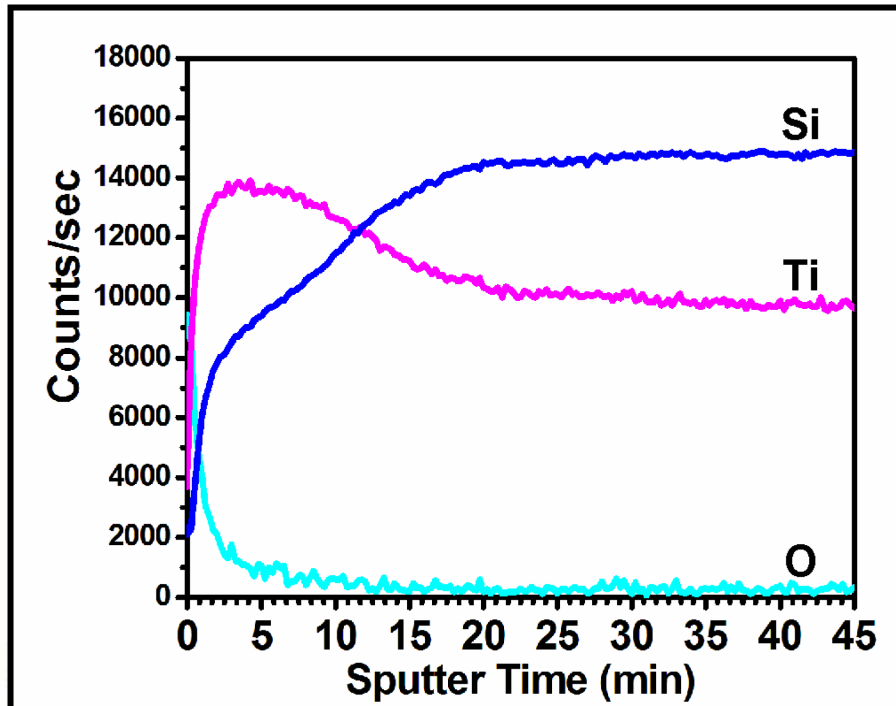


**Figure 2.7** Auger depth profile of I.

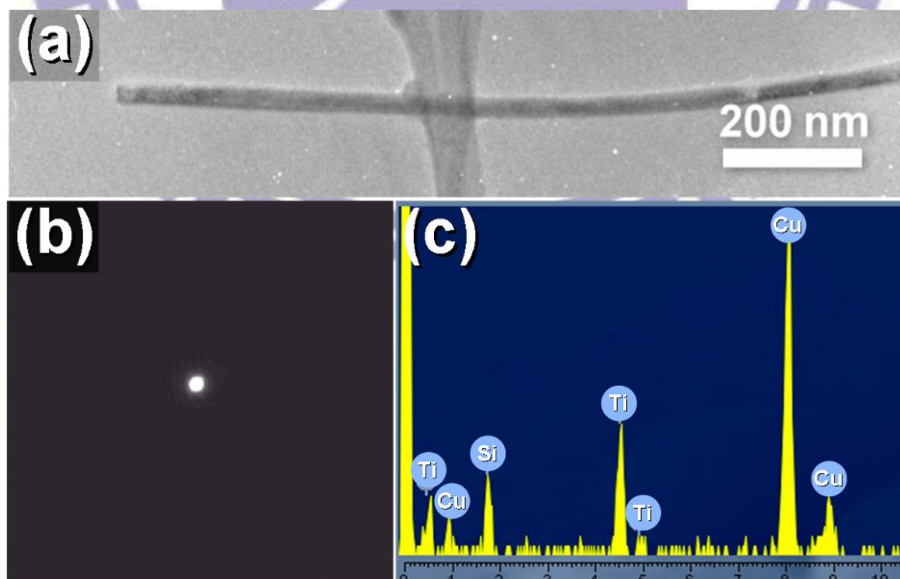


**Figure 2.8** (a) TEM image of NW isolate from sample II, (b) SAED pattern showing that the NW is amorphous, (c) EDX of the selected area in (a) indicates that the composition of the NW are Ti and Si. The NWs in II could be designated as *a*-$Ti_xSi_y$ NWs.

## 2.3.4 Influence of the Growth Conditions for the Synthesis of NWs

Both reaction temperature and time were essential factors in the synthesis of the single crystalline $Ti_5Si_3$ NWs. When the reaction temperature was decreased to 773 K, sample **II** containing abundant amorphous $Ti_xSi_y$ NWs on a C54-$TiSi_2$ thin film (designated as *a*-$Ti_xSi_y$ NWs/$TiSi_2$) was produced in 6 h. As the reaction time was reduced to 1 h, sample **III**, which showed sparse and short NWs on a layer of C54-$TiSi_2$ thin film, was obtained. Consequently, we conclude that the titanium silicide one-dimensional nanostructures could be fabricated only with sufficient reaction time. Furthermore, the crystal structures of the NWs depend highly on the reaction temperature.

The presence of Ti metal powders at the heating zone at 1173 K was important for the successful NW growth. Without it, a $TiSi_2$ film with an uneven surface was deposited on the Si substrate (Figure 2.9a). On the other hand, without the existence of $TiCl_4$, nothing will be deposited on the Si substrate (Figure 2.9b).

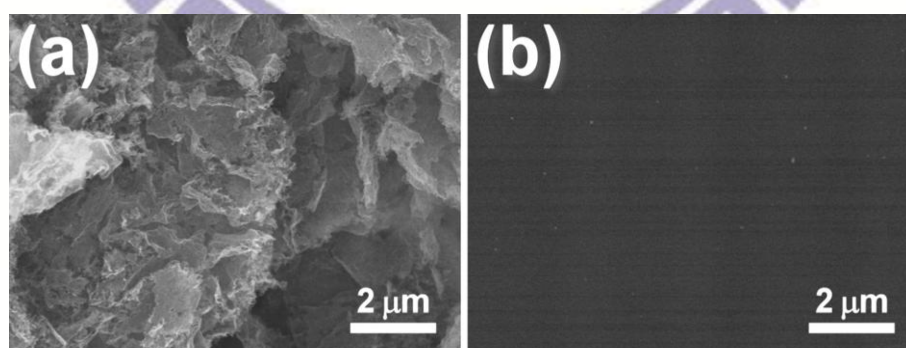


**Figure 2.9** SEM images of samples grown at similar condition but different precursors with sample I. (a) without the Ti metal, (b) without the $TiCl_4$.

## 2.3.5 Proposed Reaction Pathway

Vapor-liquid-solid (VLS) growth is employed most frequently to account for the growth of many NWs. However, according to the observations discussed above, the VLS model can be ruled out easily, owing to the absence of metal particles on the tip of the NWs.[22] Based on the experimental observations, a plausible reaction pathway is proposed in Figure 2.10 to rationalize the $Ti_5Si_3$ NW growth. It suggests that titanium subchlorides $TiCl_x$ ($x = 2, 3$), generated by the reaction between $TiCl_{4(g)}$ and Ti metal in the high temperature zone at 1173 K initially, could serve as the Ti source in two ways.[23] One is their disproportionation into $TiCl_4$ molecules and Ti atoms in the low temperature zones below 973 K. The deposited Ti atoms could react with the Si surface atoms to form $TiSi_x$ clusters for further nucleation and growth. The second one is that $TiCl_x$ could react directly with the Si substrate to form Si-rich $TiSi_x$ clusters and gaseous $SiCl_x$ byproducts, which might serve as another Si source in the formation of $TiSi_x$.[24] As the reaction proceeds further, a $TiSi_2$ thin film is grown on the substrate. In the mean time, the disproportionation of the incoming $TiCl_x$ to deposit Ti atoms remains. But the supply of Si atoms either from the substrate or from the $SiCl_x$ byproducts could be hampered by the relative inertness of the as-formed $TiSi_2$ layer. In addition, the diffusion length of Si atoms from the substrate through the $TiSi_2$ layer becomes extended.[25] All these reasons caused the Si concentration on the surface decreased at this stage. As a consequence, the $TiSi_x$ clusters nucleated are Ti-rich. Because $Ti_5Si_3$ has the highest melting point and the lowest standard heat of formation among all of the titanium silicide phases, we suggest that $Ti_5Si_3$ should be the first silicide phase solidified.[26] Further migration and coalescence of small titanium silicide clusters to these nucleation sites elongates them into the observed $Ti_5Si_3$ nanowires.

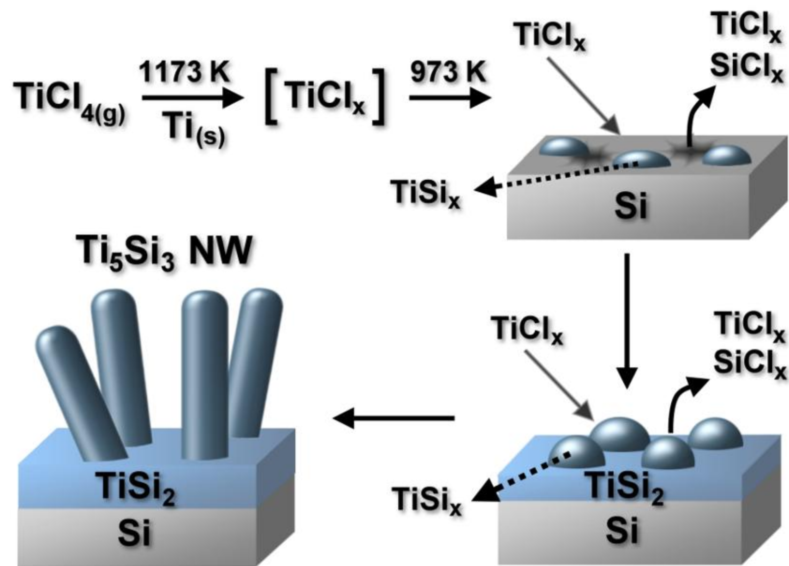


**Figure 2.10** Proposed Growth Steps of $Ti_5Si_3$ NWs.

## 2.4 Electron Field Emission Property Studies

Electron field emission (EFE) properties and the corresponding Fowler-Nordheim (F-N) plots of the samples are illustrated in Figure 2.[27] Important EFE parameters extracted from the J-E curves, including the turn-on field $E_0$, which defined as the electric field required to produce a current density of 10 $\mu Acm^{-2}$, and the field enhancement factor β, calculated from the equation $\beta = \phi^{3/2}/\phi_e$,[27] where φ is the work-function of the studied material and $\phi_e$ is the effective work-function derived from the slope of the F-N plot, are listed in Table 3.1. Among the samples studied, **I**, which is $Ti_5Si_3$ NWs on $TiSi_2$, shows the markedly superior EFE property than the others. The solid squares in Figure 2.11 illustrate that $E_0$ of **I** is only 5.4 V/μm. Sample **II**, which is composed of *a*-$Ti_xSi_y$ NWs on $TiSi_2$, displays a higher $E_0$ of 7.6 V/μm while sample **III**, which is the C54-$TiSi_2$ thin film, shows the highest $E_0$ of 10.4 V/μm. We assume that the work-functions φ of the $TiSi_2$ thin film and the $Ti_5Si_3$ NWs are the same as their bulk materials, i.e., $\phi_{TiSi2}$ = 4.53 eV and $\phi_{Ti5Si3}$ = 3.71 eV.[15]

Then, we can calculate β from ϕ and $\phi_e$. $\phi_e$ values are proportional to the slopes of the F-N plots shown in Figure 211. For sample **I**, $Ti_5Si_3$ NWs/$TiSi_2$, we suppose that most electrons were emitted from the $Ti_5Si_3$ NWs because they were closer to the anode and under higher electric field than the $TiSi_2$ film below. Thus, the β-value of **I**, estimated using $\phi_{Ti5Si3}$ and the $\phi_e$ value of **I**, is 816. This result can be regarded as $\beta_{Ti5Si3NWs}$, the β-value of $Ti_5Si_3$ NWs. It is higher than the reported β-value of $TiSi_2$ NWs, which is 500.[9a] The β-value of sample **III** is estimated to be 343. The value is high for a thin film. This may be the result from the surface roughness of **III**. Since there is no ϕ value available for *a*-$Ti_xSi_y$, it is not possible to estimate the β-value of **II**. Even though the SEM images demonstrated that **II** and **I** had similar entangled morphology, it appears that **II** could not perform better than **I** did. The amorphous NWs on **II**, may not emit electrons as efficiently as the ones on **I**. By assuming that the ϕ value of *a*-$Ti_xSi_y$ is close to those of various silicides, we can expect that the β-value of *a*-$Ti_xSi_y$ NWs is between the values found for samples **I** and **III**.

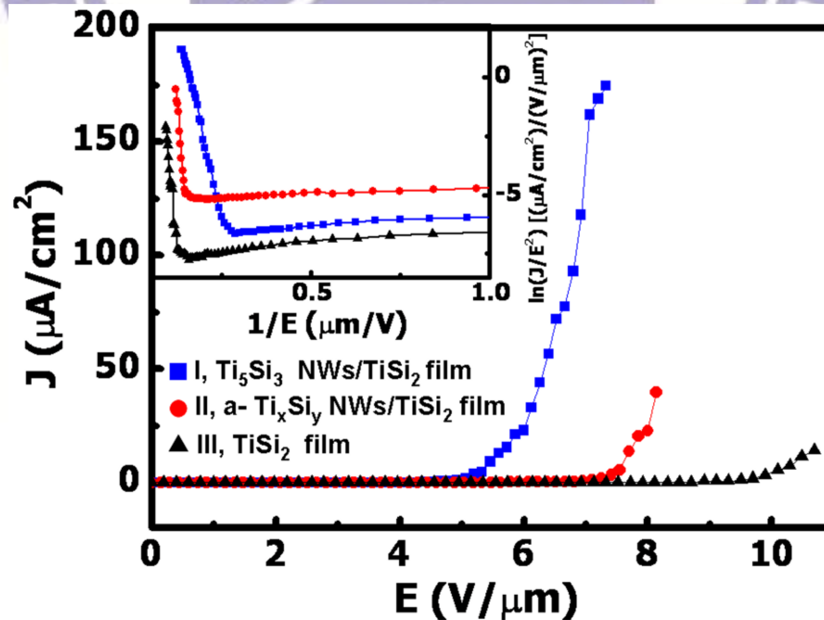


**Figure 2.11** Electron field emission current density as a function of applied electric field of samples I – III. Inset shows their corresponding Fowler-Nordheim plots.

## 2.5 Conclusions

In conclusion, this study is the first growth of $Ti_5Si_3$ NWs on C54-$TiSi_2$ thin films through a unique chemical vapor deposition process without additional catalyst. The diameters of the NWs are about 20 - 50 nm and the lengths are several micrometers. The $Ti_5Si_3$ NWs show excellent field emission properties, a low turn-on field $E_0$ of 5.4 V/μm and a high field enhancement factor β of 816. These notable results suggest that $Ti_5Si_3$ NWs could serve as a promising candidate for future field emission devices. Growth mechanism of the $Ti_5Si_3$ NWs will be further discussed in the next chapter.

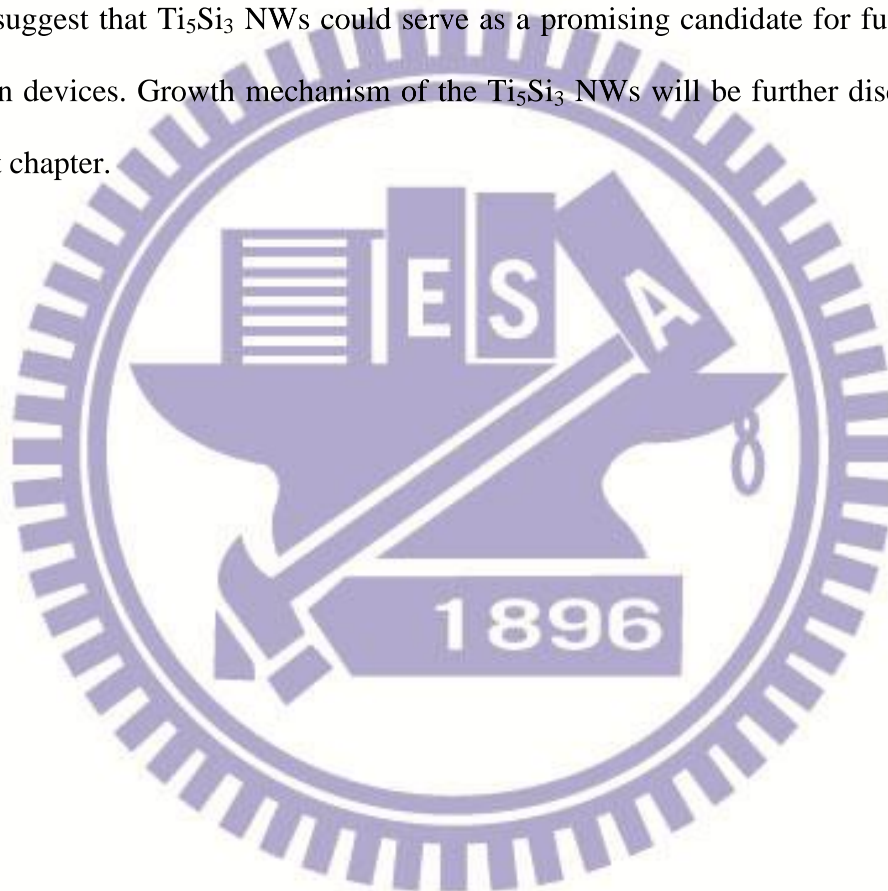

## 2.6 References

(1) Cui, Y.; Wei, Q.; Park, H.; Lieber, C. M. *Science* **2003**, *293*, 1289.

(2) Huang, M. H.; Mao, S.; Yan, H.; Wu, Y.-Y.; Kind, H.; Weber, E.; Russo, R.; Yang, P.-D. *Science* **2001**, *292*, 1897.

(3) Huang, Y.; Duan, X.; Wei, Q.; Lieber, C. M. *Science* **2001**, *291*, 630.

(4) Heer, W. A.; Chatelain, A.; Ugarte, D. *Science* **1995**, *270*, 1179.

(5) Tzeng, Y.-F.; Lee, Y.-C.; Lee, C.-Y.; Lin, I-N.; and Chiu H.-T. *Appl. Phys. Lett.* **2007**, *91*, 063117.

(6) (a) Zhou, X.-T.; Lai, H.-.; Peng, H.-Y.; Au, F. C.-K.; Liao, L.-S.; Wang, N.; Bello, I.; Lee, C.-S.; Lee, S.-T. *Chem. Phys. Lett.* **2000**, *318*, 58. ; (b) Wang, C.-H.; Lin, H.-K.; Ke, T.-Y.; Palathinkal, T. J.; Tai, N.-H.; Lin, I-N.; Lee, C.-Y.; and Chiu H.-T. *Chem. Mater.* **2007**, *19*, 3956.

(7) Tseng, Y.-K.; Huang, C.-J.; Cheng, H.-M.; Lin, I-N.; Liu, K.-S.; Chen, I-C. *Adv. Funct. Mater.* **2003**, *13*, 811.

(8) Chueh, Y.-L.; Ko, M.-T.; Chou, L.-J.; Chen, L.-J.; Wu, C.-S.; Chen, C.-D. *Nano Lett.* **2006**, *6*, 1637.

(9) (a) Xiang, B.; Wang, Q.-X.; Wang, Z.; Zhang, X.-Z.; Liu, L.-Q.; Xu, J.; Yu, D.-P. *Appl. Phys. Lett.* **2005**, *86*, 243103. (b) Du, J.; Du, P. -Y.; Hao, P.; Huang, Y.-F.; Ren, Z.-D.; Han, G.-R.; Weng, W.-J.; Zhao, G.-L. *J. Phys. Chem. C* **2007,** *111*, 10814.

(10) (a) Seo, K.; Varadwaj, K. S. K.; Cha, D.; In, J.; Kim, J; Park, J.; Kim, B. *J. Phys. Chem. C* **2007,** *111*, 9072. (b) Szczech, J. R.; Schmmitt, A. L.; Bierman, M. J.; Jin, S. *Chem. Mater.* **2007**, *19*, 3238.

(11) (a) Quyang, L.; Thrall, E. S.; Deshmukh, M. M.; Park, H. *Adv. Mater.* **2006**, *18*, 1437. (b) Schmitt, A. L.; Bierman, M. J.; Schmeisser, Dieter.; Himpsel, F. J.; Jin S. *Nano Lett.* **2006**, *6*, 1617. (c) Varadwaj, K. S. K.; Seo, K.; In, J.; Mohanty, P.; Park, J.; Kim, B. *J. Am. Chem. Soc.* **2007**, *129*, 8594.

(12) (a) Schmitt, A. L.; Zhu, L.; Schmeiber, D.; Himpsel, F. J.; Jin, S. *J. Phys. Chem. B* **2006**, *110*, 18142. (b) Seo, K.; Varadwaj, K. S. K.; Mohanty, P.; Lee, S.; Jo, Y.; Jung, M.-H.; Kim, J.; Kim, B. *Nano Lett.* **2007**, *7*, 1240.

(13) (a) Song, Y.; Jin, S. *Appl. Phys. Lett.* **2007**, *90*, 173122. (b) Song, Y.; Schmitt, A. L.; Jin, S. *Nano Lett.* **2007**, *7*, 965.

(14) Chen. L.-J. *Silicide Technology for Integrated Circuits*; IEE : London, 2004.

(15) Bucher, E.; Schultz, S.; Lux-Steiner, M. C.; Munz, P.; Gubler, U.; Greuter, F. *Appl. Phys. A* **1986**, *40*, 71.

(16) Maex, K.; Rossum, M. V. *Properties of Metal Silicides*; IEE: London, 1995.

(17) Murarka, S. P.; Fraser, D. B. *J. Appl. Phys.* **1980**, *51*, 350.

(18) Bennett, P. A.; Ashcroft, B.; He, Z.; Tromp, R. M. *J. Vac. Sci. Technol., B* **2002**, *20*, 2500.

(19) Hsu, H.-C.; Wu, W.-W.; Hsu, H.-F.; Chen, L.-J. *Nano Lett.* **2007**, *7*, 885.

(20) Choi, S.-S.; Jung, M.-Y.; Joo, M.-S.; Kim, D.-W.; Park, M.-J.; Kim, S.-B.; Jeon, H.- T. *Surf. Interface Anal.* **2004**, *36*, 435.

(21) Lee, C.-Y. *Chem. Vap. Deposition* **1999**, *5*, 69.

(22) Wagner, R. S.; Ellis, W. C. *Appl. Phys. Lett.* **1964**, *4*, 89.

(23) Ameen, M. S.; Leusink, G.; Hillman, J. T. US Patent 5926737, 1999.

(24) (a) Reynolds, G. J.; Cooper, C. B.; Faczl, P. J. *J. Appl. Phys.* **1989**, *65*, 3212. (b) Southwell, R. P.; Seebauer, E. G. *J. Vac. Sci. Technol., A* **1995**, *13*, 221

(25) Southwell, R. P.; Seebauer, E. G. *J. Electrochem. Soc.* **1997**, *144*, 2122.

(26) Wang, M. H.; Chen, L. J. *J. Appl. Phys.* **1992**, *71*, 5918.

(27) Fowler, R. H.; Nordheim, L. W. *Proc. R. Soc. London, Ser. A* **1928**, *119*, 173.

# Chapter 3

# Chemical Vapor Deposition of TiSi Nanowires on C54 $TiSi_2$ Thin Film – An Amorphous Titanium Silicide Interlayer Assisted Nanowire Growth

## 3.1 Introduction

Metal silicides, including silicides of Ti, Cr, Fe, Co and Ni, are intensively investigated because their unique physical and chemical properties could meet the requirements of modern technological applications.[1] Among the silicides, titanium silicides show high thermal stability, low electrical resistivity, low work function, and low density.[1-4] These properties make titanium silicides good candidates for enhanced electronic field emission source, field ionization source, interconnect in nanoelectronics, and solar energy assisted catalytic water splitting.[5-10] For many metal silicides, varying the synthesis conditions could alter the metal to silicon composition ratio and the crystal phase. Consequently, properties of the silicides are changed as well. Thus, it is possible to prepare silicide samples with diverse properties within one reaction system. For titanium silicides, there are six reported phases, including C54-$TiSi_2$, C49-$TiSi_2$, TiSi, $Ti_5Si_4$, $Ti_5Si_3$ and $Ti_3Si$.[11,12] Among them, C54-$TiSi_2$ is the most studied for its applications in microelectronic devices. C54-$TiSi_2$ has a low electrical resistivity 10 – 28 μΩcm and a high melting point 1773 K.[1,2,13] The other disilicide C49-$TiSi_2$, with a higher electrical resistivity ca. 100 μΩcm, is considered to be a low temperature metastable phase before the formation of C54-$TiSi_2$.[14] $Ti_5Si_3$ is a

promising high temperature material for protective refractory coating because of its high melting point 2403 K, excellent creep resistance, and high oxidation resistance.[1,15-17] For the remaining silicides TiSi, $Ti_5Si_4$ and $Ti_3Si$, applications were seldom reported due to the difficulties of preparing them in pure-phases. [2,18-24] For example, $Ti_3Si$ has rarely been described in related research because it is easily destabilized by oxygen in the processing. TiSi is another silicide with limited reports. In contrast to $Ti_3Si$, TiSi may have interesting applications because it has a high melting point 1843 K, a low electrical resistivity 60 μΩcm, and one of the highest mechanical hardness (Hμ) 18.0 among all titanium silicides.[1,3,25] Nonetheless, to this date, methods to fabricate TiSi in quantities suitable for extensive studies are limited.[22,26-28] Thus, searching for new techniques to synthesize TiSi is important in silicide research. In general, three types of techniques are commonly employed to prepare titanium silicides. The first type is powder based methods. These include arc melting and self-propagating exothermic reactions, such as ball milling, shock loading, and thermal ignition of stoichiometric mixtures of elemental powders.[18] The second one is physical vapor deposition (PVD) processes. They are frequently used to grow titanium silicide thin films. A well-known example is the salicide process.[13,29,30] It includes two steps, evaporation of Ti or coevaporation of Ti and Si atoms onto Si substrates, followed by annealing the as-deposited thin film at a high temperature to form silicides. The last one is chemical vapor deposition (CVD) reactions. By reacting $TiCl_4$ with silane or silicon chlorides at high temperatures, titanium silicide thin films can be grown.[21,31-33] CVD provides possibilities to prepare kinetically stable phases which are difficult to obtain using the other methods. Recently, by employing variations of the fabrication methods mentioned above, preparations of nanosized one-dimensional (1D) silicides of Ti, V, Cr, Mn, Fe, Co, Ni, and Ta have been reported.[5,6,34-60] For titanium silicides, these include nanowires (NWs) of TiSi and

C54-$TiSi_2$, nanopins (NPs) of TiSi, nanobats of $Ti_5Si_4$, and nanonets (NNs) of C49-$TiSi_2$, as listed in Table 3.1.[5,6,34,35,37,38] Previously, we have communicated the growth of $Ti_5Si_3$ NWs on top of C54-$TiSi_2$ thin films grown by reacting titanium subhalides $TiCl_{x(g)}$, generated by passing $TiCl_{4(g)}$ over $Ti_{(s)}$ at 1173 K, with Si substrates in a CVD process.[36] Herein, we wish to report our further investigation on this unique titanium silicide fabrication process. We have discovered that in addition to $Ti_5Si_3$ NWs, dense TiSi NW arrays can be grown by this process after adjusting the reaction parameters. In addition, this study shows the existence of an amorphous $TiSi_{2-x}$ layer between the NWs and the C54-$TiSi_2$ film below them. Importance of the amorphous $TiSi_{2-x}$ layer to the NW growth and electron field emission (EFE) properties of the NW array will also be discussed.

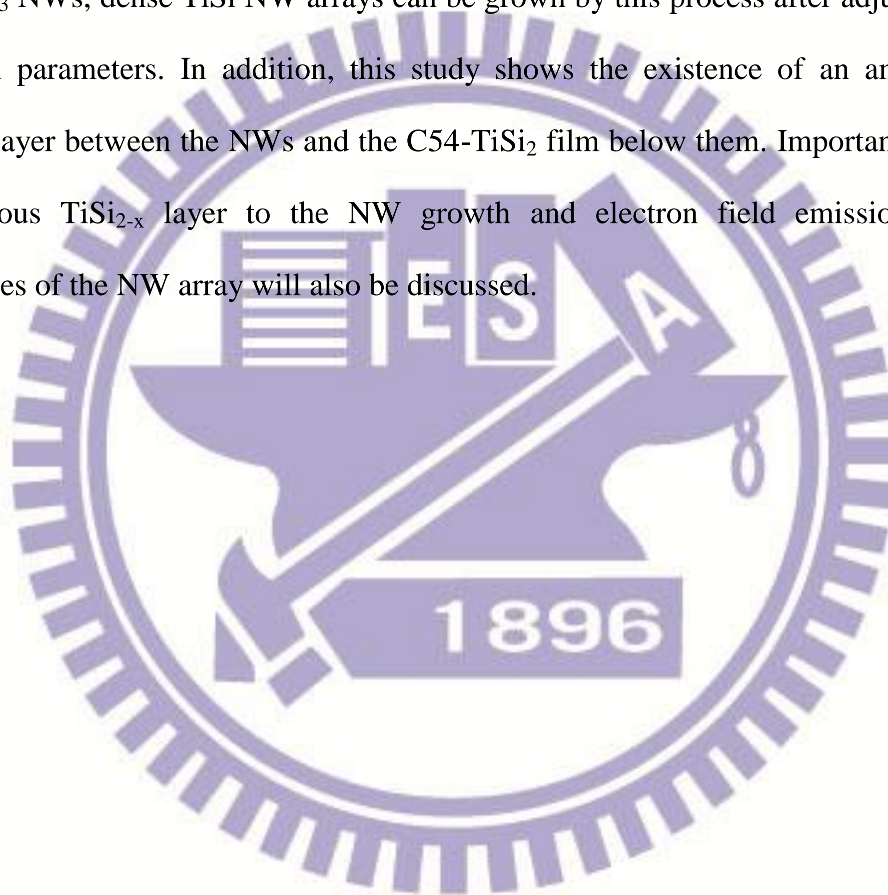

**Table 3.1** Summary of Titanium Silicide Samples

| Reference Sample | Process, Product, Morphology, and Phase | NWs Length/ Film Thickness | Growth Conditions | | $E_o$ ($V\mu m^{-1}$) | $\beta$ | $J_{max}$ ($\mu Acm^{-2}$) |
|---|---|---|---|---|---|---|---|
| | | | Temperature (K) | Time (min) | | | |
| Ref 5 | PVD (Ti powder / Si wafer) $C54\text{-}TiSi_2$ NWs | tens to hundred micrometers | 1073 | 180 | 8 | 501 | 0.23 |
| Ref 6 | PVD (Si powder / Ti foil) $Ti_5Si_4$ Nanobat | 350 nm | 1073 | 180 | 1.47[a] | 1350 | 0.36 |
| Ref 35 | CVD ($TiCl_4$, $SiH_4$ / borosilicate) TiSi NPs and NWs on $Ti_5Si_3$ film | 0.7 - 1 μm / 2 μm | 963 - 1023 | 1 - 36 | -[b] | -[b] | -[b] |
| Ref 37 | CVD ($TiCl_4$, $SiH_4$ / Si wafer) $C49\text{-}TiSi_2$ Nanonet | 2 - 10 μm | 948 | 15 | -[b] | -[b] | -[b] |
| Ref 38 | CVD ($TiCl_4$, $SiH_4$ / Si wafer) $C54\text{-}TiSi_2$ NWs | 2 - 10 μm | 898 - 973 | -[b] | -[b] | -[b] | -[b] |
| This Study | Morphologies and Phases | NWs Length/ Film Thickness | Temperature (K) | Time (min) | $E_o$ ($V\mu m^{-1}$) | $\beta$ | $J_{max}$ ($\mu Acm^{-2}$) |
| **I** | TiSi NWs on $C54\text{-}TiSi_2$ film | 2-5 μm / 10.5 μm | 1073 | 60 | 5.25 | 876 | 0.48 |
| **II** | Partial $C54\text{-}TiSi_2$ film | - | 1073 | 10 | -[c] | -[c] | -[c] |
| **III** | Short TiSi NWs on $C54\text{-}TiSi_2$ film | 0.5 - 3 μm / 8 μm | 1073 | 30 | 8.5 | 418 | 0.07 |
| **IV** | $C54\text{-}TiSi_2$ film | 2.6 μm | 973 | 60 | 10.4 | 343 | 0.014 |
| **V** | $Ti_5Si_3$ NWs on $C54\text{-}TiSi_2$ film | 2-5 μm / 6 μm | 973 | 360 | 5.4 | 816 | 0.18 |

[a] The $E_o$ is defined as the current density reaches 1 $\mu Acm^{-2}$. [b] Not reported.
[c] Partially formed $TiSi_2$ film does not emit electrons.

## 3.2 Experimental Section

### 3.2.1 Growth of Titanium Silicide Samples

Thin films and NWs of titanium silicide samples were grown by a low pressure CVD (LPCVD) using a horizontal hot-wall quartz tube reactor heated by a three-zone tube furnace (Lindberg 55346). Si(100) (n-type, 0.7 cm × 1.5 cm × 0.525 mm) wafers, pretreated by a standard RCA cleaning process, were placed at the center inside the reactor, which was at zone 2. Ti powders (0.4 g, Aldrich 99.7%) in a quartz boat were placed at zone 1, which was upstream from the Si substrates. To reduce $O_2$ and $H_2O$ partial pressures, the reactor was first purged with Ar then evacuated below 0.4 Pa before the reaction began. After zone 1 was heated to 1173 K and zone 2 reached 973-1073 K, $TiCl_4$ (Fluka 99%) kept at 298 K was vaporized into the reactor. The evaporation of $TiCl_4$ was controlled at a pressure of 2.67 Pa for 10 min to 6 h, depending on the experiments, by a low-flow metering needle valve (Swagelok, SS-SS4). The amount of $TiCl_4$ introduced was 0.42 mL/h. Assuming that the evaporation rate was constant, the flow rate of the $TiCl_4$ was estimated to be 12 mg/min (0.063 mmol/min). After the vaporization was stopped, the furnace was allowed to cool to room temperature. Deposition of gray to black films on the wafers was observed. Detailed experimental parameters for samples investigated in this study are summarized in Table 3.1.

### 3.2.2 Instruments for Characterizations

Scanning electron microscopic (SEM) images and energy dispersive X-ray spectra (EDX) of the samples were taken with a Hitachi S-4700I and a JEOL JSM-7401F operated at 15 keV. High-resolution transmission electron microscopic (HRTEM) images and EDX were acquired on a scanning transmission electron

microscope (STEM) JEOL JEM-3000F at 300 kV. A cross-sectional TEM sample was prepared using a dimpling and ion milling technique.[61] X-ray diffraction (XRD) patterns of the samples were obtained using a Bruker AXS D8 ADVANCE with Cu K$\alpha$1 radiation.

EFE measurements were carried out using a home-built apparatus, composed of a vacuum chamber and a spherical-shaped tungsten probe (diameter 1 mm) as the anode. The sample-to-anode distances were adjustable by a manipulator equipped with a micrometer. All measurements were taken below $1.05 \times 10^{-3}$ Pa at room temperature. Current-to-voltage (I — V) characteristics were measured using a Keithley 237 or 2410. The maximum applied voltage was 1100 V while the current was restricted to 10 mA. Sheet resistances of the samples were measured by a four-probe method using a Mitsubishi MCP-T600 resistivity meter.

## 3.3 Results and Discussion

In a typical reaction, $TiCl_4$ was vaporized into a hot-wall LPCVD reactor loaded with Ti powders at the heating zone at 1173 K, which was upstream from Si (100) substrates placed at the center heating zone at 973 – 1073 K. The reaction between $TiCl_4$ and Ti generated gaseous titanium subchlorides $TiCl_x$, which would undergo disproportionation to regenerate $TiCl_4$ and to deposit Ti.[62] Depending on the reaction time employed, from 10 min to 6 h, growth of products composed of gray to black thin films on the substrates was observed. In Table 3.1, effects of varying the reaction parameters on morphology and phase of the products are summarized. In this report, we will discuss more on characterizations of the samples deposited at 1073 K, including **I** and **III**, the vertically grown long and short single crystalline TiSi NWs, respectively. We will not focus on samples grown at 973 K, C54-$TiSi_2$ thin film (**IV**) and $Ti_5Si_3$ NWs (**V**) because we have reported their fabrications in chapter 4.

## 3.3.1 SEM and EDX Characterizations

SEM images of **I** are shown in Figure 3.1. Figure 3.1a is a low magnification top-view image of **I**, revealing the presence of high density 1-D nanostructures on the deposited product. The EDX spectrum shown in the inset of Figure 3.1a suggests that **I** is composed of Ti and Si only. A high magnification image in Figure 3.1b shows that the 1-D nanostructures are NWs with diameters of 30－80 nm. We do not observe metal particles on the tips of the NWs. This suggests that the NWs were not grown via a vapor－liquid－solid (VLS) mechanism.[63] Figure 3.1c displays a side-view image of **I**, indicating that the product deposited on the substrate is composed of a film (thickness 10.5 μm) and above it, a layer of NWs pointing upward. An enlarged side-view image of the NWs in Figure 3.1d shows that the NW lengths are 2-5 μm.

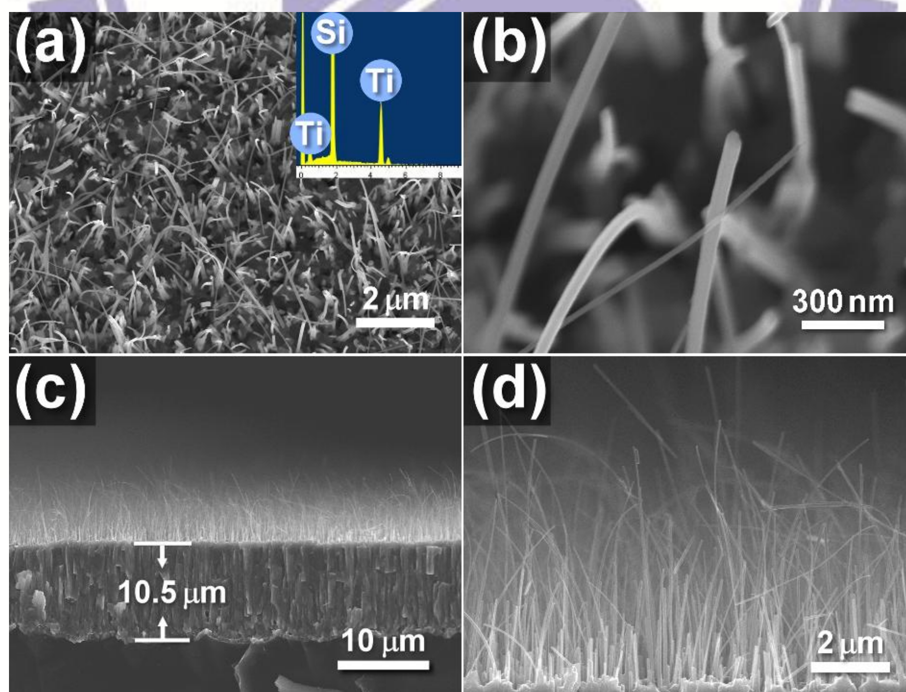


**Figure 3.1** SEM images of I grown on Si. (a) Top-view and EDX (inset), (b) high magnification image, (c) low magnification side-view, and (d) high magnification side-view image.

Figure 3.2 displays the images of **II** – **V**, the products prepared at different conditions. When the growth time was 10 min, sample **II** was obtained. As shown in Figure 3.2a, the Si substrate is partially covered (ca. 20%) by irregularly shaped islands with areas of tens to hundreds of $\mu m^2$. Unlike sample **I**, we could not find the presence of any 1-D nanostructure on the substrate of **II**. The rugged surface islands, shown in the side-view SEM image in the inset of Figure 3.2a, imply that they might be formed by etching and deposition reactions involving the Si surface and the gaseous $TiCl_x$ molecules.[64,65] Figure 3.2b shows the image of sample **III**, obtained after the reaction was carried out for 30 min at 1073 K. Growth of numerous NWs with lengths 0.5—3 μm on top of a thin film with a thickness of 8 μm is observed. Comparing samples **I** - **III**, we conclude that only a thin film was grown at the early stage of the reaction. After a certain period of time, NWs started to grow on the film. As the reaction time was lengthened, density and length of the NWs increased accordingly.

The SEM image (Figure 3.2c) of sample **IV**, which was grown at 973 K for 1 h, shows the presence of few and scattered NWs on a layer of thin film.[36] When the growth time was extended, the NWs elongated as well. For example, Figure 3.2d demonstrates the image of sample **V**, which was grown at 973 K for 6 h. It displays the growth of abundant thread-like NWs, diameter ca. 20 – 50 nm and length up to several micrometers, on top of a thin film. The above observations suggest that, before the growth of 1-D titanium silicide NWs (characterization of the products by XRD and TEM will be discussed below), an adequate reaction time was required to allow the initial deposition of a layer of titanium silicide thin film on the Si substrate.

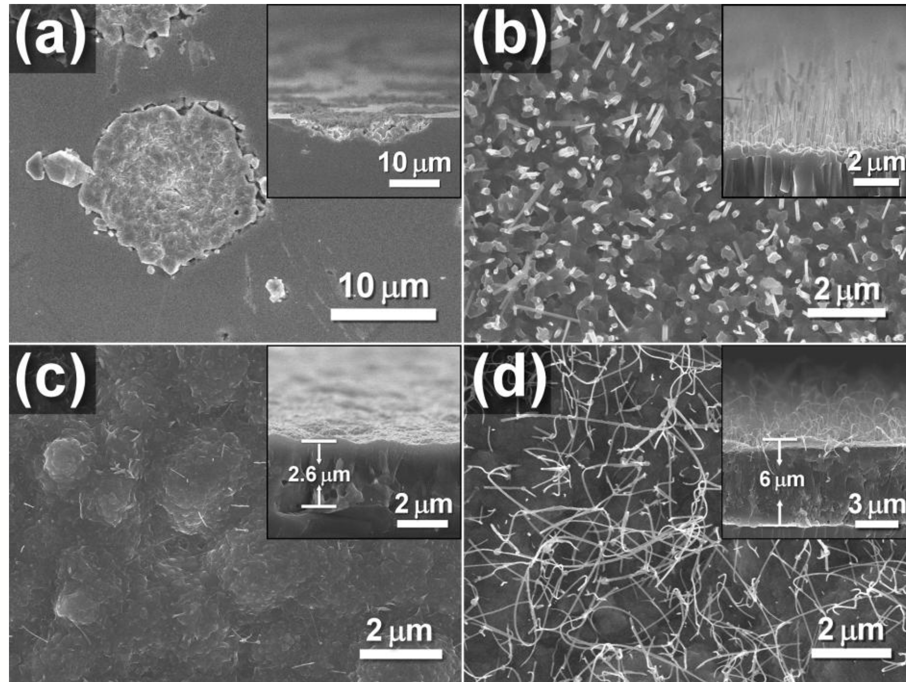


**Figure 3.2** SEM top-view and side-view (inset) of (a) II, (b) III, (c) IV, and (d) V.

## 3.3.2 XRD Characterizations

XRD patterns of the samples **I** – **V** are shown in Figure 3.3. All of them display four diffraction peaks marked by gray circles at $2\theta = 39.1^o$, $42.2^o$, $43.2^o$, and $49.7^o$. This set of peaks indicates the presence of orthorhombic C54-$TiSi_2$ (JCPDS 35-0785) as the major product. Since all of the samples have a layer of thin film several micrometers thick, we conclude that all of the thin films are composed of C54-$TiSi_2$. In addition to the C54-$TiSi_2$ pattern, sample **I** shows a strong peak at $2\theta = 50.3^o$, which is marked by a blue square in Figure 3.3. This signal is also observed for **III**, the sample with short NWs, but not for **II**, which does not show any 1D nanostructure in the SEM image. The peak is assigned to the reflection from {020} plane of orthorhombic TiSi (JCPDS 17-0424). In Figure 3.4a, a detailed XRD scan of **I** taken at $2\theta = 25 - 38^o$ was demonstrated. The diffraction peaks observed at $2\theta = 32.83^o$, $35.3^o$, and $36.93^o$ were indexed to be the reflections from TiSi {201}, {002}, and {210} planes, respectively. Thus, we conclude that in **I**, the NWs on top of the thin film, as

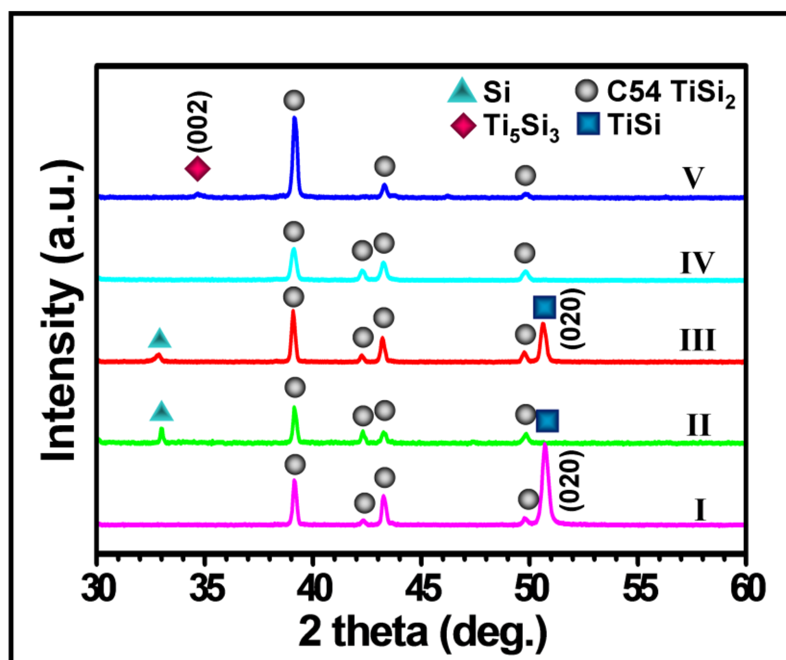


**Figure 3.3** XRD patterns of I - V. Assignment of peaks: spheres, C54-$TiSi_2$; square: TiSi (020); diamond: $Ti_5Si_3$ (002); triangle: Si (020), this forbidden signal only appears in several samples grown on a specific batch of Si substrates. For clarity, Si (400) at 69.2$^o$ is not shown.

shown in Figure 3.1, are composed of TiSi. These data differ slightly from the standard XRD pattern of TiSi. We suggest that unlike randomly oriented TiSi crystals in powders, **I** contains TiSi NWs with a preferred growth orientation in [020] direction. This is further confirmed by TEM studies and will be discussed below. All samples also showed a very strong signal at 69.2$^o$. This was assigned to Si {400} planes from the substrates. For clarity, it is not displayed in Figure 3 (see Figure 3.4b for a pattern of **I** with the substrate signal). For sample **IV**, only diffraction peaks of C54-$TiSi_2$ are observed. Accordingly, **IV** is determined to be a film composed of C54-$TiSi_2$. For sample **V**, in addition to the pattern of C54-$TiSi_2$, a weak diffraction peak at $2\theta = 34.8^o$ is shown. This is assigned to the reflection by {002} plane of $Ti_5Si_3$ (JCPDS 78-1429), the main component of the NWs in **V**. The XRD observation is in good agreement with the TEM result, which indicates that the preferred growth direction of the NWs is along [002] axis of $Ti_5Si_3$.[36] We speculate whether isolated Ti

and Si crystals could be grown during the reactions because $TiCl_x$ and $SiCl_x$ byproducts were known to deposit thin films in their elemental forms.[62,66] However, the XRD results do not show any peak which can be assigned to Ti and Si crystals.

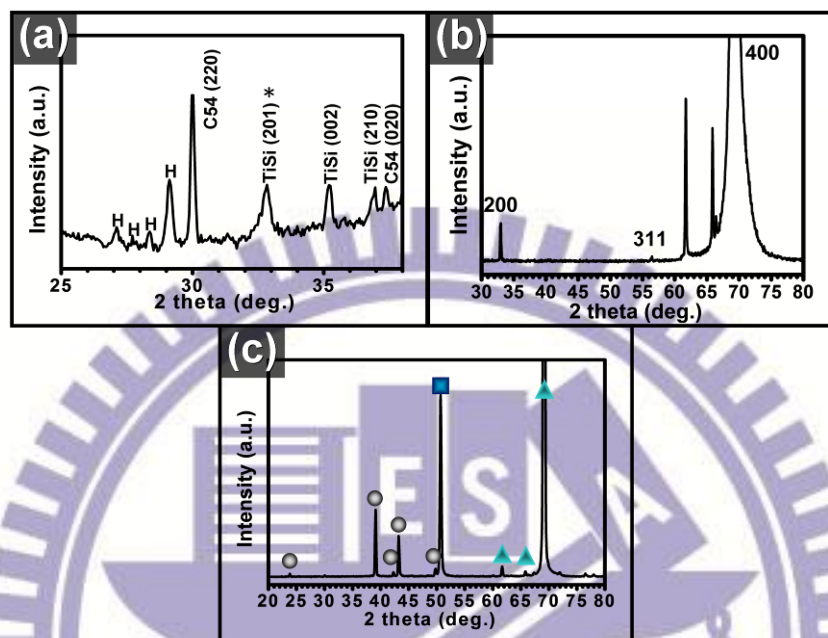


**Figure 3.4** (a) Detailed XRD of I from 25° to 38°, (b) XRD of I from 20° to 80° (spheres, C54-$TiSi_2$; square: TiSi; triangles: Si), and (c) XRD of the Si wafer used to grow silicides in samples I – III. 33.2°: Si (200), 56.5°: Si (311), 69.5°: Si (400), 61.7° and 65.9°: unable to assign.

**Table 3.2** Assignments of the XRD Peaks in Figure 3.4

| XRD 2θ | Crystal Phase (hkl) | | Calculated Value [a] | | JCPDS [b] | |
|---|---|---|---|---|---|---|
| | | | 2θ | Intensity ratio | 2θ | Intensity ratio |
| 30.02 | C54-$TiSi_2$ | (220) | 30.05 | 9 | 30.04 | 10 |
| 32.83 | TiSi | (201) | 32.68 | 32 | 32.83 | 20 |
| 35.3 | C54-$TiSi_2$ | (212) | 35.5 | 0 | - [c] | - |
| | TiSi | (002) | 35.8 | 0 | - | - |
| 36.93 | TiSi | (210) | 36.92 | 99 | 36.91 | 100 |
| 37.38 | C54-$TiSi_2$ | (020) | 37.44 | 0 | - | - |

[a] Calculated from ICSD C54-$TiSi_2$ : 96029, TiSi : 43494.

[b] JCPDS C54-$TiSi_2$ : 35-0785, TiSi : 17-0424. [c] Not reported.

### 3.3.3 TEM Studies of TiSi NWs

Figure 3.5a displays a representative TEM image of a section of a single NW obtained from **I**. The sample has a diameter ca. 80 nm and a length ca. 1 μm. The selected-area electron diffraction (SAED) pattern in Figure 4b, taken from the circled region in Figure 3.5a, suggests that the NW is single crystalline. The observed spots are determined to be from {200}, {210}, and {010} planes of orthorhombic TiSi with [001] zone axis. In Figure 3.6, the results from another NW, with dimensions similar to those of the one displayed in Figure 3.5, were shown. The SAED pattern in Figure 3.6c also confirmed that the NW was single crystalline. The diffraction spots were determined to be from {010}, {011}, and {001} planes of orthorhombic TiSi with [100] zone axis. From Figures 3.5c and 3.6c, the lattice parameters *a*, *b*, and *c* are calculated to be 0.65, 0.36, and 0.49 nm, respectively. They are close to the values of TiSi (JCPDS 17-0424), 0.654, 0.364, and 0.499 nm, respectively. Figure 3.5c exhibits the HRTEM image from the same region. The estimated lattice spacings 0.16, 0.24, and 0.18 nm are assigned to {400}, {210}, and {010} planes, respectively. From the HRTEM image shown in Figure 3.6d, the observed lattice spacings 0.36 and 0.49 nm were assigned to {010} and {001} planes, respectively. From the HRTEM images, *a*, *b*, and *c* are determined to be 0.64 nm, 0.36 nm, and 0.49 nm, respectively. An STEM image and the corresponding EDX line-scan profiles of an NW are shown in Figure 3.5d. The data indicates that the NW is mainly composed of Ti and Si, which distribute uniformly along the NW cross-section. A trace of residual O atoms, probably originated from the TEM sample preparation, is also observed. On the basis of the results from the XRD and the TEM studies, the NWs in **I** are determined to be single crystalline TiSi with a preferred growth in [010] direction. Since an NW from sample **III** showed TEM data identical to those shown in Figure 4, we conclude that

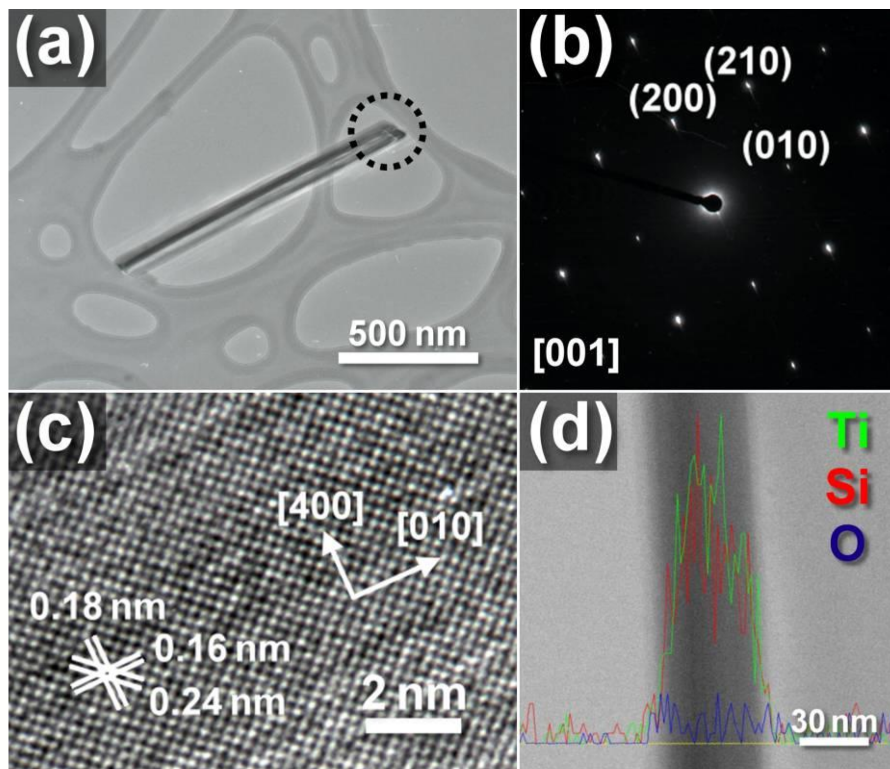


**Figure 3.5** (a) TEM image of a NW isolated from I, (b) SAED pattern and (c) HRTEM image from the circled region in (a), and (d) TEM and EDX elemental line profiles of another NW from I.

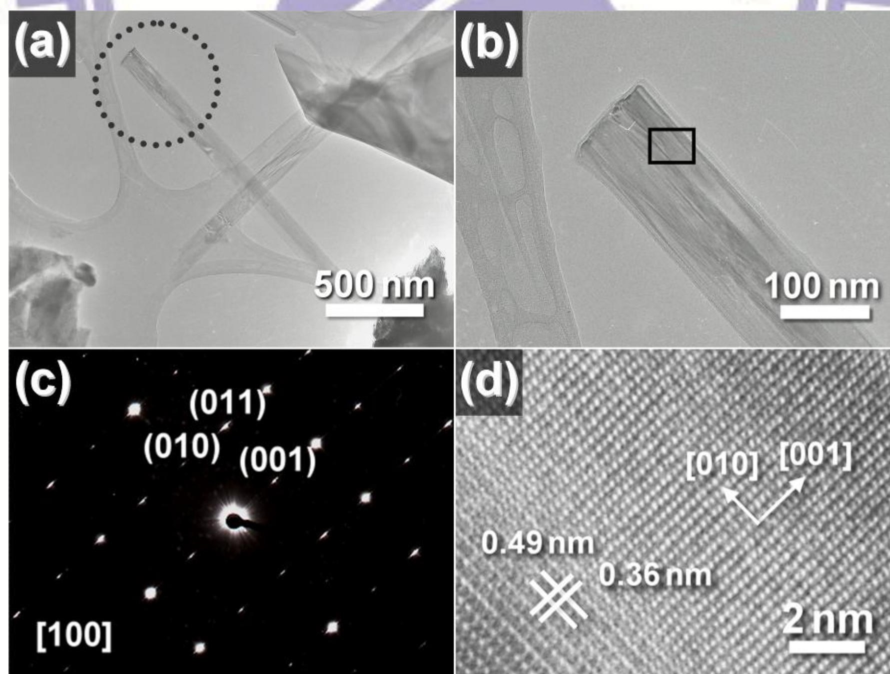


**Figure 3.6** (a) TEM image of a NW isolated from I, (b) high magnification image from (a), (c) SAED pattern from the circled region in (a), and (d) HRTEM image of the squared area in (b).

the NWs in **III** were single crystalline TiSi also. On the other hand, using the TEM result of an NW in **V** in the last chapter, we determined that it was a single crystalline titanium rich silicide, $Ti_5Si_3$, grown preferentially along the [001] direction.[36]

### 3.3.4 Characterization of the Interface between TiSi NWs and C54 $TiSi_2$ Film

From cross-sectional SEM images of **I** (Figures 3.7a and 3.7b), a layer of thin film, with a slightly different contrast and a thickness ca. 600 nm, was observed between the NWs and the C54-$TiSi_2$ film deposited on the Si substrate. This phenomenon was also observed for sample **V**. On the other hand, sample **IV**, which was a C54-$TiSi_2$ film, did not show such a layer, as shown in Figures 3.7c and 3.7d.

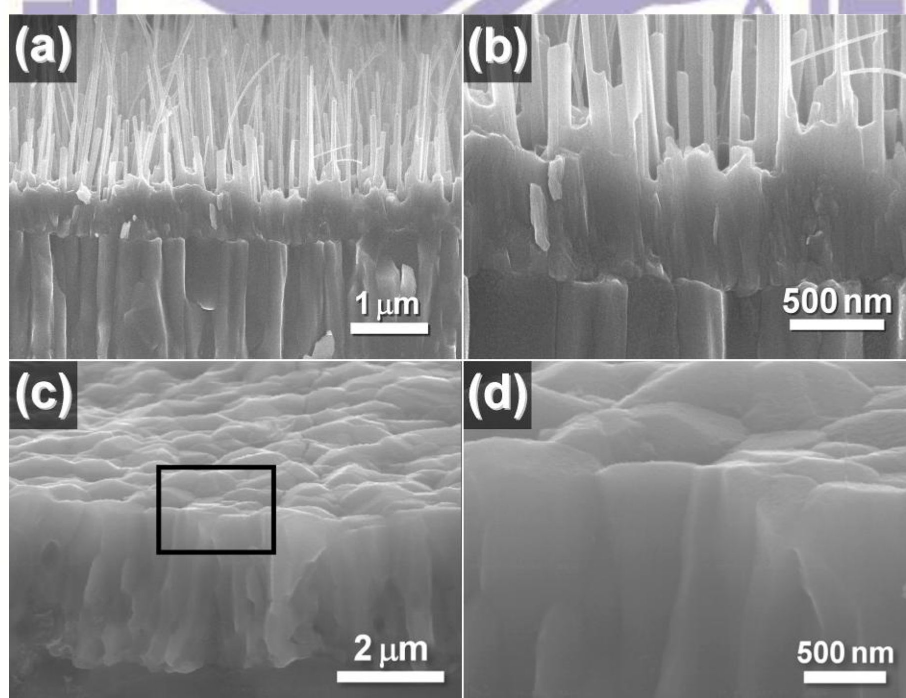


**Figure 3.7** (a) SEM side-view of I showing an interlayer between TiSi NWs and a $TiSi_2$ film, (b) enlarged view of (a), (c) SEM side-view of IV showing a $TiSi_2$ thin film, and (d) enlarged view of the rectangular region in (c).

EDX analyses of the interlayers and the films of **I** and **V** were carried out at the spots shown in Figure 3.8 The Ti contents of the interlayers were higher than those of the films below. In addition, the Ti/Si ratios of the interlayers of **I** and **V** were 0.88 and 1.57, respectively. The chemical compositions of both interlayers coincided well with those of the NWs grown on top of them. Thus, it appears that the composition and the crystal structure of the NWs are highly influenced by the interlayers. Furthermore, the EDX line-scans of **I** and **V** in Figure 3.9 revealed that the Si contents of the interlayers were lower than those of the films below them.

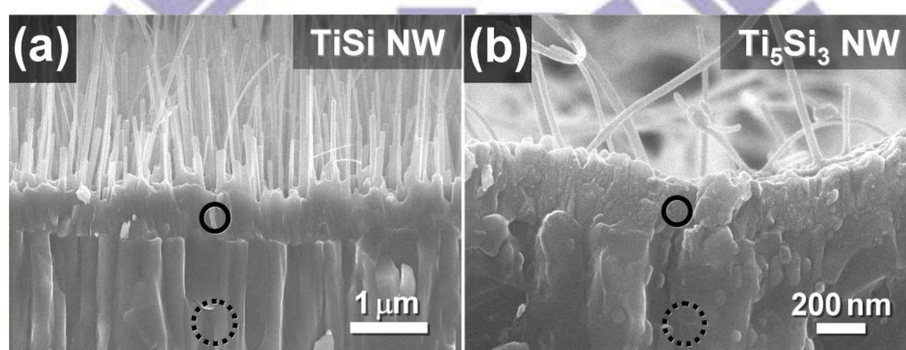


**Figure 3.8** SEM EDX analyses of (a) I and (b) V. Chemical compositions of the circled areas are listed below.

| Sample | Ti, Atomic % | Si, Atomic % |
|---|---|---|
| Interlayer of **I**, solid circle | 46.7 | 53.3 |
| Thin film of **I**, dashed circle | 31.7 | 68.3 |
| Interlayer of **V**, solid circle | 61.1 | 38.9 |
| Thin film of **V**, dashed circle | 39.9 | 60.1 |

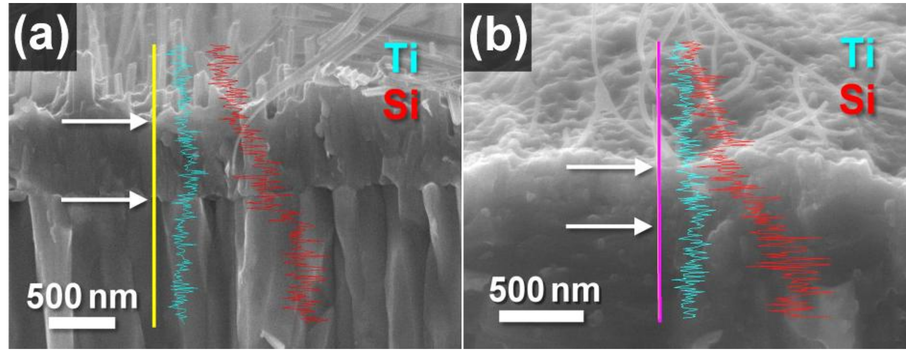


**Figure 3.9** Cross-sectional SEM EDX line-scans of (a) I and (b) V. The arrows mark the limits of the interlayers.

The interlayer between the NWs and the silicide film may provide clues to explain how and why the NWs grew in this study. Therefore, we carried out a TEM investigation of the interlayer of **I**. A thin slice of cross-section of **I** was prepared by the use of the dimpling and ion milling technique.[61] In Figure 3.10, presence of vertically grown NWs on the bottom film was shown. Unfortunately, this region was too thick for detailed HRTEM and SAED characterizations. Figure 3.11 demonstrated TEM studies from another area on the slice. This region was thin enough for detailed investigations. Except a couple of NW roots, all the NWs on the slice were removed in the polishing process. A layer with a thickness 20 - 200 nm and uneven boundary was observed in the upper regions in Figures 3.11a and 3.11b. The apparent variation

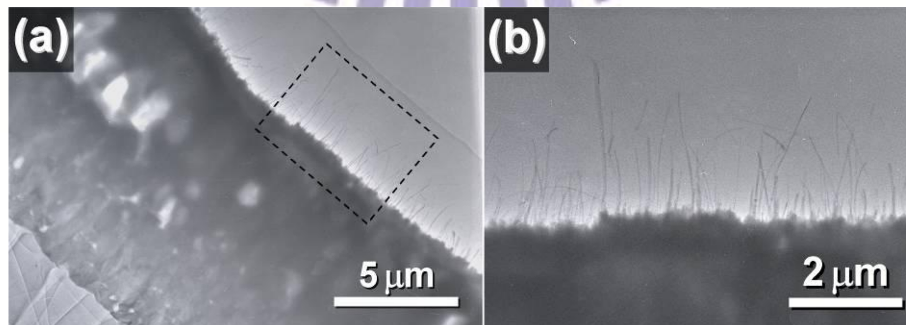


**Figure 3.10** (a) Low-magnification cross-sectional TEM image of I showing the presence of NWs on top of a thin film and (b) high-magnification image of the dashed rectangular area in (a).

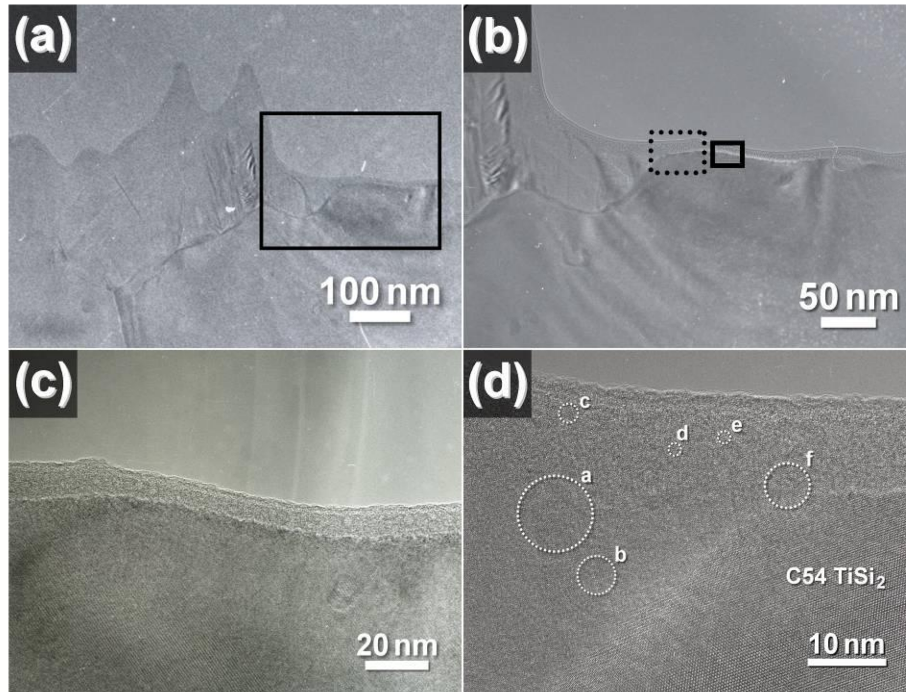


**Figure 3.11** (a) Low-magnification cross-sectional TEM image of I showing the presence of NWs on top of a thin film and (b) high-magnification image of the dashed rectangular area in (a).

of the film thickness could be the results of the irregular nature of the interlayer and the uneven processing during the sample preparation. An area of the thin layer was selected for detailed investigations (Figure 3.11b). A high magnification TEM image of this area is displayed in Figure 3.12a. It shows a top layer with a thickness ca. 10 nm. The HRTEM image (Figure 3.12b) of the rectangular area in Figure 3.12a displays the image near the interface. An amorphous layer on top of a crystalline layer can be observed. In the lower crystalline region, two sets of lattice spacings are clearly seen and are measured to be 0.23 and 0.20 nm. These coincide well with (311) and (022) lattice spacings of C54-$TiSi_2$, respectively. Figure 3.12c displays the result of an SAED study of the rectangular area shown in Figure 3.12a. The dotted pattern suggests that the single crystalline region could be indexed to [011] zone axis of orthorhombic C54-$TiSi_2$. Figure 3.12d,e presents the EDX spectra acquired from areas in the circle and the dotted circle in Figure 3.12a, respectively. The spectra confirm

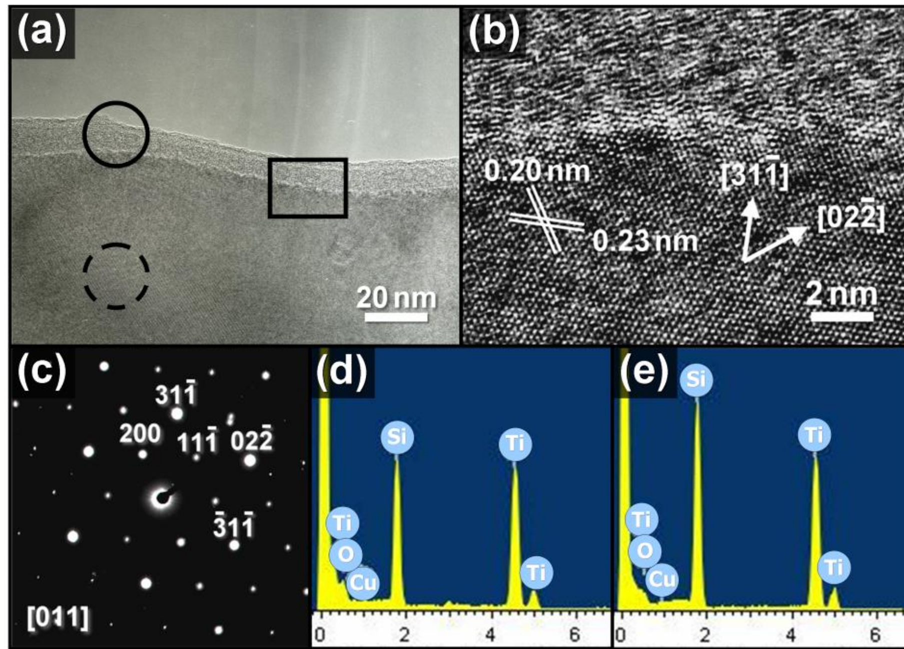


**Figure 3.12** (a) Cross-sectional TEM image of the interface in I, (b) HRTEM image and (c) SAED pattern from the solid square region in (a). EDX spectra from (d) the solid and (e) the dotted circled areas in (a). The Cu signal is from the Cu TEM grid.

that both the amorphous and the crystalline regions are mainly composed of Ti and Si. Clearly, the Ti/Si ratio of the amorphous layer is higher than that of the crystalline layer below. This is consistent with the EDX line-scan result shown in Figure 3.9. Thus, we designate the amorphous layer to have a composition $TiSi_{2-x}$, where $0 < x < 1$. This is due to the fact that along the growth direction of the layers, the Ti concentration increases while the Si concentration decreases as the reaction proceeds. Moreover, a high magnification image of the interlayer shown in Figure 3.11d indicated the presence of small crystallites. Enlarged views of some crystallites were shown in Figure 3.13. All of them displayed lattice spacings assignable to crystal planes of TiSi. Consequently, the presence of the nanocrystallites in the interlayer appears to be the key factor to induce the growth of NWs with phases different from the C54-$TiSi_2$ thin film below. Previous studies involving solid state diffusion systems have reported that amorphous titanium silicide layers at the Ti/Si interface formed

before the formation of crystalline slilicides.[67] Thus, the growth sequence of the silicide layers are determined to be in the order: growth of a $TiSi_2$ thin film on Si initially, formation of an *a*-$TiSi_{2-x}$ interlayer next, nucleation of TiSi in the interlayer subsequently, and lengthening of TiSi NWs finally. How and why the presence of the interlayer initiates the NW growth will be discussed further below.

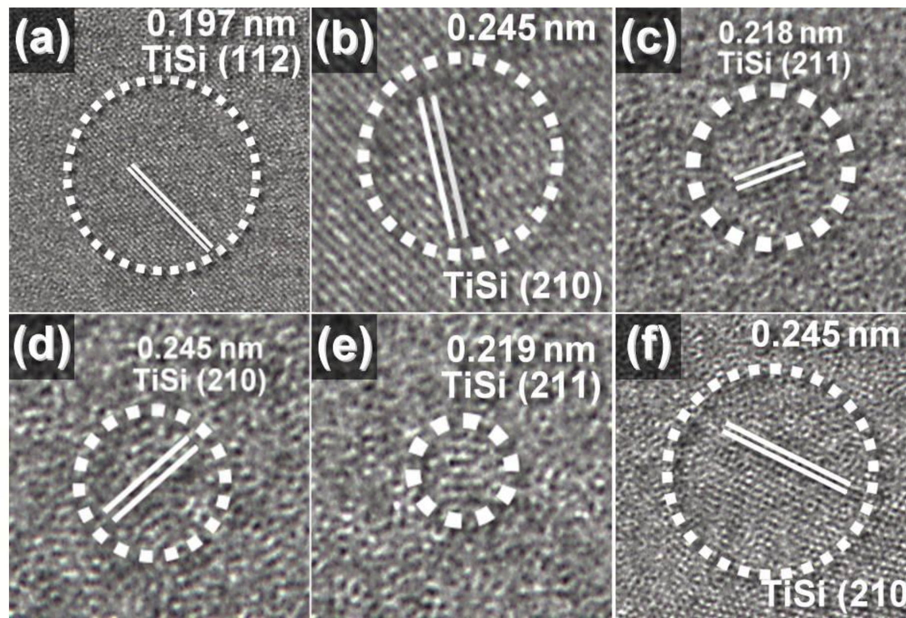


**Figure 3.13** HRTEM images of the selected crystallites shown in Figure 3.11d. Possible crystal plane assignments are designated in the images.

## 3.3.5 Growth Pathway of TiSi NWs

On the basis of the data presented above, a reaction pathway is proposed in Figure 3.14 to summarize the TiSi growth. In our CVD system, $TiCl_{4(g)}$ reacts with Ti powders to produce $TiCl_x$ subhalides at 1173 K in the first heating zone upstream from the Si substrate. Then, as the $TiCl_x$ molecules reach the substrate surface at 1073 K, they disproportionate into $TiCl_4$ molecules and Ti atoms, which deposit on the substrate surface.[62] The Ti atoms could react with the Si substrate directly to form titanium silicides, such as C54-$TiSi_2$ produced in this study. Alternatively, vapors of

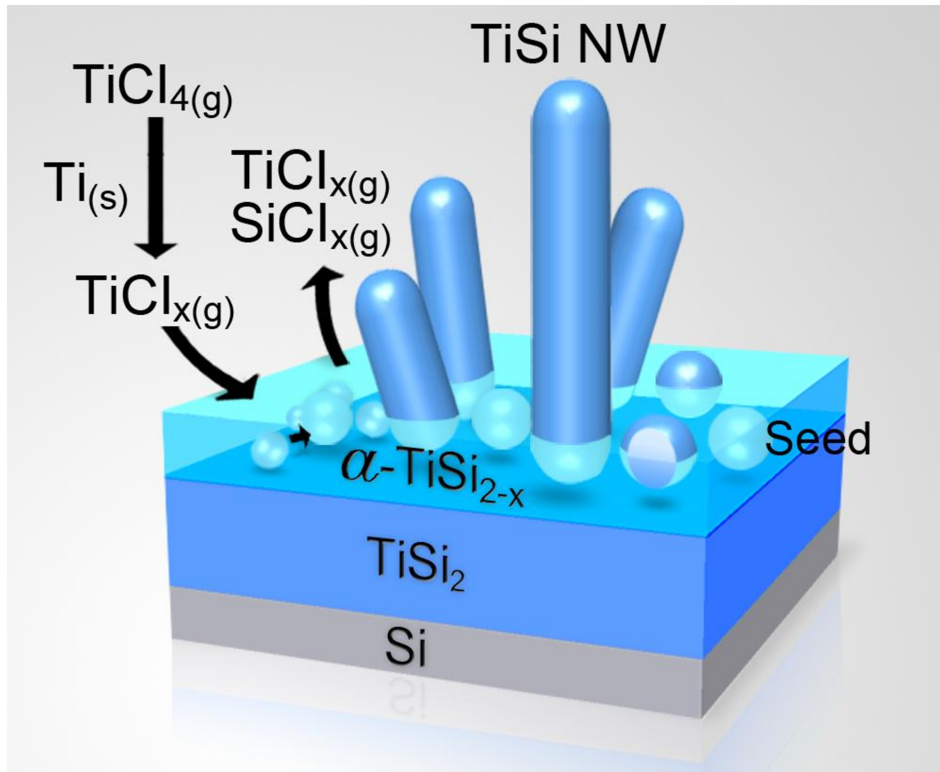


**Figure 3.14** Proposed growth pathway of the TiSi NWs. (x denotes variables).

$TiCl_4$ and $TiCl_x$ could react directly with the Si substrate to produce titanium silicides and $SiCl_x$ byproducts. $SiCl_x$ may decompose and act as another source of Si atoms for the silicide formation. After the $TiSi_2$ film grows to a certain thickness, this relatively thick and inert layer may act as a barrier to impede diffusion of Si atoms from the substrate.[68] This would hamper further interaction between the Si atoms in the substrate and the Ti atoms deposited on the surface. Consequently, the Si concentration on the surface is reduced while formation of a Si-poor *a*-$TiSi_{2-x}$ interlayer begins. We want to emphasize that the interlayer, which may be viewed as a quasi-liquid thin film, might be the key to the successful growth of titanium silicide NWs in this study.[69] After the amorphous interlayer is formed, nucleation of crystallites of a different titanium silicide phase, such as TiSi in **I** and **III**, as well as $Ti_5Si_3$ in **V** may start. Chemical composition of the interlayer, which varies with the reaction condition, affects the phase nucleated.[70] As the reaction proceeds, these

nuclei at a relatively low supersaturation condition act as the seeds for further growth of the single crystalline titanium silicides. Since quantity of the seeds is limited, sites suitable for silicide growth are limited as well. Consequently, the crystalline NWs can grow only from selected spots on top of the amorphous layer. Reports on how quasi-liquid layer affected crystal growths are known. Recently, several research groups demonstrated the fabrication of NWs of metal silicide, including $NiSi_x$, $CrSi_2$, FiSi, and CoSi, without the use of any metal nanoparticles.[41,46,48,58] These may proceed via analogous routes.

Reaction temperature has a great influence on the crystal phase and the morphology of the NWs grown in this study. We suggest that the phase of the obtained NWs is highly dependent on the elemental composition of the interlayer. At a high temperature, the diffusion rate of Si atoms from the substrate is raised.[71] This would increase the Si concentration in the interlayer, as verified in the SEM EDX data shown in Figure 3.8. In addition, the disproportionation of $TiCl_{x(g)}$ to form $TiCl_{4(g)}$ and $Ti_{(s)}$ is less favored because the estimated Gibbs free energy of reaction is more positive.[72] All of these would allow the interlayer formed at 1073 K contain more Si than that deposited at 973 K. Consequently, the NWs grown at 1073 K have more Si atoms to form the TiSi phase, while the NWs obtained at 973 K, with less Si atoms, have the $Ti_5Si_3$ phase. The distinct morphologies of the NWs may result from the difference in their diameters, which are 30 – 80 and 20 – 50 nm for TiSi and $Ti_5Si_3$, respectively. In addition, the bulk mechanical hardness of TiSi and $Ti_5Si_3$, 18.0 and 9.86 GPa, respectively, may affect their morphology too.[28] Besides, $Ti_5Si_3$ NWs may contain more defects and become thread-like, whereas the TiSi NWs might be better crystallized so that the NWs grow upward on the substrate. All of the factors may explain why the TiSi NWs are straight while the $Ti_5Si_3$ NWs are coiled.

As mentioned in the TEM studies, the TiSi NWs show preferred growth orientation in the [010] direction while the $Ti_5Si_3$ NWs show that in the [001] direction. We analyzed their crystal structures to rationalize the observed phenomena. Figures 3.15 and 3.16 displayed the crystal models of TiSi and $Ti_5Si_3$ viewed along *a*, *b*, and *c* axes. In Figure 3.15, the Si-Si distance found in the structure was 0.2171 nm. Clearly, this is much smaller than the Si-Si distances of many molecular compounds containing Si-Si single bonds, ranging from 0.2363 to 0.2370 nm.[73,74] On the other hand, the Ti-Si and the Ti-Ti distances shown in Figure 3.15 were 0.2599 and 0.3227 nm, respectively. They are longer than the Ti-Si and the Ti-Ti bond distances reported in the literature for the corresponding molecular compounds, 0.2594 – 0.2629 nm and 0.2889 – 0.2942 nm for the Ti-Si and the Ti-Ti bonds, respectively.[75,76] This suggests that the Si-Si bonds in TiSi are stronger than the Ti-Si and Ti-Ti bonds. Consequently, forming Si-Si bonds stabilizes the structure more than forming Ti-Si and Ti-Ti bonds does. In Figure 3.15, the presence of high density Si-Si bonds along *b* axis of TiSi was observed. This suggests that the growth of TiSi along the [010] direction should be more favored because the overall energy is decreased. A similar analysis is carried out to account for the preferred growth of hexagonal $Ti_5Si_3$ in the [001] direction. Figure 3.16 displayed the crystal models of hexagonal $Ti_5Si_3$ viewed along *a* and *c* axes. Formation of Ti chains with extremely short Ti-Ti distance 0.2575 nm was observed along *c* axis. The distance is shorter than the Ti-Ti distances observed for many molecules containing Ti-Ti bonds. The nearest Si-Si and Si-Ti distances were 0.3024 nm and 0.2797 nm, respectively. These are longer than the molecular Si-Si and Ti-Si bond distances mentioned above. As a result, the growth of $Ti_5Si_3$ along the [001] direction would produce more Ti-Ti bonds and lower the energy. For comparison, the growth directions of hexagonal phase $CrSi_2$ and $Fe_5Si_3$ NWs were also found to be along [001].[41,47] On the other hand, the reported growth directions of TiSi NPs and

NWs were different from our observation.[35] After comparing the XRD results, we discover that the reported nanostructures had a different TiSi phase (JCPDS-65-2585, ICSD 20375).

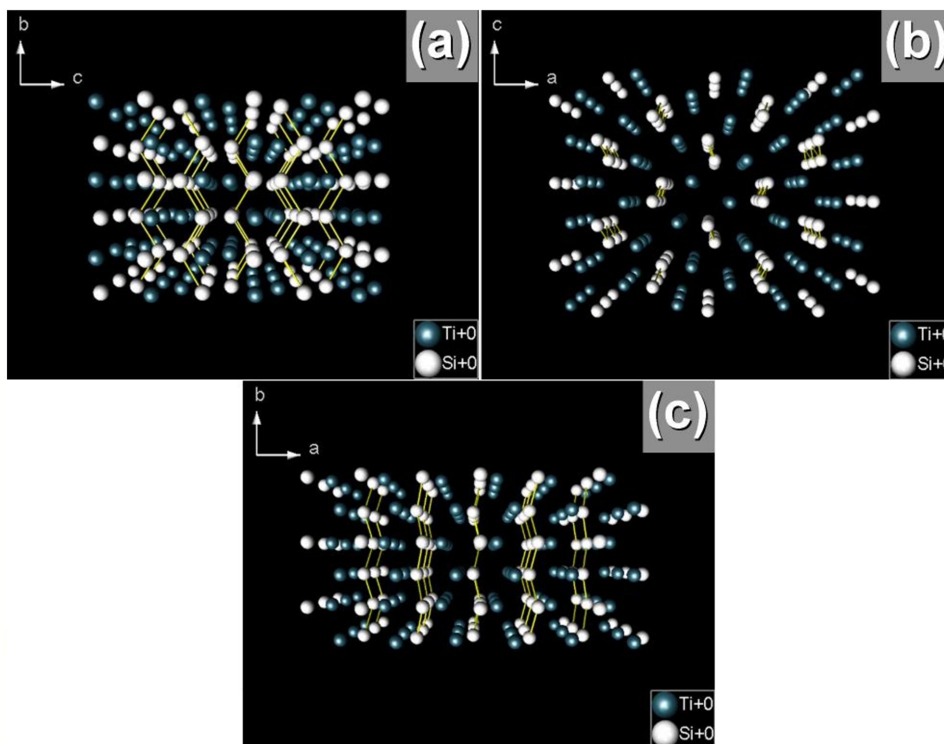


**Figure 3.15** Crystal models of orthorhombic TiSi viewing along (a) *a*, (b) *b*, and (c) *c* axes. The short Si-Si bonds (0.2171 nm) are linked in yellow sticks. Orthorhombic TiSi (JCPDS 17-0424, ICSD 43494): space group P*nma* (no. 62), *a* = 0.6544 nm, *b* = 0.3638 nm, ***c*** = 0.4997 nm.

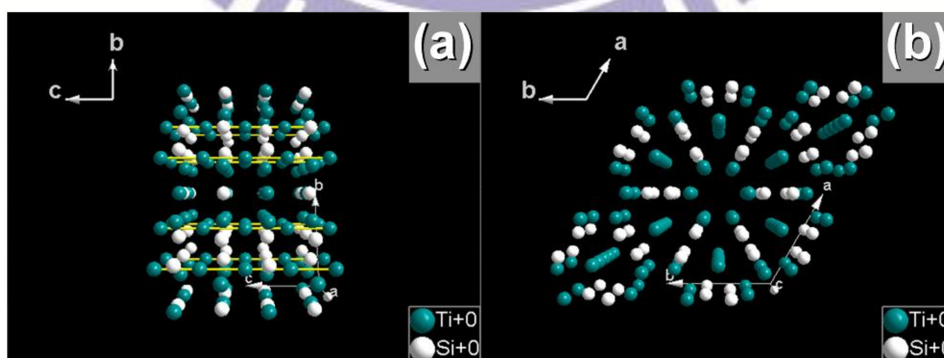


**Figure 3.16** Crystal models of hexagonal $Ti_5Si_3$ viewing along (a) *a* and (b) *c* axes. Viewing along *b* axis is equivalent to viewing along *a* axis. The short Ti-Ti bonds (0.25754 nm) are linked in yellow sticks. Hexagonal $Ti_5Si_3$ (JCPDS 78-1429, ICSD 62591): space group $P6_3$/mcm (no. 193), *a* = 0.7610 nm, *c* = 0.51508 nm.

### 3.3.6 Electron Field Emission Properties of Titanium Silicide Samples

Titanium silicides are suitable for EFE applications, due to their high melting points, low work functions (3.71 - 4.53 eV), and high conductivities.[1,28] Thus EFE properties of the samples obtained in this study were investigated. The results are shown in Figure 6. Detailed EFE properties, such as turn-on field $E_o$, which is defined as the electric field required to generate a current density ($J$) of 10 μAcm$^{-2}$, and field enhancement factor $\beta$, which is deduced from the Folwer-Nordheim (F-N) plot (the inset of Figure 6 showing the ln($JE^{-2}$)-($E^{-1}$) relationship, are summarized in Table 1.[36] Sample **I** demonstrates the best EFE performance among our samples. The $E_o$ of **I** is low, only 5.25 Vμm$^{-1}$, while the $J_{max}$ (at an applied voltage 1100 V) is high, 0.48 mAcm$^{-2}$. The low $E_o$ value is associated with its high NW aspect ratio. The high $J_{max}$ could be attributed to its high NW density, low TiSi resistivity, and low sheet resistance, which is 8.6 × 10$^{-2}$ Ω/□. $\beta$ of **I** is 876, calculated from the equation $\beta = \phi^{3/2}/\phi_e$, where $\phi$ is the work function of TiSi, 3.99 eV, while $\phi_e$ is the effective work-function derived from the slope of the F-N plot of **I** shown in the inset of Figure 3.17.[77] Other samples from this study did not perform equally well because they lack the proper combination of NW density, aspect ratio, and overall NW/thin film resistance. For example, **II** could not emit electrons even under the highest possible field applied. This is because **II** was a partially formed $TiSi_2$ film lacking 1-D nanostructures for emission. Sample **III** shows an $E_o$ 8.5 Vμm$^{-1}$ which is higher than **I**'s value because **III** has shorter NWs and consequently, a lower aspect ratio. The same reason is also applicable to explain **IV**'s poor performance. Sample **V** has an $E_o$ 5.4 Vμm$^{-1}$, which is slightly higher than **I**'s result, but a $J_{max}$ only a third of the value of **I**. This is attributed to **V**'s low NW density, high $Ti_5Si_3$ resistivity, and high sheet

resistance, $1.9 \times 10^{-1}$ Ω/□. In contrast, **I** is composed of high density, high aspect ratio and vertically aligned crystalline TiSi NWs. These ensure that nearly all NWs in **I** could emit electrons effectively. The result is that **I** is one of the best titanium silicide NW emitting materials reported so far.[5,6]

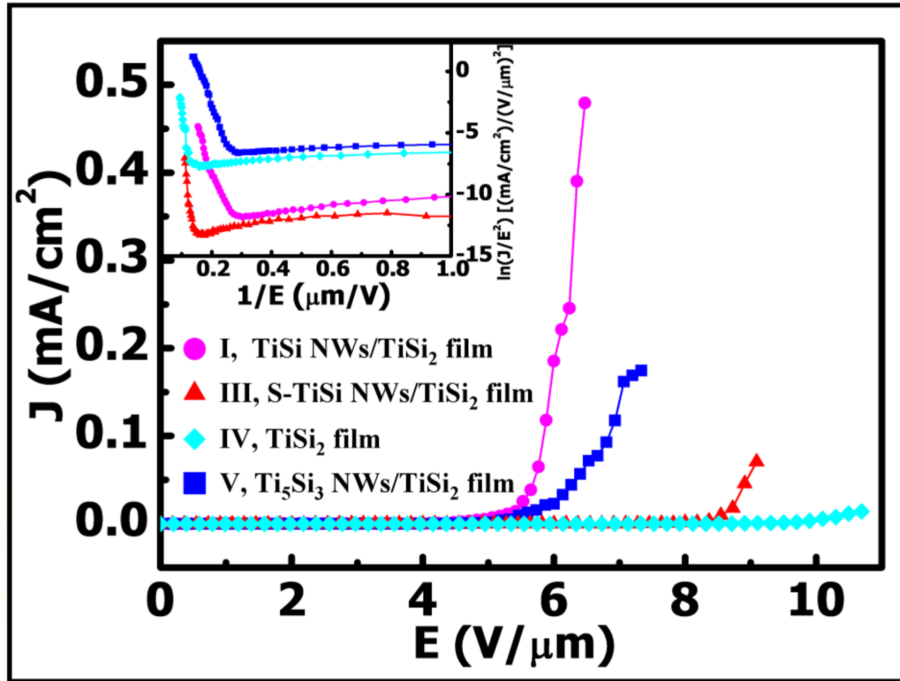


**Figure 3.17** EFE current density as a function of applied electric field of samples I, and III–V. Inset shows their corresponding Fowler-Nordheim plots.

1896

# 3.4 Conclusions

In conclusion, TiSi NWs were grown vertically on a C54-$TiSi_2$ film employing a unique CVD process. Disproportionation of gaseous $TiCl_x$ subhalides, formed by reacting $TiCl_{4(g)}$ and $Ti_{(s)}$ at high temperatures, provided Ti atoms while the Si substrate supplied Si atoms. Presence of an amorphous $TiSi_{2-x}$ interlayer was observed between the NWs and the film. This interlayer, probably existed as a quasi-liquid thin film during the growth, appears to be the key factor to assist the development of 1-D nanostructures. Varying the reaction conditions, such as time and temperature, would modulate reactivity and diffusion rate of the Ti and Si containing reactive species and limit the number of nucleation sites. This would influence not only composition and morphology but also physical and chemical properties of the product. Growth direction of the TiSi NWs was determined to be along [010]. The phenomenon could be attributed to the presence of strong Si-Si bonds along TiSi's *b* axis. This would lower the energy and provide high stability for the growth of TiSi in [010]. The vertically grown TiSi NWs demonstrates superior EFE properties with a low $E_o$ 5.25 $V\mu m^{-1}$ and a high $\beta$ 876. The high performance is attributed to TiSi's low work function, growth of high density, high aspect ratio, and vertically aligned 1D nanostructures, and the existence of a highly conductive $TiSi_2$ film below. Our study has provided a new route to grow unusual TiSi NWs which cannot be fabricated by other means so far. The synthesis will offer opportunities to study other physical and chemical properties of this unique material in the future.

# 3.5 References

(1) Maex, K.; Rossum, M. V. *Properties of Metal Silicides*; IEE: London, 1995.

(2) Murarka, S. P.; Fraser, D. B. *J. Appl. Phys.* **1980**, *51*, 350.

(3) Murarka, S. P. *Silicides for VLSI Applications*; Academic Press: Orlando, FL, 1983.

(4) Bucher, E.; Schultz, S.; Lux-Steiner, M. C.; Munz, P.; Gubler, U. G., F *Appl. Phys. A* **1986**, *40*, 71.

(5) Xiang, B.; Wang, Q.-X.; Wang, Z.; Zhang, X.-Z.; Liu, L.-Q.; Xu, J.; Yu, D.-P. *Appl. Phys. Lett.* **2005**, *86*, 243103.

(6) Chang, C.-M.; Chang, Y.-C.; Lee, C.-Y.; Yen, P.-H.; Lee, W.-F.; Chen, L.-J. *J. Phys. Chem. C* **2009**, *113*, 9153.

(7) Riley, D. J.; Mann M.; MacLaren, D. A.; Dastoor, P. C.; Allison, W. *Nano Lett.* **2003**, *3*, 1455.

(8) Singh, J. P.; Karabacak, T.; Lu, T. M.; Wang, G. C.; Koratkar, N. *Appl. Phys. Lett.* **2004**, *85*, 3226.

(9) Ritterskamp, P.; Kuklya, A.; Wustkamp, M.-A.; Kerpen, K.; Weidenthaler, C.; Demuth, M. *Angew. Chem., Int. Ed.* **2007**, *46*, 7770.

(10) Li, Q.; Lu, G. *Catal. Lett.* **2008**, *125*, 376.

(11) Massalski, T. B.; Okamoto, H.; Subramanian, P. R.; L, K. *Binary Alloy Phase Diagrams*; American Society for Metals: Metals Park, OH, 1990.

(12) Beyers, R.; Sinclair, R. *J. Appl. Phys.* **1985**, *57*, 5240.

(13) Murarka, S. P.; Fraser, D. B. *J. Appl. Phys.* **1980**, *51*, 342.

(14) Mann, R. W.; Clevenger, L. A. *J. Electrochem. Soc.* **1994**, *141*, 1347.

(15) Willams, J. J.; Akinc, M. *Oxid. Met.* **2002**, *58*, 57.

(16) Zhang, L.; Wu, J. *Acta Mater.* **1998**, *46*, 3535.

(17) Shah, D. M.; Berczik, D.; Anton, D. L.; Hecht, R. *Mat. Sci. Eng., A* **1992**, *155*, 45.

(18) Yen, B. K.; Aizawa, T.; Kihara, J. *J. Am. Ceram. Soc.* **1998**, *81*, 1953.

(19) Doppiu, S.; Monagheddu, M.; Cocco, G. *J. Mater. Res.* **2001**, *16*, 1266.

(20) Bentini, G. G.; Nipoti, R.; Armigliato, A.; Berti, M.; Drigo, A. V.; Cohen, C. *J. Appl. Phys.* **1985**, *57*, 270.

(21) Clevenger, L. A.; Cabral, C.; Roy, R. A.; Lavoie, C.; JordanSweet, J.; Brauer, S.; Morales, G.; Ludwig, K. F.; Stephenson, G. B. *Thin Solid Films* **1996**, *289*, 220.

(22) Wakelkamp, W. J. J.; Loo, F. J. J. V.; Metselaar, R. *J. Eur. Ceram. Soc.* **1991**, *8*, 135.

(23) Cockeram, B.; Wang, G. *Thin Solid Films* **1995**, *269*, 57.

(24) Ramos, A. S.; Nunes, C. A.; Coelho, G. C. *Mater. Charact.* **2006**, *56*, 107.

(25) Fouad, O. A.; Yamazato, M.; Nagano, M. *Appl. Surf. Sci.* **2002**, *195*, 130.

(26) Brukl, C.; Nowotny, H.; Schob, O.; Benesovsky, F. *Monatsh. Chem.* **1961**, *92*, 781.

(27) Samsonov, G. V.; Okhremchuk, L. N.; Podgrushko, N. F.; Podchernyaeva, I. A.; Fomenko, V. S. *Inorg. Mater.* **1976**, *12*, 720.

(28) Kosolapova, T. Y. *Handbook of High Temperature Compounds: Properties, Production, Applications;* Hemisphere Publishing Corporation: New York, 1990.

(29) Chopra, K. L. *Thin Film Phenomena*; McGraw-Hill: New York, 1969.

(30) Hoffman, D. W.; Thronton, J. A. *Thin Solid Films* **1977**, *40*, 355.

(31) Yim, W. M.; Stotko, E. J. *J. Electrochem. Soc.* **1974**, *121*, 965.

(32) Hallais, J. P.; Boccon-Gibod, D.; Chane, J. P.; Durand *J. Electrochem. Soc.* **1977**, *124*, 1290.

(33) Lacombe, J.; Duchemin, J. P.; Bonnet, M.; Huyghe, D. *Electron. Lett.* **1977**, *13*, 472.

(34) Du, J.; Du, P.-Y.; Hao, P.; Huang, Y.-F.; Ren, Z.-D.; Han, G.-R.; Weng, W.-J.; Zhao, G.-L. *J. Phys. Chem. C* **2007**, *111*, 10814.

(35) Du, J.; Ren, Z.-D.; Tao, K.-Y.; Hu, A.-H.; Hao, P.; Huang, Y.-F.; Zhao, G.-L.; Weng, W.-J.; Han, G.-R.; Du, P.-Y. *Cryst. Growth Des.* **2008**, *8*, 3543.

(36) Lin, H.-K.; Tzeng, Y.-F.; Wang, C.-H.; Tai, N.-H.; Lin, I.-N.; Lee, C.-Y.; Chiu, H.-T. *Chem. Mater.* **2008**, *20*, 2429.

(37) Zhou, S.; Liu, X.-H.; Lin, Y.-J.; Wang, D.-W. *Angew. Chem., Int. Ed.* **2008**, *47*, 7681.

(38) Zhou, S.; Liu, X.-H.; Lin, Y.-J.; Wang, D.-W. *Chem. Mater.* **2009**, *21*, 1023.

(39) In, J.; Seo, K.; Lee, S.; Yoon, H.; Park, J.; Lee, G.; Kim, B. *J. Phys. Chem. C* **2009**, *113*, 12996.

(40) Seo, K.; Varadwaj, K. S. K.; Cha, D.; In, J.; Kim, J.; Park, J.; Kim, B. *J. Phys. Chem. C* **2007**, *111*, 9072.

(41) Szczech, J. R.; Schmmitt, A. L.; Bierman, M. J.; Jin, S. *Chem. Mater.* **2007**, *19*, 3238.

(42) Zhou, F.; Szczech, J.; Pettes, M. T.; Moore, A. L.; Jin, S.; Shi, L. *Nano Lett.* **2007**, *7*, 1649.

(43) Higgins, J. M.; Schmitt, A. L.; Guzei, L. A.; Jin, S. *J. Am. Chem. Soc.* **2008**, *130*, 16086.

(44) Ham, M.-H.; Lee, J.-W.; Moon, K.-J.; Choi, J.-H.; Myoung, J.-M. *J. Phys. Chem. C* **2009**, *113*, 8143.

(45) Quyang, L.; Thrall, E. S.; Deshmukh, M. M.; Park, H. *Adv. Mater.* **2006**, *18*, 1437.

(46) Schmitt, A. L.; Bierman, M. J.; Schmeisser, D.; Himpsel, F. J.; Jin, S. *Nano Lett.* **2006**, *6*, 1617.

(47) Varadwaj, K. S. K.; Seo, K. I., J.; Mohanty, P.; Park, J.; Kim, B. *J. Am. Chem. Soc.* **2007**, *129*, 8594.

(48) Schmitt, A. L.; Zhu, L.; Schmeiber, D.; Himpsel, F. J.; Jin, S. *J. Phys. Chem. B* **2006**, *110*, 18142.

(49) Seo, K.; Varadwaj, K. S. K.; Mohanty, P.; Lee, S.; Jo, Y.; Jung, M.-H.; Kim, J.; Kim, B. *Nano Lett.* **2007**, *7*, 1240.

(50) Seo, K.; Lee, S.; Yoon, H.; In, J.; Varadwaj, K. S. K.; Jo, Y.; Jung, M. H.; Kim, J.; Kim, B. *ACS Nano* **2009**, *3*, 1145.

(51) Decker, C. A.; Solanki, R.; Freeouf, J. L.; Carruthers, J. R.; Evans, D. R. *Appl. Phys. Lett.* **2004**, *84*, 1389.

(52) Kim, J.; Anderson, W. A. *Thin Solid Films* **2005**, *483*, 60.

(53) Kim, J.; Anderson, W. A.; Song, Y. J.; Kim, G. B. *Appl. Phys. Lett.* **2005**, *86*, 253101.

(54) Song, Y.; Jin, S. *Appl. Phys. Lett.* **2007**, *90*, 173122.

(55) Song, Y.; Schmitt, A. L.; Jin, S. *Nano Lett.* **2007**, *7*, 965.

(56) Kim, C.-J.; Kang, K.; Woo, Y. S.; Ryu, K.-G.; Moon, H.; Kim, J.-M.; Zang, D.-S.; Jo, M.-H. *Adv. Mater.* **2007**, *19*, 3637.

(57) Kim, J.; Shin, D. H.; Lee, E.-S.; Han, C.-S.; Park, Y. C. *Appl. Phys. Lett.* **2007**, *90*, 253103.

(58) Kang, K.; Kim, S.-K.; Kim, C.-J.; Jo, M.-H. *Nano Lett.* **2008**, *8*, 431.

(59) Lee, C. Y.; Lu, M. P.; Liao, K. F.; Lee, W. F.; Huang, C. T.; Chen, S. Y.; Chen, L. J. *J. Phys. Chem. C* **2009**, *113*, 2286.

(60) Chueh, Y.-L.; Ko, M.-T.; Chou, L.-J.; Chen, L.-J.; Wu, C.-S.; Chen, C.-D. *Nano Lett.* **2006**, *6*, 1637.

(61) Weaver, L. *Microsc. Res. Tech.* **1997**, *36*, 368.

(62) Lee, C.-Y. *Chem. Vap. Deposition.* **1999**, *5*, 69.

(63) Wagner, R. S.; Ellis, W. C. *Appl. Phys. Lett.* **1964**, *4*, 89.

(64) Reynolds, G. J.; Cooper, C. B.; Faczl, P. J. *J. Appl. Phys.* **1989**, *65*, 3212.

(65) Southwell, R. P.; Seebauer, E. G. *J. Vac. Sci. Technol., A* **1995**, *71*, 5918.

(66) Mendicino, M. A.; Seebauer, E. G. *J. Electrochem. Soc.* **1993**, *140*, 1786.

(67) Chen, L. J. *Mat. Sci. Eng., R* **2000**, *29*, 115.

(68) Southwell, R. P.; Seebauer, E. G. *J. Electrochem. Soc.* **1997**, *144*, 2122.

(69) Luo, J. *Crit. Rev. Solid State* **2007**, *32*, 67-109.

(70) Wang, M. H.; Chen, L. J. *Appl. Phys. Lett.* **1991**, *59*, 2460.

(71) Gossmann, H. J.; Rafferty, C. S.; Luftman, H. S.; Unterwald, F. C.; Boone, T.; Poate, J. M. *Appl. Phys. Lett.* **1993**, *63*.

(72) Reaction-Web, Facility for the Analysis of Chemical Thermodynamics; CRCT, Ecole Polytechnique de Montréal: Montréal, http://www.crct.polymtl.ca/fact/.

(73) Chisholm, M. H.; Chiu, H.-T.; Folting, K.; Huffman, J. C. *Inorg. Chem.* **1984**, *23*, 4097.

(74) Stueger, H.; Fuerpass, G.; Renger, K.; Baumgartner, J. *Organometallics* **2005**, *24*, 6374.

(75) McAlexander, L. H.; Hung, M.; Li, L.; Diminnie, J. B.; Xue, Z.; Yap, G. P. A.; Rheingold, A. L. *Organometallics* **1996**, *15*, 5231.

(76) Thorn, M. G.; Vilardo, J. S.; Lee, J.; Hanna, B.; Fanwick, P. E.; Rothwell, I. P. *Organometallics* **2000**, *19*, 5636.

(77) Fowler, R. H.; Nordheim, L. W. *Proc. R. Soc. London, Ser. A* **1928**, *119*, 173.

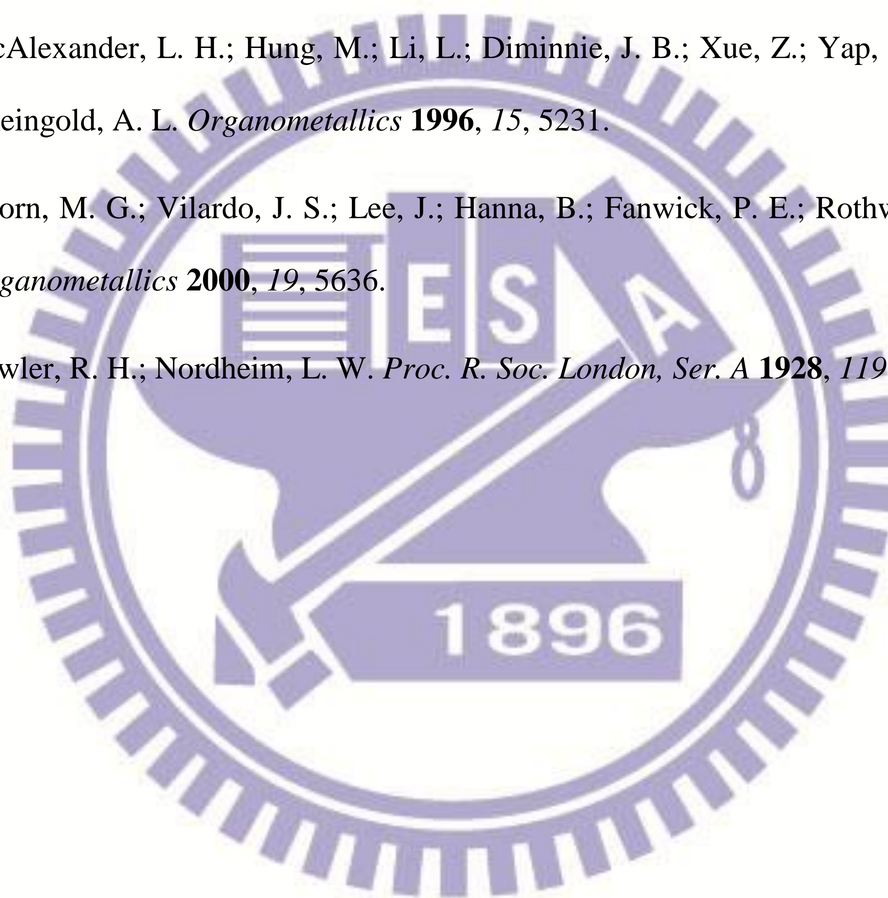

# Chapter 4

# Chemical Vapor Deposition of $Ti_xSi_y$ Film and Single Crystalline C49 $TiSi_2$ Nanoplates

## 4.1 Introduction

In addition to one-dimension nanostructures, two-dimensional nanostructures also show unique physical and chemical properties for future applications.[1-11] There are some synthetic strategies to obtained two-dimensional nanostructures. For example, Ag nanoplates were synthesized with capping agent to confine the crystal growth into two dimensions.[1] Second, self-assembly block copolymer was used as template to synthesize ZnSe nanoplates.[2] In addition, under proper reaction condition, nanoplates could be obtained with compounds that have anisotropic structure nature.[3],[4] In chapters 2 and 3, we have investigated the preparation of titanium silicide samples through a unique CVD process without using the hazardous $SiH_4$ gas and catalyst for one-dimensional nanostructures. $TiCl_x$, generated by reaction between $TiCl_4$ vapor and Ti metal, was used as the precursor to grow titanium silicide thin films or NWs on Si substrate.[12-14] Also, in this chapter, we will demonstrate the synthesis of C49 $TiSi_2$ nanoplates on Si substrate via our CVD process under low $TiCl_4$ vapor pressure condition. The characterization and the growth mechanism of the two-dimensional nanostructure will be discussed below. Moreover, influence of the reaction temperature and time on the morphologies, crystal structures, and film growth rate of the titanium silicide samples are investigated in detail to better understand the reaction process.

## 4.2 Experimental Section

### 4.2.1 Synthesis Procedure

A summary of reaction conditions and experimental observations is listed in Table 4.1. The detail reaction procedure is described below. Ti powders (0.3 g) were placed at the highest temperature zone at 1173 K. Si (100) wafers with size of 0.7 x 1.5 $cm^2$, cleaned by RCA process were placed at a low temperature zone at 723 – 1073 K downstream. After the chamber was evacuated to lower than 2 mtorr, $TiCl_4$ immersed in a 298 K water bath was vaporized into the reaction chamber at a pressure of 20 mtorr, which is manipulated by a needle valve. After 30 min to 6 h, the supply of $TiCl_4$ was stopped and the reaction system was cooled to room temperature. Samples of gray or black thin films deposited on Si substrates were obtained. By changing the reaction condition, thin film samples with different morphologies and crystal structure could be obtained. On the other hand, when the $TiCl_4$ was changed to a 273 K ice bath and the partial pressure was reduced to 10 mtorr. After 30 min, C49-$TiSi_2$ nanoplates on Si substrate could be obtained at 973 K.

### 4.2.2 Characterization Instrument

The SEM and EDX data were collected using JEOL JSM-6330F and Hitachi S-4700I at 15 kV. The TEM, SAED, and high-resolution transmission electron microscopic (HRTEM) images and EDX were acquired on a scanning transmission electron microscope (STEM) JEOL JEM-3000F at 300 kV. The X-ray photoelectron spectroscopy (XPS) measurement were carried out using a Perkin-Elmer PHI 1600 spectrometer with Mg Kα (1253.6 eV) radiation. The sample surface was cleaned by an $Ar^+$ ion sputter gun. The XRD studies were carried out using a MAC MXP-18 and a BRUKER AXS D8 ADVANCE with Cu Kα1 radiation.

## 4.3 Results and Discussion

All reactions were performed in a low pressure reactor as shown in Figure 2.1. $TiCl_4$, the precursor, was vaporized into the reaction chamber at a controlled partial pressure. Close to the precursor inlet, Ti powders were placed at the heating zone at 1173 K. Si (100) wafers were placed at the center heating zone at 723 - 973 K. After 30 min to 6 h, deposition of a gray layer on the substrates was observed. A summary of the representative samples prepared in this study is listed in Table 2.1.

**Table 4.1** Summary of Samples

| Sample | Morphologies and Phases | NWs Length/ Film Thickness | Temperature (K) | Time (min) | $TiCl_4$ Temp (K) | $TiCl_4$ Pressure (mtorr) | Growth rate (nm/min) [b] |
|---|---|---|---|---|---|---|---|
| I | C49-$TiSi_2$ film | 100 nm | 723 | 60 | 298 | 20 | 1.6 |
| II | C49-$TiSi_2$ and C54-$TiSi_2$ film | 550 nm | 773 | 60 | 298 | 20 | 9.2 |
| III | C54-$TiSi_2$ film | 2 μm | 873 | 60 | 298 | 20 | 33.3 |
| IV | C54-$TiSi_2$ film | 2.6 μm | 973 | 60 | 298 | 20 | 43.3 |
| V | TiSi NWs on C54-$TiSi_2$ film | 2-5 μm / 10.5 μm | 1073 | 60 | 298 | 20 | 170 |
| VI | C54-$TiSi_2$ film | 2.2 μm | 973 | 30 | 298 | 20 | 73.3 |
| VII | $Ti_5Si_3$ NWs on C54-$TiSi_2$ film | 0.5-3 μm / 3.5 μm | 973 | 180 | 298 | 20 | 19.4 |
| VIII | $Ti_5Si_3$ NWs on C54-$TiSi_2$ film | 2-5 μm / 6 μm | 973 | 360 | 298 | 20 | 16.6 |
| IX | C49-$TiSi_2$ nanoplates | 30-100 nm / 0.5-5 μm [a] | 973 | 30 | 273 | 10 | - |

[a] Thickness / lateral dimension of the nanoplates. [b] Estimated from the SEM image.

### 4.3.1 Titanium Silicide Films Grown at Different Temperatures

Figure 4.1 shows SEM images of samples synthesized at different temperatures for 60 min. The growth temperature of sample **I**, **II**, **III**, **IV**, and **V** are 723 K, 773K, 873 K, 973 K, and 1073 K, respectively. SEM images of **I**, Figure 4.1a and b display a thin film with small grains on the top and a thickness of 100 nm. Figure 4.1c and d demonstrate that **II** has rough film surface and the film thickness is raised to 550 nm. **III**, prepared at 873 K, shows a thickness of 1.8 – 2 μm and an uneven surface. As shown in Figure 4.1g and h, **IV** obtained at 973 K for 60 min also displays a 2.6 μm-thick film and scarce and short nanowires on it. Figure 4.1i is a low magnification top-view image of **V**, revealing the presence of high density Two-dimensional nanostructures on the deposited product. Figure 4.1j displays a side-view image of **V**, indicating that the product deposited on the substrate is composed of a film (thickness 10.5 μm) and above it, a layer of NWs pointing upward. The growth rate of the thin film, 1.6 – 170 nm/min, was evaluated from the cross-sectional SEM images. As the data shown in table 4.1, the growth rates of the sample synthesized for 60 min (**I**-**V**) increase with the reaction temperature. At 723 K, **I**, the growth rate was very low (1.6 nm/min). When the reaction temperature was raised to 1073 K, the deposition rate increased notably to a rate of 170 nm/min. As a consequence, the growth rate was increased with the reaction temperature.

XPS studies were performed to verify the chemical state of the Ti and Si in the samples. XPS spectra of sample **IV** grown at 973 K for 60 min are shown as a typical example, since the spectra of the samples are quite similar. Figure 4.2a shows the high-resolution spectra of Ti. The signals of Ti $2p_{1/2}$ and Ti $2p_{3/2}$ are observed at 460.4 eV and 454.4 eV, respectively. These are close to the values of Ti-Si binding energy.

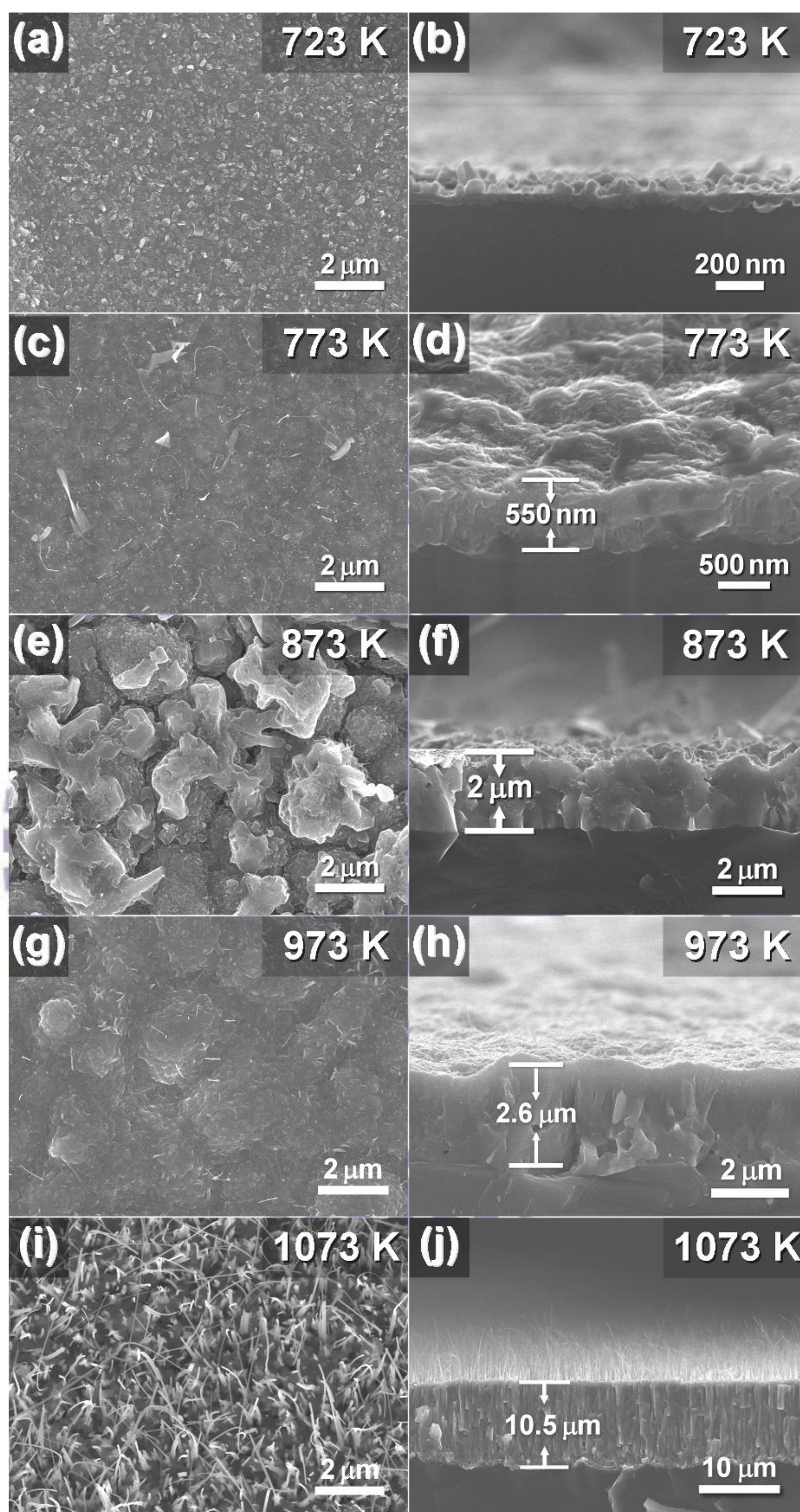


**Figure 4.1** Top-view and side-view SEM images of samples grown at different reaction temperatures for 60 min. (a)-(b) 723 K (I), (c)-(d) 773 K (II), (e)-(f) 873 K (III), (g)-(h) 973 K (IV), and (i)-(j) 1023 K (V).

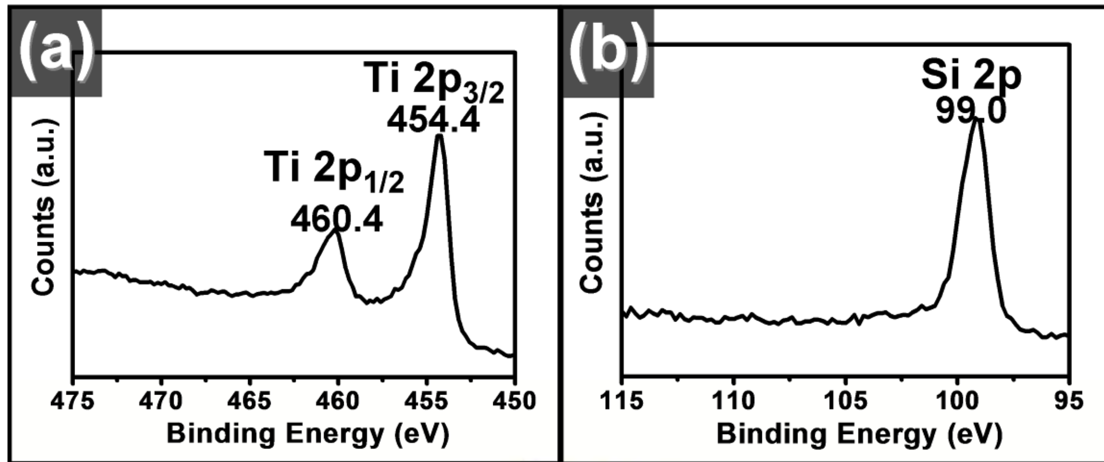


**Figure 4.2** High-resolution XPS spectra of the film grown at 973 K for 60 min. (a) Ti 2p1/2 and Ti 2p3/2 electrons and (b) Si 2P electron.

The binding energy of Si 2p electrons, Figure 4.2b, shows one binding energy of 99.0eV and could be assigned to Si-Ti binding energy. Thus, the chemical states of the Ti and Si in the samples are determined to be Ti-Si bonding.[14]

The crystal structures of the films were examined by XRD. In Figure 4.3, sample **I**, synthesized at 723 K for 60 min showing two broad peaks at $2\theta = 40.8^o$ and $50.9^o$ marked with blue circles were assigned to the {131} and {002} reflections of orthorhombic C49-$TiSi_2$ (JCPDS 10-0225), which suggested that the film was composed mainly of orthorhombic C49-$TiSi_2$ phase. Sample **II** displays one strong diffraction peak at $2\theta = 33^o$, which could be assigned to be the Si {020} reflection, which results from the Si substrate used. Four peaks around $2\theta = 39.1^o$, $42.3^o$, $43.5^o$, and $50^o$ marked with gray circles could be assigned to the {311}, {040}, {022}, and {331} planes of C54-$TiSi_2$ (JCPDS 35-0785), respectively. In addition, two minor reflections at $2\theta = 40.8^o$ and $50.9^o$ marked with blue circles corresponds well with the {131} and {002} planes of C49-$TiSi_2$. Thus, we conclude that **II**, synthesized at 773 K for 60 min, is composed mainly of C54-$TiSi_2$ and a portion of C49-$TiSi_2$. As the reaction temperature was further raised to 873 K and 973 K, for sample **III** and **IV**, respectively, only diffraction patterns of C54-$TiSi_2$ could be observed. Therefore, **III**

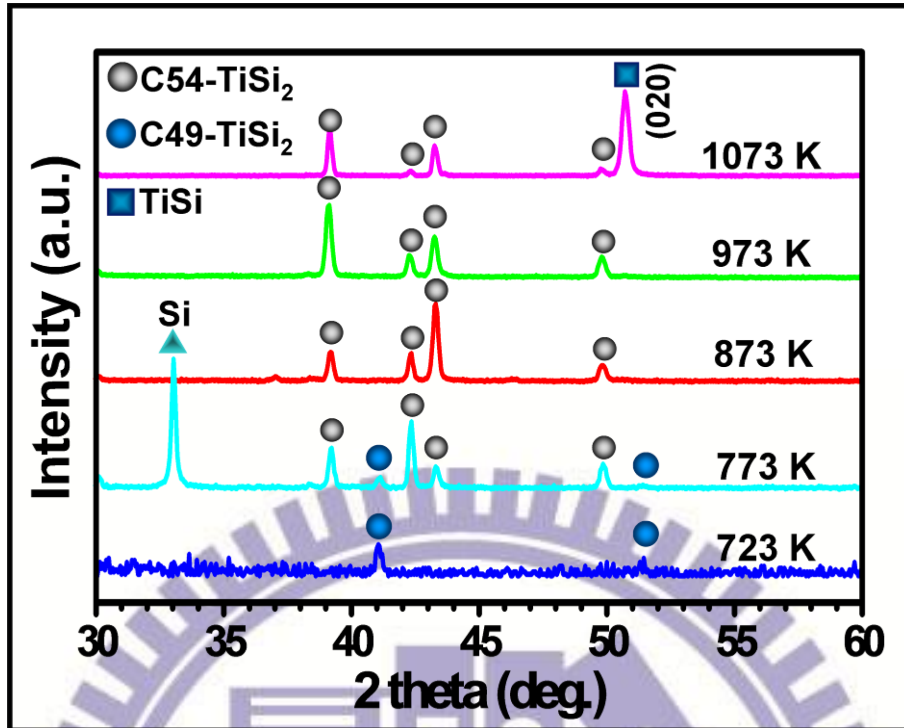


**Figure 4.3** XRD patterns of samples prepared at different temperatures for 60 min (I-V).

and **IV** are determined to be C54-$TiSi_2$ films. As mention in chapter 3, sample fabricated at 1073 K for 60 min, **V**, contains TiSi NWs with a preferred growth orientation in [020] direction on the top of a C54-$TiSi_2$ film. The presence of pure C49-$TiSi_2$ phase at low reaction temperature of 723 K, mix phases of C54 and C49 $TiSi_2$ at 773 K, and pure C54 $TiSi_2$ at temperatures higher than 873 K imply that the C49-$TiSi_2$ is a low temperature metastable phase before the formation of C54-$TiSi_2$. This result coincides well with the previous research on titanium silicide.[15]

## 4.3.2 Titanium Silicide Film Grown at Different Time

Influence of the reaction time on the samples is discussed in this section. Figure 4.4 demonstrates the top-view and cross-sectional SEM images of the samples fabricated at 973 K with different reaction time, which are 30 min, 60 min, 180 min,

and 360 min for sample **VI**, **IV**, **VII**, and **VIII**, respectively. The SEM images (Figure 4.4a and b) of sample **VI**, which was grown at 973 K for 30 min, displays a film with an uneven surface and a film thickness of 2.2 μm. When the growth time was 60 min, sample **IV** was obtained. As shown in Figure 4.4c and d, there are few NWs on a layer of thin film with a thickness of 2.6 μm. Figure 4.4e and f display the image of sample **VII**, obtained after the reaction was carried out for 180 min at 973 K. Growth of some thread-like NWs with lengths 0.5 - 3 μm on top of a thin film with a thickness of 3.5 μm is observed. When the reaction time was increased to 360 min, as shown in Figure 4.4g and h sample **VIII**, abundant thread-like NWs with lengths 2 – 5 μm were grown on a film with thickness of 6 μm. Thus, we can conclude that only a thin film was grown initially. When the reaction time was extended to a certain period of time, growth of 1-D nanostructure was started. As the reaction time increased, density and length of the NWs raised accordingly. Besides, the film growth rate was decreased with the lengthening of reaction time, which were 73.3 nm/min and 16.6 nm/min for sample synthesized at 30 min and 360 min, respectively. As discussed in chapter 3, In our CVD system, the $TiCl_x$ molecular, generated through the reaction between $TiCl_{4(g)}$ and the Ti powders at 1173 K, could react directly with the Si substrate to form titanium silicides and $SiCl_{x(g)}$ byproduct. The $SiCl_x$ could decompose and serve as another source of Si atom for the silicide formation. As the reaction progressed, the presence of the relatively inert C54-$TiSi_2$ film could impede the reaction between the $TiCl_x$ and the Si substrate as well as the production of $SiCl_x$. Consequently, the deposition rate of the $TiSi_2$ thin film decreased with the lengthening of the reaction time.

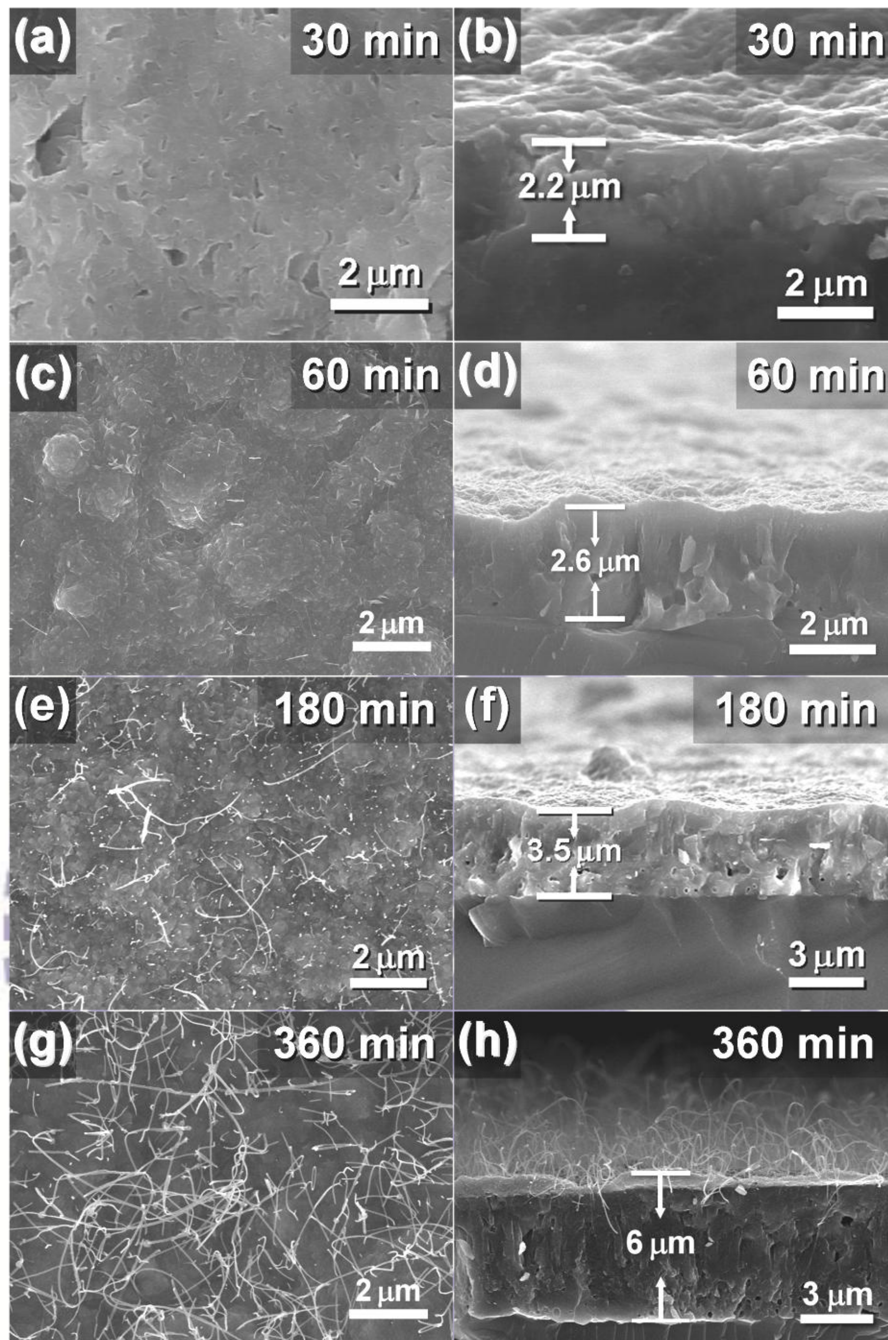


**Figure 4.4** Top-view and side-view SEM images of samples grown at 973 K for 30 - 360 min. (a)-(b) 30 min (VI), (c)-(d) 60 min (IV), (e)-(f) 180 min (VII), (g)-(h) 360 min (VIII).

Figure 4.5 displays the XRD patterns of the sample synthesized at 973 K for different reaction time. All of them show four diffraction peaks marked by gray circles at $2\theta = 39.1^o$, $42.2^o$, $43.2^o$, and $49.7^o$, which indicates that these samples are mainly composed of orthorhombic C54-$TiSi_2$ (JCPDS 35-0785) thin film. For sample

obtained for 30 min, **VI**, a diffraction peak at $2\theta = 33^{o}$, which is assigned to Si {020} plane. The Si diffraction was resulted from the Si substrate used. Only diffraction peaks of C54-$TiSi_2$ are observed for sample synthesized at 30 and 60 min. Therefore, **IV** and **VI** are determined to be C54-$TiSi_2$ films. As the reaction time increased more than 180, in addition to the C45-$TiSi_2$ diffraction peaks, a weak diffraction peak at $2\theta = 34.8^{o}$ is shown. This could be assigned to the reflection by by {002} plane of $Ti_5Si_3$ (JCPDS 78-1429), the main component of the NWs in **VII** and **VIII**. In addition, the XRD data coincided well with the TEM data of the $Ti_5Si_3$ NWs, which reveals that the NWs is grown preferentially along [002] axis of $Ti_5Si_3$.

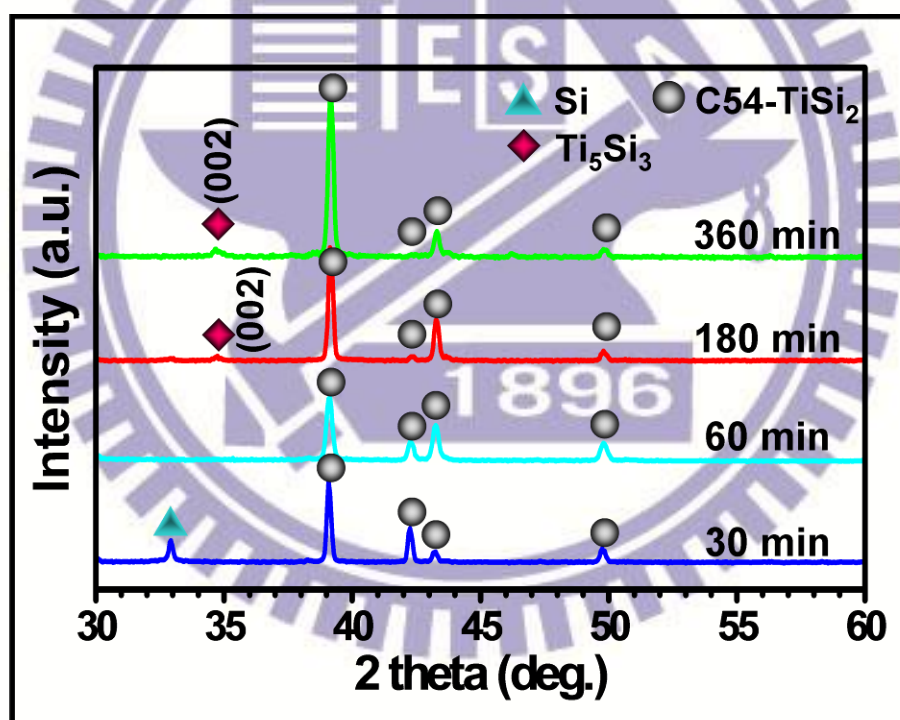


**Figure 4.5** XRD patterns of samples synthesized at 973 K for different time.

## 4.3.3 Synthesis of C49 $TiSi_2$ Nanoplates

### 4.3.3.1 Characterization of the C49 $TiSi_2$ Nanoplates

Two-dimensional titanium silicide nanostructures spontaneously formed by reacting $TiCl_{x(g)}$, producing by reaction between $TiCl_{4(g)}$ and Ti metal at 1173 K, with Si substrate at 973 K for 30 min. Unlike the samples discussed previously, the $TiCl_{4(g)}$ partial pressure in this study was reduced to 10 mtorr by keeping the $TiCl_{4(l)}$ precursor in an ice bath at 273 K. Figure 4.6 shows the SEM image and XRD of sample IX, grown on Si wafer at 973 K for 30 min as the $TiCl_4$ was immersed in an ice bath. Top-view SEM image of IX, Figure 4.6a, reveals numerous thin plate structures on the Si substrate. Inset is the EDX spectrum taken at the center part in Figure 1a, which implying that the nanoplates are composed of Ti and Si only. In addition, Ti and Si atom% estimated from the EDX are 34 % and 66 %. Figure 4.6b indicates that the thickness and lateral dimension of the nanoplates are about 30 – 100 nm and 0.5 - 5 μm. In addition to the plate-like structures, some net-like structures could be observed. Enlarged-view of the nanoplate is shown in Figure 4.6c. The nanoplates are composed of arrays of one-dimensional nanostructures in two directions, which are perpendicular to one another, with diameters of 20 – 50nm. Figure 4.6d demonstrates the XRD pattern of IX. Diffraction peaks at $2\theta = 33^o$, which is assigned to Si {020} plane, results from the Si substrate. In addition, there are two sets of diffraction peaks could be observed. Minor diffraction peaks at $2\theta = 39.1^o$, $43.5^o$, and $50^o$ marked with gray circles could be assigned to the {311}, {022}, and {331} planes of orthorhombic C54-$TiSi_2$ (JCPDS 35-0785). Two strong peaks at $2\theta = 40.8^o$ and $50.9^o$ marked with blue circles were assigned to the {131} and {002} reflections of orthorhombic C49-$TiSi_2$ (JCPDS 10-0225). Thus, we attributed the presence of C54-$TiSi_2$ to the underlying film on the surface, similar with sample **II** in chapter 3, partial C54-$TiSi_2$

film obtained at 1073 K for 10 min. The C49-$TiSi_2$ signals are resulted from the nanoplates, which is further confirmed by TEM studies and will be discussed below.

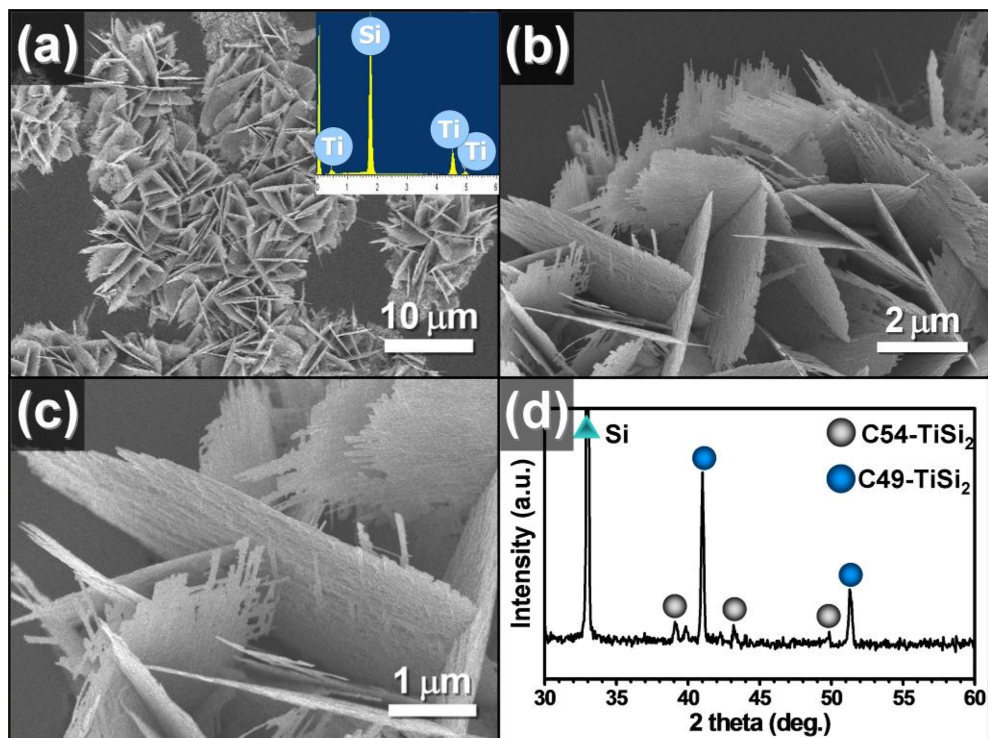


**Figure 4.6** Characterization of sample **IX**, grown on Si wafer at 973 K for 30 min as the $TiCl_4$ was immersed in an ice bath. SEM studies: (a) low magnification image, and EDX spectrum (inset), (b) high magnification image of the nanoplates, (c) enlarged-view of the nanoplats, and (d) XRD pattern.

Figure 4.7a shows a representative TEM image of a nanoplate isolated from **IX**. The lateral-dimension of this nanoplate is about 480 – 800 nm. The various contrast through the plate implies that the plate have an uneven surface. Figure 4.7b demonstrates EDX spectrum taken from the square area in (a). The data indicates that the nanoplate contains Ti and Si only. In addition, the Si/Ti atomic ratio is 2.3, which is close to that of C49-$TiSi_2$. SAED shown in Figure 4.7c represents well-defined ED spots denoting that the nanoplate is single-crystalline. In addition, the ED are determined to be from {200}, {002}, and {202} planes of orthorhombic TiSi with

[010] zone axis. Figure 4.7d represents the HRTEM image from the same region. The lattice spacings 0.181, 0.179, and 0.127 nm are assigned to {200}, {002}, and {202} planes of C49-$TiSi_2$, respectively. According to the SAED and HRTEM results, the nanoplates in **IX** are determined to be single crystalline C49-$TiSi_2$ with a basal plane of (010) plane.

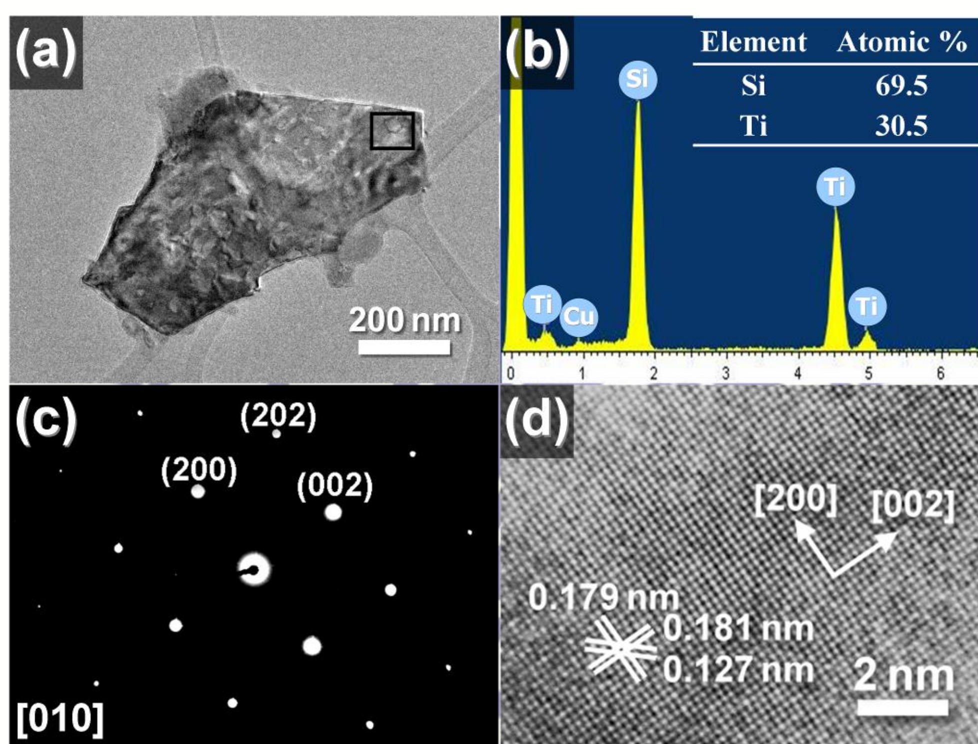


**Figure 4.7** TEM studies of sample **IX**. (a) Low-magnification TEM image, (b) EDX spectrum, (c) SAED, and (d) HRTEM image were obtained at the square area in (a).

### 4.3.3.2 Proposed Reaction Pathway of the C49 $TiSi_2$ Nanoplates

In our CVD system, titanium subchlorides $TiCl_x$ (x = 1-3), produced by the reaction between $TiCl_{4(g)}$ and Ti atoms at 1173 K, could disproportitonate into $TiCl_4$ and Ti atom below 973 K. Alternatively, the $TiCl_x$ and $TiCl_4$ vapor could react with the Si substrate to produce Si-rich $TiSi_x$ clusters and gaseous $SiCl_x$ byproducts, which might act as another Si source in the formation of small $TiSi_x$ clusters.[14] Existence of etched holes with small clusters around them further confirms this reaction progress.

As the reaction continues, titanium silicides clusters start to grow into two-dimensional C49-$TiSi_2$ nanoplates. Sample **VI**, obtained at 973 K with $TiCl_{4(g)}$ partial pressure of 20 mtorr for 30 min shows a C54-$TiSi_2$ thin film with a thickness of 2.2 μm. On the other hand, when the partial pressure of $TiCl_{4(g)}$ was reduced to 10 mtorr, by immersing the $TiCl_{4(l)}$ precursor in an ice bath at 273 K, abundant two-dimensional C49-$TiSi_2$ nanoplates were formed. Different morphology of samples obtained in **VI** and **IX** could be explained by the supersaturation crystal growth theory, anisotropic growth of $TiSi_x$ nuclei occurs at a relative low supersaturation condition. Similar two-dimensional C49-$TiSi_2$ nanostructures have been reported. The author claimed that the growth of two-dimensional structures may be attributed to the orthorhombic symmetry and corresponding atomic arrangements. The assumed that the Cl terminations serve as a passivation layer that prevents further deposition on the *b* planes. Here, we propose another hypothesis to rationalize the growth mechanism of the C49 nanoplates. The formation of C49-$TiSi_2$ nanoplates is possibly due to their anisotropic structure, which will be discussed below. Figure 4.8 displayed the crystal models of orthorhombic C49-$TiSi_2$ viewed along *a*, *b*, and *c* axes. In Figure 4.8a, Si-Si bonds with distance of 0.232 nm, which are smaller than the Si-Si single bond distances reported (0.2363 – 0.2370 nm), were observed along the c axis.[16,17] In addition, Figure 4.8b-c demonstrate the model have the Ti-Si bonds shortest distance of 0.264 nm, which are only slightly higher than the reported value of 0.2594 - 0.2629 nm, were linked with yellow sticks.[18,19] According to Figure 4.8b and c, crystal structure viewed along the *a* and *c* axes, respectively, C49-$TiSi_2$ was determined to be a layer structure with a basal plane parallel to the (010) plane. The anisotropic structure nature makes the preferred growth along the (100) and (001) faces. The results were consisted with the TEM studies of the C49-$TiSi_2$ nanoplate, which shows a basal plane of (010). According to the TEM studies, the top-right

corner of the nanoplate seems to have edges of (202) and (-202) facets. This phenomenon could be attributed to the higher growth rates of the (100) and (001) faces. The faster crystal facets grow the more easily there facets disappear.

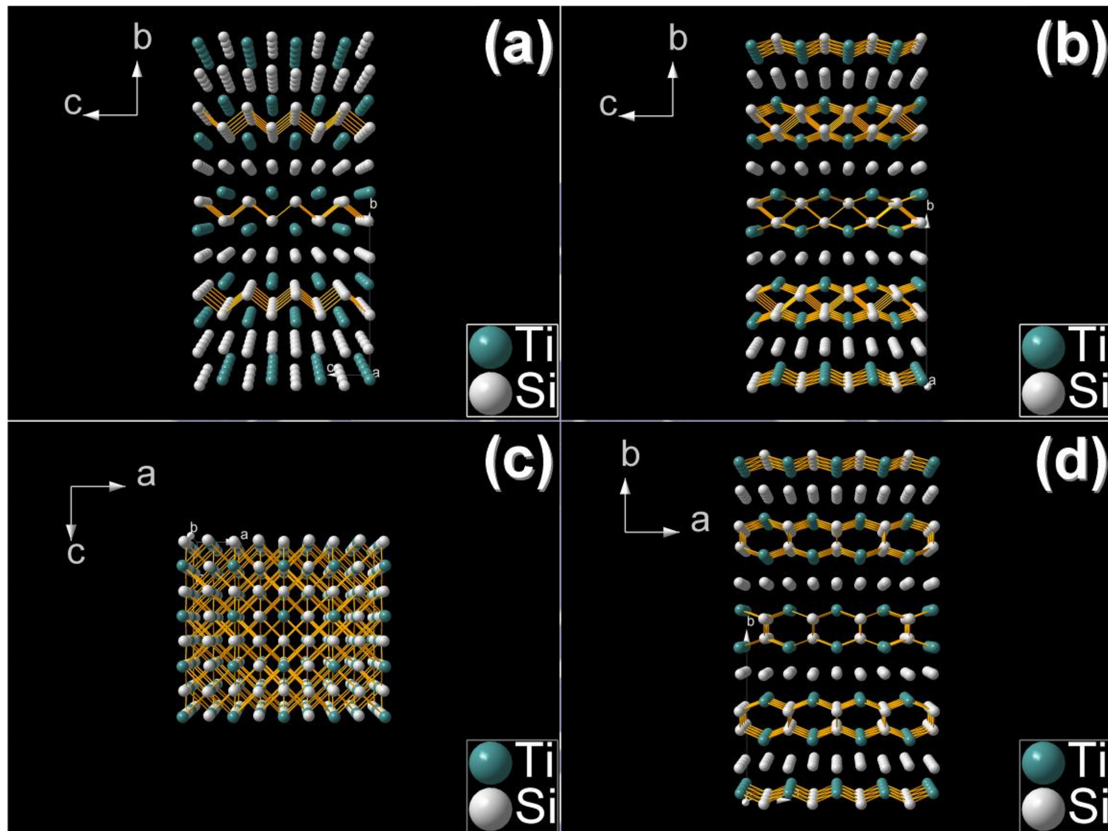


**Figure 4.8** Crystal models of orthorhombic C49-$TiSi_2$ viewing along (a) *a*, (b) *a*, (c) *b*, and (d) *c* axes. The short Si-Si bonds (0.232 nm) are linked in yellow sticks in (a). The Si-Si and Ti-Si, with the shortest distance, are linked in yellow sticks for clarity in (b)-(d). Orthorhombic C49-$TiSi_2$ (JCPDS 10-0225): space group C*mcm* (no. 63), $a$ = 0.362 nm, $b$ = 1.376 nm, $c$ = 0.3605 nm.

## 4.4 Conclusions

Titanium silicides samples were obtained through our unique CVD system. In this chapter, we have discussed how the reaction temperature and reaction time influence the morphologies, crystal structures, and the film growth rate of the samples obtained. For samples grown at different temperatures for 60 min. C49-$TiSi_2$ film was fabricated at 723 K. When the reaction temperatures were raised to higher than 873 K, C49-$TiSi_2$ disappears and C54-$TiSi_2$ becomes the major product. TiSi NWs on top of C54-$TiSi_2$ film was fabricated at 1073 K. For samples grown at 973 K for different time, only thin film samples were obtained. Only with sufficient time, more than 180 min, one-dimensional nanostructures will be obtained. In addition, the film growth rates were increased, when the reaction temperature was raised. While, for reaction obtained at 973 K for different reaction time, the film growth rates were reduced, with reaction time. In the third part, C49-$TiSi_2$ nanoplates were synthesized when the vapor pressure of the $TiCl_4$ was reduced to 10 mtorr. The preferred basal plane of the C49-$TiSi_2$ nanoplates was determined to be parallel to the (010) plane. This could be attributed to the anisotropic nature of the C49-$TiSi_2$, which shows a layer structure with layers parallel to the (010) plane. That is, the growth rates of the (100) and (001) faces would be higher than those of other faces. Comparing with the titanium silicide NWs discussed in chapter 2 and 3, with preferred growth direction of [002] and [010] for $Ti_5Si_3$ NWs and TiSi NWs, respectively. The crystal structure nature takes an important role on the growth of anisotropic nanostructures.

## 4.5 References


(1) Wiley, B.; Sun, Y.; Mayers, B.; Xia, Y. *Chem.-Eur. J.* **2005**, *11*, 454.

(2) Karanikolos, G. N.; Law, N. L.; Mallory, R.; Petrou, A.; Alexandridis, P.; Mountziaris, T. J. *Nanotechnology* **2006**, *17*, 3121.

(3) Zhang, C.; Zhu, Y. F. *Chem. Mater.* **2005**, *17*, 3537.

(4) Han, J. T.; Huang, Y. H.; Jia, R. J.; Shan, G. C.; Guo, R. Q.; Huang, W. *J. Cryst. Growth* **2006**, *294*, 469.

(5) Chen, S. H.; Fan, Z. Y.; Carroll, D. L. *J. Phys. Chem. B* **2002**, *106*, 10777.

(6) Kuo, C. L.; Kuo, T. J.; Huang, M. H. *J. Phys. Chem. B* **2005**, *109*, 20115.

(7) Zhou, G. T.; Wang, X. C.; Yu, J. C. *Cryst. Growth Des.* **2005**, *5*, 1761.

(8) Jang, E. S.; Won, J. H.; Hwang, S. J.; Choy, J. H. *Adv. Mater.* **2006**, *18*, 3309.

(9) Wu, J.; Duan, F.; Zheng, Y.; Xie, Y. *J. Phys. Chem. C* **2007**, *111*, 12866.

(10) Lim, B.; Wang, J. G.; Camargo, P. H. C.; Jiang, M. J.; Kim, M. J.; Xia, Y. N. *Nano Lett.* **2008**, *8*, 2535.

(11) Zhou, S.; Liu, X.-H.; Lin, Y.-J.; Wang, D.-W. *Angew. Chem. Int. Ed.* **2008**, *47*, 7681.

(12) Lin, H.-K.; Tzeng, Y.-F.; Wang, C.-H.; Tai, N.-H.; Lin, I.-N.; Lee, C.-Y.; Chiu, H.-T. *Chem. Mater.* **2008**, *20*, 2429.

(13) Lin, H. K.; Cheng, H. A.; Lee, C. Y.; Chiu, H. T. *Chem. Mater.* **2009**, *21*, 5388.

(14) Lee, C.-Y. *Chem. Vap. Deposition* **1999**, *5*, 69.

(15) Mann, R. W.; Clevenger, L. A. *J. Electrochem. Soc.* **1994**, *141*, 1347.

(16) Chisholm, M. H.; Chiu, H. T.; Folting, K.; Huffman, J. C. *Inorg. Chem.* **1984**, *23*, 4097.

(17) Stueger, H.; Fuerpass, G.; Renger, K.; Baumgartner, J. *Organometallics* **2005**, *24*, 6374.

(18) McAlexander, L. H.; Hung, M.; Li, L.; Diminnie, J. B.; Xue, Z.; Yap, G. P. A.; Rheingold, A. L. *Organometallics* **1996**, *15*, 5231.

(19) Thorn, M. G.; Vilardo, J. S.; Lee, J.; Hanna, B.; Fanwick, P. E.; Rothwell, I. P. *Organometallics* **2000**, *19*, 5636.

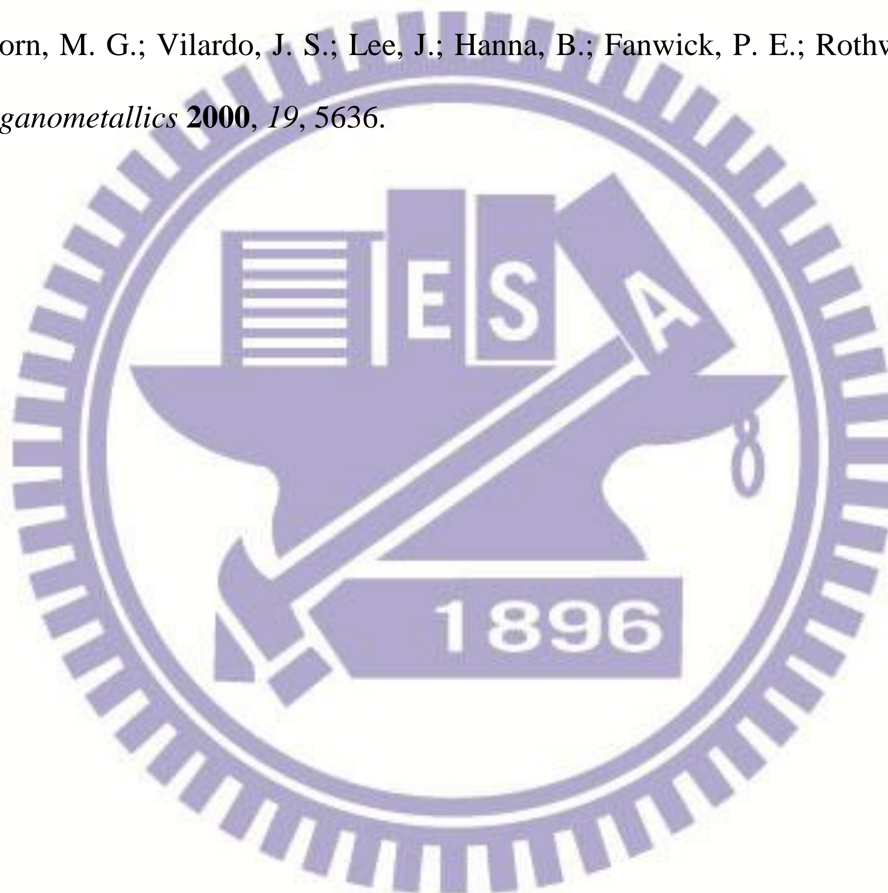

# Chapter 5

# Conclusions

Titanium silicide samples, with different crystal phases and morphologies, including nanowires ($Ti_5Si_3$ and TiSi), nanoplates (C49 $TiSi_2$), and thin films (C49 and C54 $TiSi_2$) have been successfully synthesized via a unique chemical vapor deposition process. Disproportionation of gaseous $TiCl_x$ subhalides, formed by reacting $TiCl_{4(g)}$ and $Ti_{(s)}$ at high temperatures, provided Ti atoms while the Si substrate supplied Si atoms. Varying the reaction conditions, such as time and temperature, would modulate reactivity and diffusion rate of the Ti and Si containing reactive species. That is, the composition, morphology, physical and chemical properties of the products could be manipulated within one synthesis system.

This study is the first growth of single crystalline $Ti_5Si_3$ NWs on C54-$TiSi_2$ thin films through CVD without additional catalyst. The diameters of the NWs are about 20 - 50 nm and the lengths are several micrometers. In addition, the growth direction of the $Ti_5Si_3$ NWs is determined to be along the [001] axis. Furthermore, TiSi NWs grown perpendicularly on the C54-$TiSi_2$ thin films were also fabricated in the study. These TiSi NWs have diameters of about 20 – 80 nm and several micrometers in length. The growth direction of the obtained TiSi NWs is identified to be along the b-axis of TiSi. In NWs samples, we have observed the existence of an amorphous $TiSi_{2-x}$ interlayer between the NWs and the film below. This interlayer, probably existed as a quasi-liquid thin film during the growth, is believed to be important to assist the growth of 1-D nanostructures. This result may shad light on the growth

mechanism of other 1-D nanomaterials.

In addition, C49-$TiSi_2$ nanoplates on Si substrate were synthesized under low $TiCl_4$ vapor condition. The thickness of the the thickness and lateral dimension of the nanoplates are about 30 – 100 nm and 0.5 - 5 μm. The preferred basal plane of the C49-$TiSi_2$ nanoplates are determined to be parallel to the (010) plane. This could be attributed to the anisotropic crystal structure of the orthorhombic C49-$TiSi_2$, which shows a layer structure with layers parallel to the (010) plane. Preferred growth phenomenon of $Ti_5Si_3$ NWs, TiSi NWs, and C49 $TiSi_2$ nanoplates indicates that the crystal nature of the samples plays an important role on the growth of anisotropic nanostructures.

EFE properties of the titanium silicide samples are studied in this research. The EFE properties of these titanium silicide emitters are highly depended on the morphology and crystal structure of the NWs and thin films. The turn-on field $E_o$ of $Ti_5Si_3$ NWs and TiSi NWs are 5.4 V$\mu m^{-1}$ and 5.25 V$\mu m^{-1}$, respectively. The titanium silicide NWs also show remarkable field enhancement factor β, which are 816 for $Ti_5Si_3$ NWs and 876 for TiSi NWs. The high performance is attributed to TiSi's low work function, growth of high density, high aspect ratio, and vertically aligned 1D nanostructures, and the existence of a highly conductive $TiSi_2$ film below. These notable results suggest that titanium silicide emitters could serve as promising candidates for future field emission devices. Our study has provided a new route to grow titanium silicide nanomaterials with various morphologies and phases. Metal silicide nanostructures with different metal component might be produced through this synthetic method with appropriate precursor. In addition, these novel titanium nanostructures offer opportunities to study their physical and chemical properties, such as field emission properties of single NW, electrical conductivity of the NWs, and photoelectrochemical water-splitting properties, the future.

# List of Publications

1. H.-K. Lin, Y.-F. Tzeng, C.-H. Wang, N.-H. Tai, I-N. Lin, C.-Y. Lee, and H.-T. Chiu
"$Ti_5Si_3$ Nanowire and Its Field Emission Property", *Chem. Mater*. **2008**, *20*, 2429.

2. H.-K. Lin, H.-A. Cheng, C.-Y. Lee, and H.-T. Chiu
"Chemical Vapor Deposition of TiSi Nanowires on C54 $TiSi_2$ Thin Film – An Amorphous Titanium Silicide Interlayer Assisted Nanowire Growth", *Chem. Mater*. **2009**, *21*, 5388.

3. C.-H. Chien, P.-S. Sheng, C.-H. Wang, C.-H. Huang, H.-K. Lin, C.-Y. Lee and H.-T. Chiu,
"Preparation of $Mo_2C$@a-C Core-shell Powders via Carburization of Mo Particles by 1-chlorobutane and Hexachlorobenzene", *Mater. Lett*. **2007**, *61*, 3593.

4. C.-H. Huang, Y.-H. Chang, H.-K. Lin, C.-W. Peng, W.-S. Chung, C.-Y. Lee, and H.-T. Chiu,
"Phase Segregation Assisted Morphology Sculpting -Growth of Graphite and Silicon Crystals via Vapor-Solid Reactions", *J. Phys. Chem. C* **2007**, *111*, 4138.

5. C.-H. Wang, H.-K. Lin, T.-Y. Ke, T.-J. Palathinkal, N.-H. Tai, I.-N. Lin, C.-Y. Lee, and H.-T. Chiu.
"Growth of Polycrystalline Tubular Silicon Carbide - Yajima-Type Reaction at the Vapor-Solid Interface", *Chem. Mater*. **2007**, *19*, 3956.

6. C.-H. Chien, P.-S. Sheng, C.-H. Wang, C.-H. Huang, H.-K. Lin, C.-Y. Lee, and H.-T. Chiu.
"Synthesis of Carbon Particles and Hollow Shells from $CCl_4$ and Mo", *Mater. Lett*. **2008**, *62*, 1176.

7. T.-K. Huang, Y.-C. Chen, H.-C. Ko, H.-W. Huang, C.-H. Wang, H.-K. Lin, F.-R. Chen, J.-J. Kai, C.-Y. Lee, and H.-T. Chiu.
"Growth of High-Aspect Ratio Gold Nanowires on Silicon by Surfactant Assisted Galvanic Reductions", *Langmuir* **2008**, *24*, 5647.

8. I.-C. Chang, T.-K. Huang, H.-K. Lin, Y.-F. Tzeng, C.-W. Peng, F.-M. Pan, C.-Y. Lee, and H.-T. Chiu.
"Growth of Pagoda-Topper Tetragonal Copper Nanopillar Arrays", *ACS Appl. Mater. Interfac*. **2009**, *1*, 1375.

9. H.-K. Lin, Y.-F. Tzeng, C.-H. Wang, N.-H. Tai, I-N. Lin, C.-Y. Lee, and H.-T. Chiu. "Field Emission Properties of $TiSi_x$ Nanowires and Thin Films," Materials Research Society 2008 Spring Meeting, San Francisco, United State, **2008**.

10. H.-K. Lin, H.-A. Cheng, C.-Y. Lee, and H.-T. Chiu. "Chemical Vapor Deposition of Titanium Silicide Nanowires," Japan-Taiwan Joint Symposium on New Functional Materials and Their Nano-Scale Analysis, Kyoto, Japan, **2009**.